CRASH MODELING OF A LIGHT COMPOSITE AIRCRAFT

MOELETSI AUGUSTINUS MOLETSANE

A THESIS SUBMITTED IN FULFILMENT OF THE REQUIREMENTS OF THE MASTERS DEGREE IN TECHNOLOGY TO THE DEPARTMENT OF MECHANICAL ENGINEERING AT THE DURBAN UNIVERSITY OF TECHNOLOGY

APPROVED FOR FINAL SUBMISSION

……. ……..

SUPERVISOR **DATE**

PROF. DAVID JONSON

DURBAN, SOUTH AFRICA

APRIL 2014

DECLARATION

I declare that this thesis is my own un-aided work except where due acknowledgement is made to others. This thesis is being submitted for the Masters Degree in Technology to the Department of Mechanical Engineering at the Durban University of Technology, and has not been submitted previously for any other degree or examination.

Moeletsi Augustinus Moletsane Date

ACKNOWLEDGEMENTS

I would like to thank Professor David Jonson for giving me the opportunity to study towards my master's degree in technology. I would also like to thank my parents for their encouragement and support throughout all my studies, my colleagues for their assistance, and National Research Foundation (NRF) for their financial support that helped me throughout my research.

Table of Contents

DECLARATION i
ACKNOWLEDGEMENTS ii
LIST OF FIGURES vi
LIST OF TABLES x
ABSTRACT xi
CHAPTER 1 1
INTRODUCTION 1
CHAPTER 2 5
LITERATURE REVIEW 5
2.1 Crash environment 5
2.1.1 Impact terrain 5
2.1.2 Impact attitude and descent angle 6
2.1.3 Aircraft coordinate system 7
2.1.4 Acceleration and velocity related terms 10
2.1.5 Force related terms 11
2.2 Composite materials 13
2.2.1 Fibrous composites 13
2.2.2 Fibre reinforcement 14
2.2.3 Types of matrix 15
2.2.4 Stiffness and Strength of composites 15
2.2.5 Stress/strain relations in composites 16
2.2.6 Composite with the off-axis fibre orientation 18
2.2.7 Stiffness of composites 20
2.3 Properties of composite materials 24
2.3.1 Rules of mixtures 24
2.3.2 Failure theories in fibrous composites 26
2.4 Basic Classical laminate theory of multilayered shells in MSC.Dytran 30
2.5 Modeling Using MSC.Patran/Dytran 31
2.6 Theory of contact 33
2.7 Validation of Computational Tools 34

CHAPTER 3 37
RESEARCH METHODOLOGY 37
3.1 Failure criteria associated with a lamina 37
3.1.1 Fibre-composite material with failure criteria in MSC.Dytran. 37
3.1.2 Evaluation of fibre-composite material with failure criteria in MSC.Dytran. 38
3.1.3 Modeling approach of the composite strip 42
3.1.4 Results review of stress-time and failure flag-time graphs with different failure criteria. 43
3.1.5 Results review of displacement-time graphs with different criteria. 56
3.1.6 Progressive ply failure in MSC.Dytran 58
3.2 Evaluation of the fuselage sandwich core 60
3.2.1 Modeling the sandwich core 60
3.2.2 Failure flags of the sandwich core before and after failure prediction 61
3.2.3 Failure flag plots of the sandwich core materials 63
3.3 Evaluation of failure criteria associated with beams with MSC.Dytran 65
3.4 Progressive crushing of a composite square tube 68
3.4.1 Modeling methodology of the composite square tube 68
3.4.2 Finite element model of the composite square tube 69
3.4.3 Material properties for the composite square tube model 70
3.4.4 Boundary conditions for the composite tube crushing 71
3.4.5 Results review of the composite tube crushing 72
3.5 Crash modeling approach of the Ravin 500 light composite aircraft. 74
3.5.1 Description of the FEM model of the aircraft 74
3.5.3 Boundary conditions of the aircraft crash model 79
3.5.3.1 Concentrated masses applied to the model 79
3.5.3.2 Contact definition in the crash model 80
3.5.3.3 Aircraft crash parameters 80
CHAPTER 4 82
RESULTS AND DISCUSSION 82
CHAPTER 5 88
CONCLUSIONS AND RECOMMENDATIONS 88

REFERENCES.....90

LIST OF FIGURES

Figure 1.1 Ravin 500 light composite aircraft 2

Figure 2.1 Descent angle and impact attitude 6

Figure 2.2 Aircraft coordinates and attitude directions 8

Figure 2.3 Flight path angle, terrain angle and impact angle 9

Figure 2.4 Typical aircraft floor acceleration pulse 10

Figure 2.5 Resultant crash force, vertical crash and horizontal crash force 12

Figure 2.6 Crash force angle and related terms 12

Figure 2.7 Plain weave woven roving 14

Figure 2.8 Unidirectional composite fibre specimen 16

Figure 2.9 Principal material axes of unidirectional lamina 16

Figure 2.10 Unidirectional lamina with principal axes rotated by relative angle θ to the x-y axes 18

Figure 2.11 Definition of plies within a laminate 20

Figure 2.12 The in-plane and bending components of the laminate 21

Figure 2.13 Equivalent loads acting on a laminate 22

Figure 2.14 Time step loop of the explicit method 32

Figure 2.15 Graphs of numerical analysis and experimental plots of the left sidewall acceleration responses of a vertical drop test of B737 fuselage section 35

Figure 2.16 Comparison of predicted deformation of MSC.Dytran with experiments from a high speed camera 36

Figure 2.17 Experimental and Dytran analysis comparison of fuselage drop test 36

Figure 3.1 Nodes with initial velocity of -132m/s along z-axis 40

Figure 3.2 Nodes with initial velocity of -116m/s along z-axis 40

Figure 3.3 Nodes with initial velocity of -100m/s along z-axis 41

Figure 3.4 Stress vs. time plots with no failure criteria defined 43

Figure 3.5 Stress vs. time graph of the Tsai-Hill criteria 44

Figure 3.6 Failure flags vs. time graph of the Tsai-Hill criteria 45

Figure 3.7 Stress vs. time plots of the Tsai-Wu criteria 46

Figure 3.8 Failure flag vs. time plots of the Tsai-Wu criteria 47

Figure 3.9 Stress vs. time plots of the Modified Tsai-Wu criteria 48

Figure 3.10 Failure flags of the Modified Tsai-Wu criteria 49

Figure 3.11 Stress vs. time plots of the Maximum stress criteria 50

Figure 3.12 Failure flag vs. time plots of the Maximum stress criteria 51

Figure 3.13 Stress vs. time plots of the Hashin criteria 52

Figure 3.14 Failure flag vs. time plots of the Hashin criteria 53

Figure 3.15 Stress vs. time plots of the Chang-Chang criteria 54

Figure 3.16 Failure flags vs. time plots of the Chang-Chang criteria 55

Figure 3.17 Displacement vs. time plots of node 31 with no failure criteria 56

Figure 3.18 Displacement vs. time plots of node 31 with failure criteria defined 57

Figure 3.19 No failure at t=0.256 milliseconds with Tsai-Wu criteria 59

Figure 3.20 Failure at t=0.272 milliseconds with Tsai-Wu criteria 59

Figure 3.21 Failure flag plot up to t=0.261 milliseconds with Tsai-Wu criteria 59

Figure 3.22 Sandwich core of Rohacell foam and two plies of carbon fibre 60

Figure 3.23 Failure flag plots of layer 1 defined with carbon fibre properties 61

Figure 3.24 Failure flag plot of layer 2 defined with Rohacell foam properties 62

Figure 3.25 Failure flag plot of layer 3 defined carbon fibre properties 62

Figure 3.26 Carbon fibre failure flag of element 31 layer 1 63

Figure 3.27 Rohacell foam failure flag not dropped down to zero after failure of element 31 layer 2 64

Figure 3.28 Carbon fibre failure flag of element 31 of layer 3 64

Figure 3.29 Clamped nodes, nodes with initial velocity and concentrated mass 65

Figure 3.30 Beam failure flag at t=1.762 milliseconds and t=181.9 milliseconds 66

Figure 3.31 Beam stresses vs. time graph 67

Figure 3.32 Beam failure flags vs. time graph 67

Figure 3.33 Set-up model for the composite tube crush analysis 68

Figure 3.34 Meshed models of the moving rigid surface and the square tube 70

Figure 3.35 Composite tube plots with no failure criteria defined 72

Figure 3.36 Composite tube plots with Tsai-Wu criteria defined 73

Figure 3.37 Half model of the ravin 500 light composite aircraft 75

Figure 3.38 Components of the Ravin floor structure 76

Figure 3.39 Connected mesh of both the floor structure and the fuselage section 76

Figure 3.40 Concentrated masses representing the wings, stabilizers and engine loadings 79

Figure 3.41 Soil model, aircraft model, crash velocity and crash angle 81

Figure 4.1 Element 37470 not failed at t=55.4 milliseconds for both layer 1 and 9 of the fuselage at 20 crash angle 83

Figure 4.2 Element 37470 failed at t=56.5 milliseconds for both layer 1 and 9 of the fuselage at 20 crash angle 83

Figure 4.3 Aircraft crash sequence at 10° crash angle and a portion of a fuselage with minimum amount of damage 84

Figure 4.4 Aircraft crash sequence at 15° crash angle and failure in the wheel-well structure 85

Figure 4.5 Aircraft crash sequence at a 20° crash angle and crushed forward, fuselage structure 86

Figure 4.6 Aircraft crash sequence at a 30° crash angle and the entire fuselage heavily damaged 87

LIST OF TABLES

TABLE 1 Typical fibre and resin properties 25

TABLE 2 Material properties for the composite half strip 39

TABLE 3 Rohacell foam material properties 60

TABLE 4 Material properties for the tube wall laminate ply 71

TABLE 5 Nominal layup schedule for the aircraft fuselage skin 75

TABLE 6 Nominal layup schedule for the aircraft internal structure 76

TABLE 7 Equivalent material properties for fuselage facings (orthotropic) 77

TABLE 8 Equivalent material properties for internal facings (orthotropic) 77

TABLE 9 Material properties for foam core (isotropic) 78

TABLE 10 Material properties for the steel beam elements 78

TABLE 11 Material properties for soil model (isotropic) 78

TABLE 12 Components with concentrated masses 79

TABLE 13 Different aircraft crash conditions used for the crash model 81

ABSTRACT

The study presented here was focused on the crash analysis of light composite aircraft on relatively survivable accidents. The crash analysis approach was based on the numerical simulation using the finite element software (MSC.Dytran). The aircraft crash environment, impact terrain, impact angles and material properties were identified, and later introduced into the aircraft crash model.

The background on composite materials is discussed and more focus was given to their response at high strain rates. The modeling methodology is also discussed with more emphasis on the finite element analysis approach and the failure theories behind composite materials. The failure criteria are based on assumptions considered for the classical lamination theory, and each of the failure theories in MSC.Dytran were evaluated before being introduced into the crash model. The Tsai-Wu failure criterion was found to be capable of predicting the progressive ply failure of the composite lamina.

The Ravin 500 light composite aircraft model was used for the purpose of this study and four crash scenarios of impacting the aircraft onto the soil model were considered. The aircraft was impacted at the same crash velocity but different flight path angles were considered. The 10°, 15°, 20° and 30° crash angles together with a crash velocity of 22m/s were used. The impact approach was influenced by the previous literature; it shows that the structural damage of an aircraft during crash accident is affected largely by the crash angle.

The results of each crash scenario are presented and mainly focused on the failure response of the aircraft structure. The conclusion on the crashworthiness of the Ravin 500 light composite aircraft is also drawn based on the numerical work. Details

regarding the future work or recommendations for the design philosophy and means of improving the crashworthiness of the light composite aircraft are also presented. In addition, more emphasis is focused in the occupant's space within the aircraft.

CHAPTER 1

INTRODUCTION

In the world today aircraft crashworthiness has become the major concern with regard to civil aviation. There is a high need for safety improvements in order to achieve reliable means of transportation. This includes the ability of an aircraft to eliminate unnecessary injuries and fatalities in relatively survivable accidents. Even though in some instances the structural damage, especially the bottom fuselage which may be heavily deformed or crashed, it is believed that the occupant volume must still provide adequate protection to the crew.

In the past decades aluminum used to be the primary material in the aircraft and automotive industries. Its strength to weight ratio offered good performance compared to other traditional materials in terms of weight savings and strength. Most homogenous materials have different strengths; this implies that each material can withstand a certain amount of loading for the same volume of the material. Therefore, in any design of a load carrying structure, it is important to consider the strength of the material to be selected and if the material is not strong enough, the geometry or the volume of the load carrying parts may be increased so as to increase the load bearing capacity. But on the other hand, the structure becomes bulky and the weight also increases. Therefore, to avoid this problem, modern aircrafts are manufactured from composite materials which are strongly replacing the use of aluminum.

The increasing state of the art in material development has shifted from metals to alternative materials. Therefore, much research effort has gone into the technology of composite materials which performs better in comparison to the homogenous

materials. This is mostly due to high specific strength and stiffness properties but still maintaining high corrosion resistance capability compared to metal alloys. Since composite materials are non-homogenous, the resulting properties are the combination of individual constituent materials, therefore resulting in outstanding performances. In addition, composite structures can offer high specific energy absorption under crash loadings.

Since the properties of composites are entirely derived from the experimental testing, it is important to first identify the suitability of the composite material for a specific application. This includes static or dynamic performances. Finally, the major concern is crashworthiness and it was studied based on computational modeling of the Ravin 500 light composite aircraft shown in Figure 1.1.

Figure 1.1 Ravin 500 light composite aircraft. [1]

Modern advances in computer technology, improvements of the current generation of software, allow for the evaluation and development process of the crash test at a reduced cost as compared to experimental tests. Therefore, previous researchers conducted similar work on the implementation and the understanding on simulation of actual crash dynamics [2], [3], [4]. But there are some uncertainties on various modeling techniques involved in this type of study. Therefore, the aircraft crashworthiness study is still an ongoing research especially with the use of the commercially available computational tools.

The main objective of this investigation was focused on achieving an appropriate methodology in order to perform a controlled dynamic aircraft crash analysis. Therefore, a simple test was conducted on multilayered composite plate; it was a means of verifying the capability of MSC.Dytran to predict progressive ply failure using available criteria within the code. Furthermore, a composite tube was impacted onto a rigid floor in order to display the crushing behavior of a composite structure. Later the aircraft was modeled with appropriate material properties, crash angle, crash velocity, failure criteria and impacted onto the soil model.

The study, discussed in chapter 2, includes the main areas of literature survey done in accordance with the objective of the research work. This includes the conditions of crash environment of fixed wing aircraft. This provided adequate means of setting a proper approach or methodology for the purpose of analysis. It is of great importance for a designer of an aircraft structure to have background knowledge of the crash scenarios before any attempt to build the actual product.

A more detailed survey was also conducted on composite materials and is discussed in chapter 2 as well. In chapter 3, a procedure to set up a proper crash environment for the purpose of investigating the crashworthiness of the light composite aircraft is described. In chapter 4, the results obtained from the crashworthiness analysis of a

light composite aircraft are discussed in this section. The concluding remarks and future recommendations are discussed in chapter 5.

CHAPTER 2

LITERATURE REVIEW

2.1 Crash environment

Aircraft crash conditions vary considerably depending on a number of factors. Velocity, attitude and deceleration are some of the factors that strongly contribute towards setting up appropriate crash impact conditions for analysis.

In some of the technical reports for the US (Federal Aviation Agency) in Washington [5], [6], [7], [8], [9]; assumptions regarding the crash environment were necessary in the design principles affecting the airframe of an aircraft. Impact terrain, descend angles, impact attitude, impact deceleration and airplane velocity are the primary parameters affecting the assumptions. It is also important to consider the local environment (aircraft interior design) of the occupant at all potential seating locations [8]. In this study, focus is directed towards the effect of crash on the impacted structure especially the "livable volume". This is the area sufficient in size to maintain space between the occupant and the structure [10].

2.1.1 Impact terrain

It was stated earlier that the crash conditions contribute towards a number of factors. The nature of the aircraft impacting a surface during crash landing also determines the degree of survivability of the occupant and structural damage. If the impacted surface is extremely tough, then the level of damage is likely to be high. On a soft surface some of the energy maybe absorbed by both the aircraft and the surface as they are likely to deform hence minimizing the damage. But more kinetic energy of the mass can be absorbed if a crushable subfloor structure is included in the aircraft.

In some previous studies it was noted that under some conditions of impact and structural deformation, the forward section of an impacting aircraft deforms changing to a scoop shape, it removes the mass of earth and carry it along to the velocity of the aircraft [5], [8]. Greer et al further noticed that the primary energy is dissipated due to soil plowing and compression. As each part of the airplane makes contact with the terrain, whether at initial impact or during subsequent motion, the kinetic energy and velocity are decreased and the decelerations are produced.

2.1.2 Impact attitude and descent angle

The impact attitude of an aircraft is the relationship of the aircraft axes with respect to the ground and determines the part of the airplane first affected by impact [5]. This means that during crash entry into the terrain, there are possibilities of the airplane to roll, yaw and pitch. If during the crash event, the pilot loses flight control on the aircraft axes, then the impact attitude is highly likely to be introduced, consequently minimizing the level of survivability. For example, Greer et al indicated that a roll attitude can influence the wing to impact first, producing side accelerations and increasing the danger of fuel spillage by crushing the wing fuel tanks or breaking the wing through the tank. On the other hand, a pitch attitude increases the likelihood of breaking the fuselage in the occupied area.

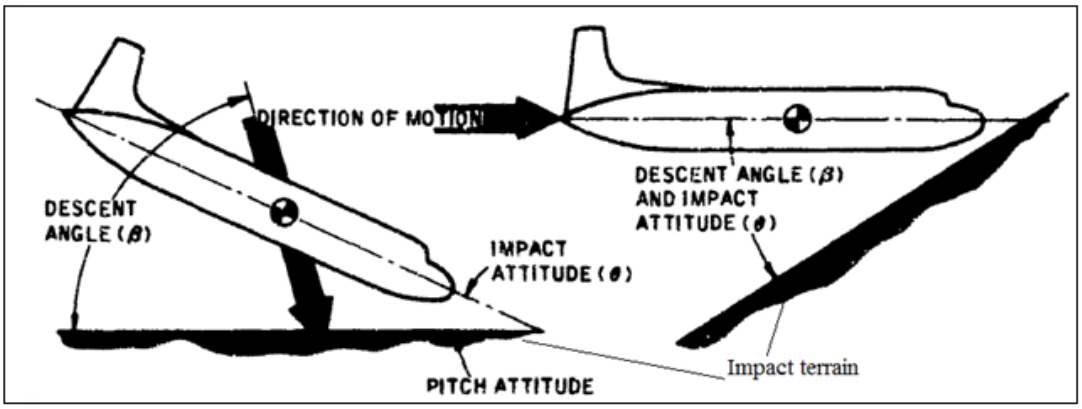

Figure 2.1 Descent angle and impact attitude. [5]

It can be seen in Figure 2.1 that the pitch attitude can be out of the descent angle which is determined by the direction of motion but at some instances they can both share the same flight path angle. This is largely influenced by the crash accident, for example, a wing structure can fail due to fatigue or crack propagation which can then lead to aerodynamic imbalance of the airplane during crash landing.

In the report prepared for the applied technology laboratory of the U.S Army, further studies were conducted focusing on the aircraft coordinate systems, acceleration, velocity, force and dynamic related terms. Some of the parameters related to aircraft crash accidents are also defined. A summary of some parameters discussed in the report is presented below: [6]

2.1.3 Aircraft coordinate system

- **Aircraft coordinates**

Positive directions for velocity, acceleration, and force components, together with pitch, roll and yaw are illustrated in Figure 2.2. When referring to an aircraft in any flight attitude, it is standard practice to use a basic set of orthogonal axes in x, y and z referring to the longitudinal, lateral, and vertical directions respectively.

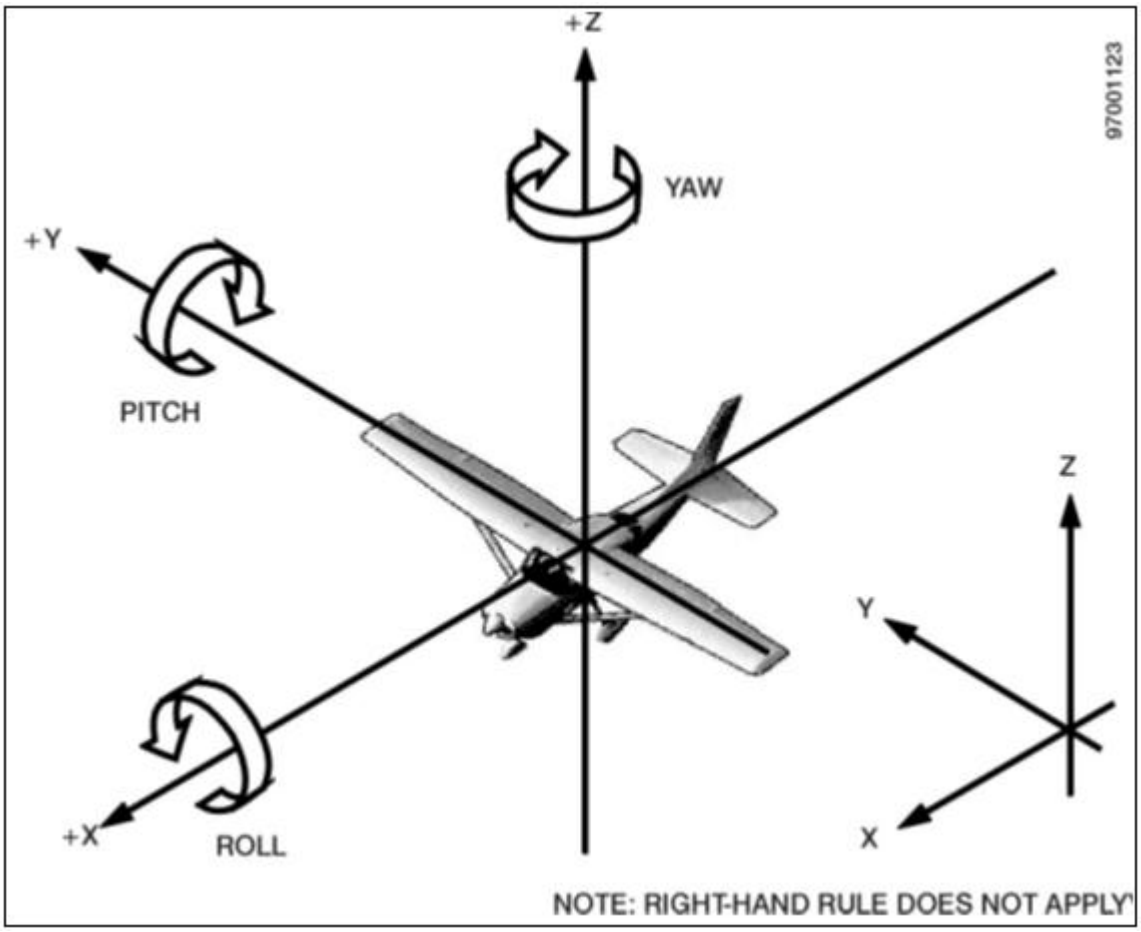

Figure 2.2 Aircraft coordinate and attitude directions. [11]

However, care must be taken when analyzing ground impact cases where structural failure occurs. The aircraft geometry changes and reaction loading at the ground takes place. In the simulation of such impacts, it is often necessary to use aircraft axis of rotation and the earth-fixed system shown in Figure 2.2.

- **Flight Path Angle**

The flight path angle is the angle between the aircraft flight path and the horizontal at the moment of impact. The algebraic sign of the flight path angle is positive if the aircraft is moving downward immediately prior to impact. The sign is negative if impact occurs while the aircraft is moving upward.

- **Terrain Angle**

The terrain angle is the angle between the impact surface and the horizontal, measured in a vertical plane. The algebraic sign of the terrain angle is positive when the direction of the flight is uphill and negative when the direction of flight is downhill.

- **Impact Angle**

The impact angle is the angle between the flight path and the terrain, measured in a vertical plane. This is also the algebraic sum of the flight path and terrain angle as shown in Figure 2.3.

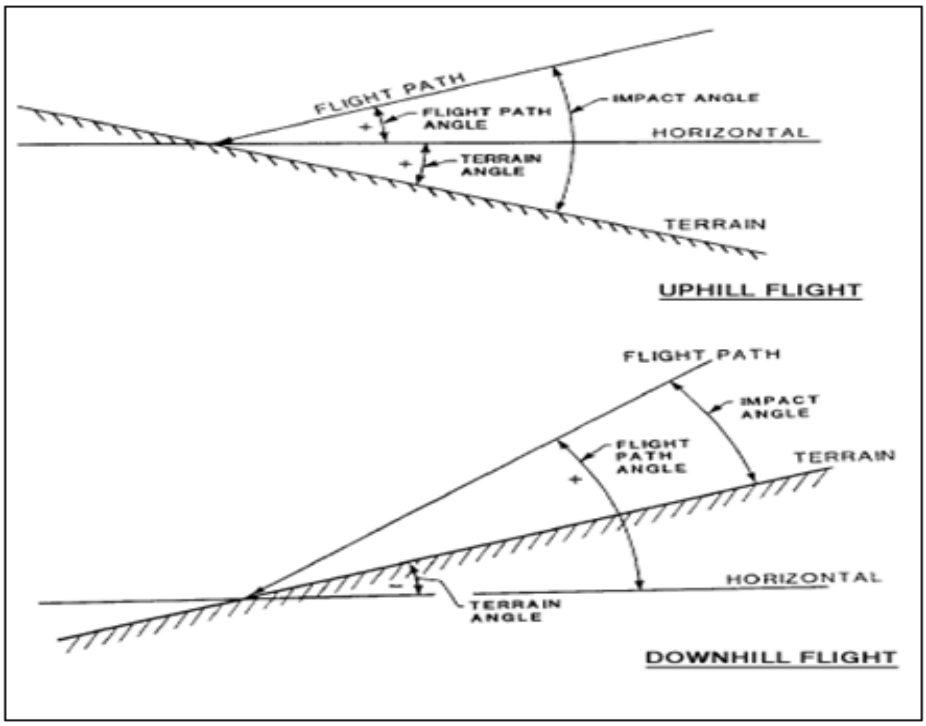

Figure 2.3 Flight path angle, terrain angle and impact angle. [11]

- **Attitude at Impact**

The attitude at impact is the aircraft attitude in degrees at the moment of initial impact. The attitude at impact is stated in degrees of pitch, yaw, and roll.

2.1.4 Acceleration and velocity related terms

- **Acceleration**

An acceleration is required to produce any velocity change, whether in magnitude or in direction. Acceleration may produce either an increase or a decrease in velocity. There are two basic types of accelerations: linear, which changes translational velocity, and angular (or rotational) which changes angular (or rotational) velocity. With respect to the crash environment, unless otherwise specified, all acceleration values are those at a point approximately at the center of the floor structure. Figure 2.4 shows a typical aircraft floor acceleration pulse during landing crash event.

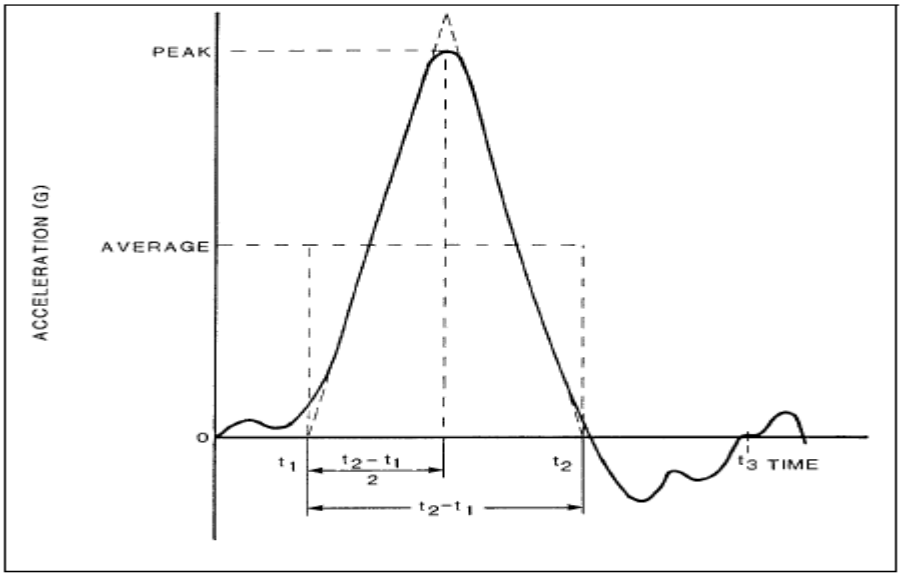

Figure 2.4 A typical aircraft floor acceleration pulse. [11]

Velocity changes

- **Longitudinal Velocity Change**

This is the decrease in velocity during the major impact; it is measured along the longitudinal (roll) axis of the aircraft. The velocity does not necessarily reach zero during the major impact.

- **Vertical Velocity Change**

This is the decrease in velocity during the major impact and it is measured along the vertical (yaw) axis of an aircraft. The vertical velocity generally reaches zero during the major impact.

- **Lateral Velocity Change**

This is the decrease in velocity during the major impact measured along the lateral (pitch) axis of the aircraft.

2.1.5 Force related terms

- **Crash Force Resultant**

This is the geometric sum of horizontal and vertical crash forces; horizontal and vertical velocity components at impact, and horizontal and vertical stopping distances. The crash force resultant is fully defined by the determination of both its magnitude and direction as illustrated in Figure 2.5. The algebraic sign of the resultant crash force angle is positive when the line of action of the resultant is above the horizontal, and negative if the line of action is below the horizontal.

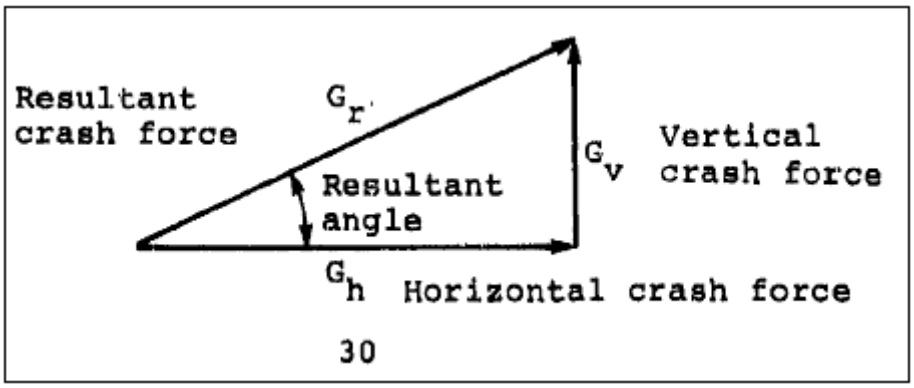

Figure 2.5 Resultant crash force, vertical crash and horizontal crash force. [6]

- **Crash Force Angle**

This is the angle between the resultant crash force and the longitudinal axis of the aircraft. For impacts with little lateral components of force, It is also the algebraic sum of the crash force resultant angle plus the aircraft pitch angle as shown in Figure 2.6.

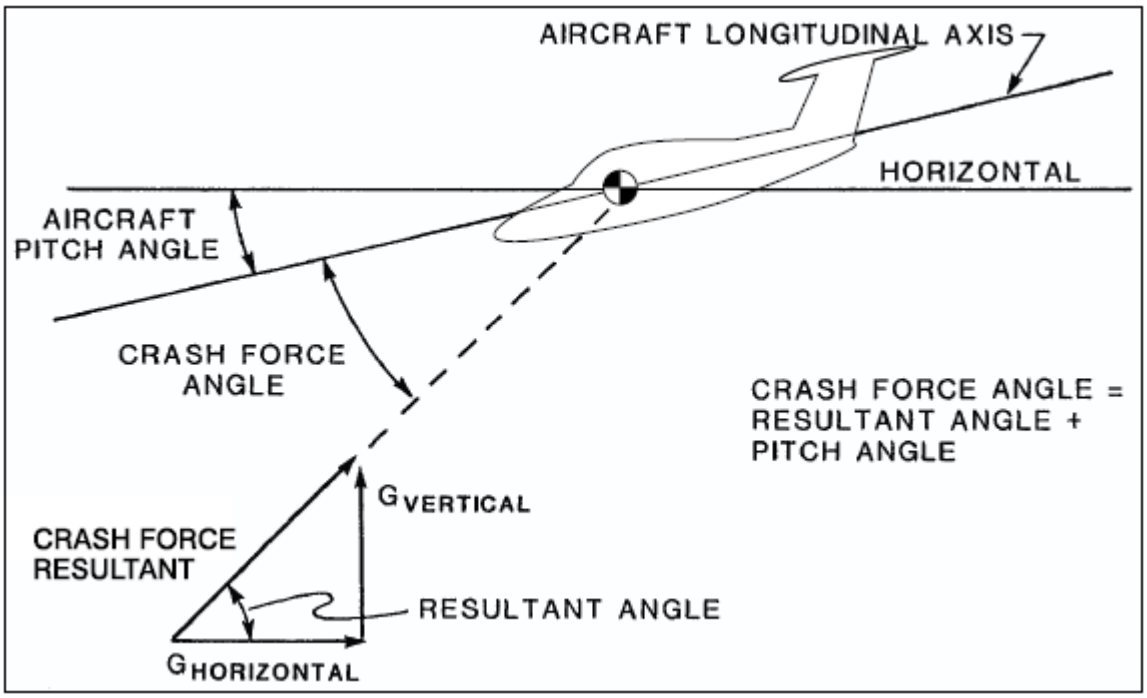

Figure 2.6 Crash force angle and related terms. [11]

2.2 Composite materials

Composites are produced by combining two or more materials to achieve a property that cannot be obtained from the individual constituents. Normally a composite material consists of matrix and the filler. In engineering design, a composite material usually refers to a material consisting of constituents within the micro and macro scale range, and even favors the macros [12]. The matrix bonds the filler together to form one bulk of a material. The filler is the material that is impregnated into the matrix to contribute its property to the composite. The desired composite material may be selected to produce a specific stiffness, strength, weight saving, corrosion resistance and many more depending on the specific engineering requirements.

Composites can be classified roughly into two categories: particulate and fibrous. A particulate composite is a mixture of a filler material of granular or pellet type particles; an example is concrete which comprises a mixture of gravel and cement. Fibrous composites are normally derived based on the filler material having a specific length to diameter ratio and may be further grouped into long and short fibre composite materials. Fibrous composites are popular in automotive and aircraft industries. Some of the applications of strong composites in the aircraft design include the fuselage, floor structure and wing structures.

2.2.1 Fibrous composites

As previously stated fibrous composites are common in automotive and aircraft industries, therefore, they were given more attention in this study. This type of composite materials are considered to consist of either continuous (long) or discontinuous (chopped or short) fibres suspended in the matrix material [13]. In many instances, the type of composite entirely depends on the nature of reinforcement. Discontinuous reinforcement is considered to produce a material that is anisotropic; this is due to the random nature of the reinforcement [14].

2.2.2 Fibre reinforcement

Fibre-reinforced composites are extremely popular and have a fast growing demand for different applications. The interest in the reinforcement is based entirely on the performance of a final composite structure. The fibre arrangement provides desired material properties more especially the specific strength of the final component. The reinforcing fibres are usually glass, carbon and aramid. The matrix is normally an epoxy, vinylester or thermosetting plastic. The fibres are mostly used in chopped or continuous form. The chopped form is a collection of short length fibres held together by a binding agent. The continuous form is a stack of fibres called rovings. In Figure 2.7 is a commercially available plain weave roving, the fibres are arranged together at 90 degrees to each other which results in biaxial properties.

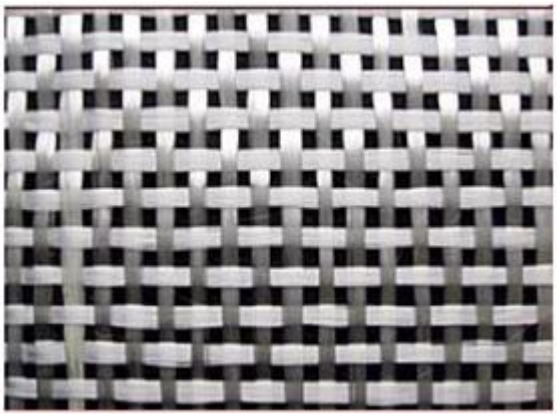

Figure 2.7 Plain weave woven roving.

2.2.3 Types of matrix

The matrix is the binder that supports and protects the fibres within the composite material. It allows for a proper load transfer and redistribution in the event of fibre breakage. Normally the matrix has a lower density, stiffness, and strength than the fibres. Matrices vary widely depending on their properties and can display brittle, elastic, or plastic properties. They can exhibit linear or nonlinear stress-strain behavior. It is important to ensure that the matrix is capable of being fed around the reinforcement at some manufacturing stage of the composite. On the other hand, the fibre must allow for adhesion of the matrix.

2.2.4 Stiffness and Strength of composites

Composites have their respective properties like other homogeneous materials even though they are obtained from a combination of different constituents as discussed earlier. The properties of composite materials depend most on the fibre orientations. A good design of a composite structure is such that the load is always carried by the fibres as the matrix holds the fibres together. A typical example of a unidirectional composite specimen is shown in Figure 2.8, the specimen will carry its maximum load capacity along the x-axis but if the specimen is loaded along the y-axis, its weakness is revealed since the matrix will be the only constituent carrying the load. In addition, the matrix strength is extremely low compared to that of the fibres.

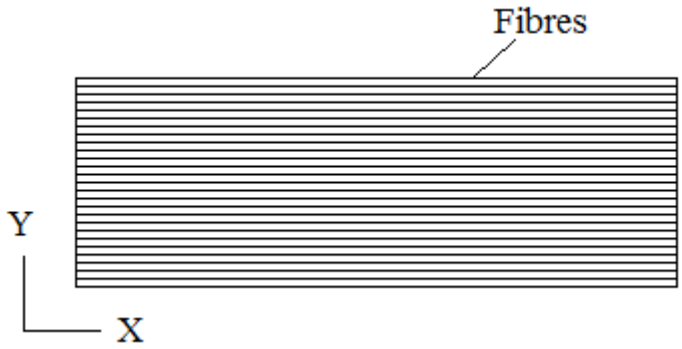

Figure 2.8 Unidirectional composite fibre specimens.

2.2.5 Stress/strain relations in composites

As discussed previously, in composites, the properties of a laminate are primarily dependent on the fibres not the matrix. But the stresses and strains in a laminate are related, this can be clearly understood by considering a single lamina of unidirectional fibre orientation in Figure 2.9 below.

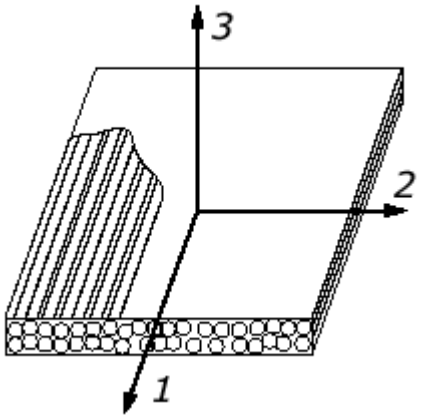

Figure 2.9 Principal material axes of unidirectional lamina.

Therefore, the stress-strain relations on the principal axes may be formulated by the compliance matrix [$\boldsymbol{S}$] such that

$$[\varepsilon] = [\boldsymbol{S}][\sigma] \tag{2.1}$$

$$\begin{Bmatrix} \varepsilon_1 \\ \varepsilon_2 \\ \gamma_{12} \end{Bmatrix} = \begin{bmatrix} \frac{1}{E_1} & -\frac{v_{12}}{E_1} & 0 \\ -\frac{v_{21}}{E_2} & \frac{1}{E_2} & 0 \\ 0 & 0 & \frac{1}{G_{12}} \end{bmatrix} \begin{Bmatrix} \sigma_1 \\ \sigma_2 \\ \sigma_{12} \end{Bmatrix} \tag{2.2}$$

Or by the stiffness matrix [$\boldsymbol{C}$] such that

$$[\sigma] = [\boldsymbol{C}][\varepsilon] \tag{2.3}$$

$$\begin{Bmatrix} \sigma_1 \\ \sigma_2 \\ \sigma_{12} \end{Bmatrix} = \begin{bmatrix} \frac{E_1}{1-v_{12}v_{21}} & \frac{v_{12}E_2}{1-v_{12}v_{21}} & 0 \\ \frac{v_{21}E_1}{1-v_{12}v_{21}} & \frac{E_2}{1-v_{12}v_{21}} & 0 \\ 0 & 0 & G_{12} \end{bmatrix} \begin{Bmatrix} \varepsilon_1 \\ \varepsilon_2 \\ \varepsilon_{12} \end{Bmatrix} \tag{2.4}$$

for both the compliance and stiffness matrices are symmetric, that is

$$\frac{v_{12}}{E_1} = \frac{v_{21}}{E_2} \tag{2.5}$$

And only four of the material constants $E_1 E_2 G_{12} v_{12}$ and v_{21} are independent properties. In addition, it must be noted that $\boldsymbol{C}_{12}$ is equal to $\boldsymbol{C}_{21}$ and also $\boldsymbol{S} = \boldsymbol{C}^{-1}$.

2.2.6 Composite with the off-axis fibre orientation

In many instances laminates are constructed by stacking a number of fabric layers, normally unidirectional and positioned in various orientations. In Figure 2.10, the principal axes of the lamina are orientated by an angle θ relative to the x-y axes.

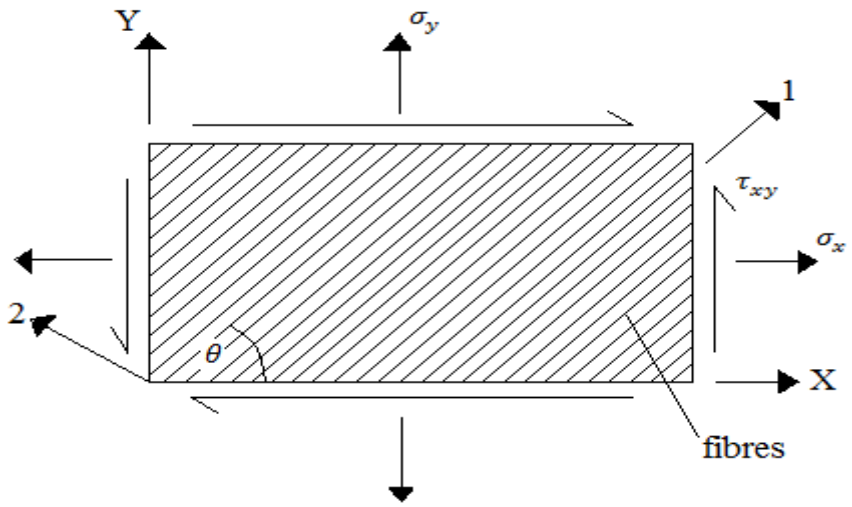

Figure 2.10 Unidirectional lamina with principal axes rotated by relative angle θ to the x-y axes.

The condition illustrated above can be seen to correspond to the analysis of principal stress for isotropic materials. Therefore, the stress/strain relationship can be written as:

$$\sigma_{12} = T\sigma_{xy} \tag{2.6}$$

and

$$\bar{\varepsilon}_{12} = T\bar{\varepsilon}_{xy} \tag{2.7}$$

where

$$\sigma_{12} = \{\sigma_1 \quad \sigma_2 \quad \tau_{12}\} \tag{2.8}$$

$$\sigma_{xy} = \{\sigma_x \quad \sigma_y \quad \tau_{xy}\} \tag{2.9}$$

$$\bar{\varepsilon}_{12} = \left\{\varepsilon_1 \quad \varepsilon_2 \quad \frac{1}{2}\gamma_{12}\right\} \tag{2.10}$$

$$\bar{\varepsilon}_{xy} = \left\{ \varepsilon_x \quad \varepsilon_y \quad \frac{1}{2}\gamma_{xy} \right\} \tag{2.11}$$

And the transformation matrix, T is given by

$$T = \begin{bmatrix} m^2 & n^2 & 2mn \\ n^2 & m^2 & -2mn \\ -mn & mn & (m^2 - n^2) \end{bmatrix} \tag{2.12}$$

where m = $\cos\theta$ and n = $\sin\theta$.

The strain for a set of known stresses (or vice versa) can be obtained when the elastic properties are known. If the properties are known for the 1-2 axes they need to be referred to as the x-y axes, this is done with the some mathematical manipulation which leads to:

$$\sigma_{xy} = \bar{Q}\varepsilon_{xy} \tag{2.13}$$

The transformed stiffness matrix is $\bar{Q}$, the elements of which are

$$\bar{Q}_{11} = Q_{11}m^4 + 2(Q_{12} + 2Q_{33})n^2m^2 + Q_{22}n^4 \tag{2.14}$$

$$\bar{Q}_{22} = Q_{11}n^4 + 2(Q_{12} + 2Q_{33})n^2m^2 + Q_{22}m^4$$

$$\bar{Q}_{12} = (Q_{11} + Q_{22} - 4Q_{33})n^2m^2 + Q_{12}(m^4 + n^4)$$

$$\bar{Q}_{33} = (Q_{11} + Q_{22} - 2Q_{12} - 2Q_{33})n^2m^2 + Q_{33}(m^4 + n^4)$$

$$\bar{Q}_{13} = (Q_{11} - Q_{12} - 2Q_{33})nm^3 + (Q_{12} - Q_{22} + 2Q_{33})n^3m$$

$$\bar{Q}_{23} = (Q_{11} - Q_{12} - 2Q_{33})n^3m + (Q_{12} - Q_{22} + 2Q_{33})nm^3$$

It can be seen that if the fibre orientation θ and the unidirectional properties Q in the principal directions are known, the stiffness of the rotated lamina can be calculated. To obtain the strains, the equation can be inverted to give

$$\varepsilon_{xy} = \bar{Q}^{-1}\sigma_{xy} \tag{2.15}$$

or

$$\varepsilon_{xy} = \bar{S}^{-1}\sigma_{xy} \tag{2.16}$$

where $\bar{S}$ is the transformed compliance matrix, the elements of which can be found by using the similar process to that used for obtaining the elements of $\overline{Q}$ i.e.

$$\bar{S}_{11} = S_{11}m^4 + (2S_{12} + Q_{33})n^2m^2 + S_{22}n^4 \quad (2.17)$$

$$\bar{S}_{22} = S_{11}n^4 + (2S_{12} + S_{33})n^2m^2 + S_{22}m^4$$

$$\bar{S}_{12} = (S_{11} + S_{22} - S_{33})n^2m^2 + S_{12}(m^4 + n^4)$$

$$\bar{S}_{33} = 2(2S_{11} + 2S_{22} - 4S_{12} - S_{33})n^2m^2 + S_{33}(m^4 + n^4)$$

$$\bar{S}_{13} = (2S_{11} - 2S_{12} - S_{33})nm^3 + (2S_{12} - 2S_{22} + S_{33})n^3m$$

$$\bar{S}_{23} = (2S_{11} - 2S_{12} - S_{33})n^3m + (2S_{12} - 2S_{22} + S_{33})nm^3$$

2.2.7 Stiffness of composites

A composite laminate consists of a number of laminae/plies each with independent fibre orientations and ply thicknesses to achieve a preferred material stiffness and strength properties. The significance of the stacking sequence is to acquire the desired material stiffness and strength of the laminate. The definition of the plies in the laminate is shown in Figure 2.11.

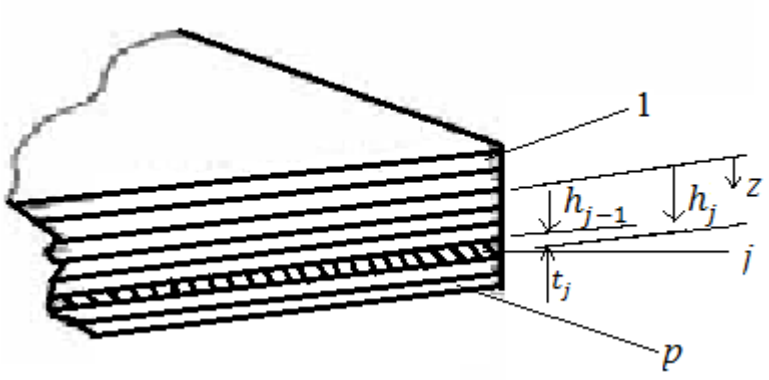

Figure 2.11 Definition of plies within a laminate. [14]

A composite laminate is normally subjected to in-plane and bending loading, which means each of the layers will be susceptible to stretching and bending. Figure 2.12 shows both these effects and they have to be taken into consideration.

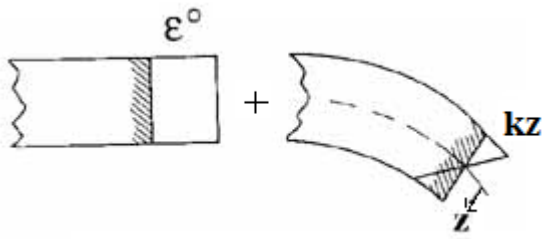

Figure 2.12 The in-plane and bending components of the laminate strain. [14]

The relationship between the lamina in-plane and bending strain is written as

$$\varepsilon_{xy} = \varepsilon^{\circ} + zk \tag{2.18}$$

or

$$\begin{bmatrix} \varepsilon_x \\ \varepsilon_y \\ \varepsilon_{xy} \end{bmatrix} = \begin{bmatrix} \varepsilon_x^{\circ} \\ \varepsilon_y^{\circ} \\ \varepsilon_{xy}^{\circ} \end{bmatrix} + z \begin{bmatrix} k_x \\ k_y \\ k_{xy} \end{bmatrix} \tag{2.19}$$

Since the plies are bonded together from the manufacturing process, it can be assumed that the in-plane strains and curvatures are the same on all layers.

Hence Hooke's law for the layer *j* is given by

$$\sigma_{xyj} = \bar{Q}_j \varepsilon^{\circ} + z\bar{Q}_j k \tag{2.20}$$

where $\bar{Q}_j$ is the transformed stiffness matrix for the j^{th} layer.

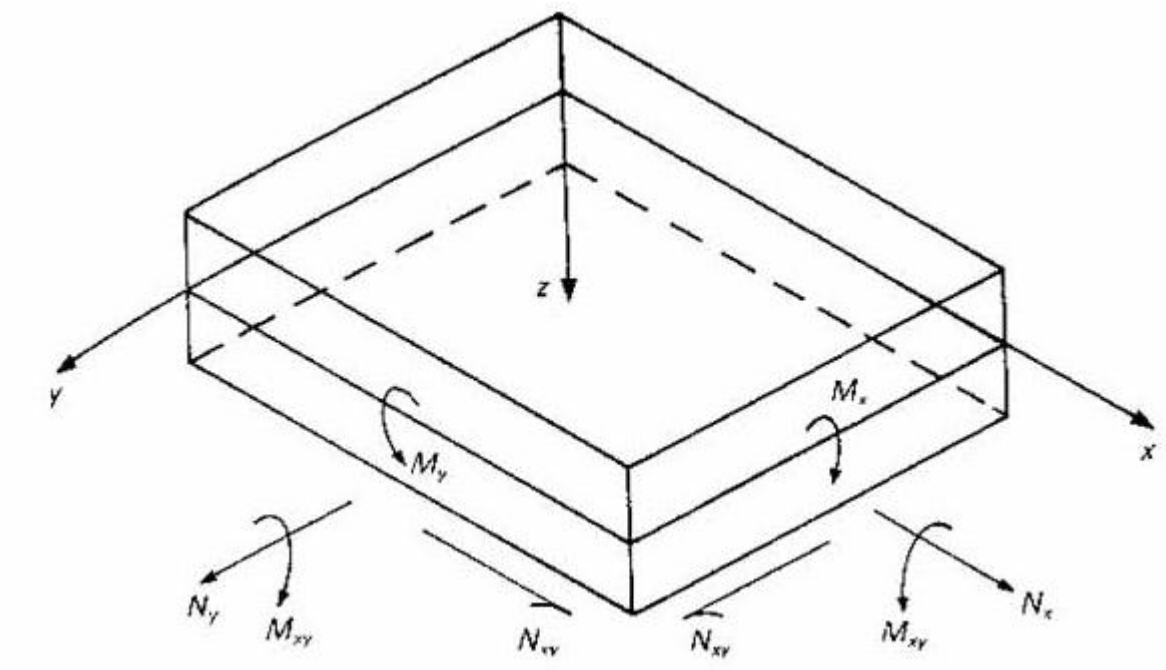

Figure 2.13 Equivalent loads acting on a laminate. [14]

It is seen in Figure 2.13 that the entire equivalent stresses act in the plane of the laminate and moments about the mid-plane. The stresses can be converted into equivalent forces, therefore $\sigma_x$from the load $N_{xj} = \sigma_{xj} t_j$ (where t_j is the thickness of the layer *j*). Similarly, the equivalent moments can be obtained on any layer, so once more from σ_x we get $M_{xj} = \sigma_{xj} t_j z_j$, (where z_j is the distance from the laminate mid-plane to the mid-thickness of a particular layer). If all the equivalent load components are added they will be equal to the external value, this applies to both the forces and the moments.

Relationship between the stress resultants, the strains and curvatures is given by;

$$N = A\varepsilon^{\circ} + Bk \tag{2.21}$$

and

$$M = B\varepsilon^{\circ} + Dk \tag{2.22}$$

Equations (2.19) and (2.20) are known as the 'plate constitutive equations' and are fundamental equations of the laminate theory.

The above equations can be assembled into matrix form giving;

$$\begin{bmatrix} N \\ M \end{bmatrix} = \begin{bmatrix} A & B \\ B & D \end{bmatrix} \begin{bmatrix} \varepsilon^{\circ} \\ k \end{bmatrix} \tag{2.23}$$

The elements of A, B and D matrices are given by

$$A_{rs} = \sum_{j=1}^{p} \bar{Q}_{rsj} \left[h_j - h_{j-1} \right] \tag{2.24}$$

$$B_{rs} = \sum_{j=1}^{p} \bar{Q}_{rsj} \left[h_j^2 + h_{j-1}^2 \right] \tag{2.25}$$

$$D_{rs} = \sum_{j=1}^{p} \bar{Q}_{rsj} \left[h_j^3 + h_{j-1}^3 \right] \tag{2.26}$$

where r, s = 1, 3. Matrix A represents the in-plane direct stiffness, B represents the bending stretching coupling and C represents the bending stiffness. [16]

2.3 Properties of composite materials

2.3.1 Rules of mixtures

A rule of mixtures is a method of approach to estimate composite material properties. It is normally based on an assumption that a composite property is the volume weighed average of the individual constituent's contribution to the total material by volume. The criteria used are the fibre volume fraction to estimate the properties of the entire composite. The summation of the fibre volume fraction V_f and a matrix volume fraction V_m must always be one, that is

$$V_f + V_m = 1 \tag{2.27}$$

where m and f refer to matrix and fibre,

According to the rule of mixtures, a particular property d_c may be estimated from the constituent properties, d_f and d_m of the fibres and the matrix respectively as

$$d_c = V_m\, d_m + V_f\, d_f \tag{2.28}$$

For example the rule of mixture is used to predict the Poisson's ratio of the composite as follows

$$\nu = \nu_m d_m + d_f \nu_f \tag{2.29}$$

where: ν_m = Poisson's ratio of the matrix material.

ν_f = Poisson's ratio of the fibre material.

As stated earlier that the resulting properties of a composite material are a combination of the constituents, it is important to identify the properties of the individual material before attempting to build a composite. Reinforcing fibres usually have a diameter of 5-10μm, but they may approximately reach 100μm, and a modulus and strength of order 70-800GPa and 1000-7000MPa, respectively. The

failure strains are estimated at 0.27-5% [31], but carbon and aramid may exhibit an increasing modulus with increasing strain due to changes in their internal structure during stressing. The resins have a modulus and strength of the order of 2-5GPa and 50-100GPa respectively. It also has a failure strain of approximately 1% [15]. Some typical fibre and resin properties are summarized in Table 1 below.

Material	**Density (Mgm^{-3})**	**Tensile modulus (GPa)**	**Tensile strength (MPa)**	**Strain to failure (%)**
Glass fibre	2.49-2.55	73-86	3400-4500	3.5-5.4
Carbon fibre	1.7-2.0	160-827	1400-7070	0.27-1.9
Aramid fibre	1.33-1.45	73-160	2400-3400	1.4-4.6
Inorganic fibre	2.0-3.97	152-462	1720-3900	
Phenolic resin	1.0-1.35	3.0-4.0	60-80	~1.8
Polyester resin	1.1-1.23	3.1-4.6	50-75	1.0-6.5
Epoxy resin	1.2	2.6-3.8	60-85	1.5-8.0
Bismaleimaide resin	1.2-1.32	3.2-5.0	48-110	1.5-3.3

Table 1 Typical fibre and resin properties. [15]

The static properties of composite materials maybe affected by the strain rate effect during impact crush behavior. The modulus and the strength normally increase over the static values exhibiting high stress/strain non-linearity. The high strain rate properties were not available for this study, therefore, their effect were not included.

2.3.2 Failure theories in fibrous composites

In general, fibrous composite materials fail in different modes depending on their loading state and the mechanical properties of the material. Therefore, this makes failure criteria for composites more complex than the yield criteria for metals. A failure criterion compares the loading state at a point of stress or strain with a set of values reflecting the strength of material at that point. The loading and strength value should be reflected in the same material co-ordinate system. For instance, for unidirectional composite material, this is normally in the direction of the fibres, but for a material of different fibre direction, the direction is not obvious. The theories which reflect detailed mechanisms of failure are still being developed, but the empirical data derived from experiment have been used for decades. Furthermore, the study on the application of finite element analysis on damage modeling approach with computational tools continues as a means of reducing the expense of experimental work [16], [17], [18].

The following is a list some failure criteria associated with fibrous composites:

Tsai-Hill

$$\frac{\sigma_{11}^2}{X^2} - \frac{\sigma_{11}\sigma_{22}}{X^2} + \frac{\sigma_{22}^2}{Y^2} + \frac{\sigma_{12}^2}{S^2} \geq 1 \qquad (2.30)$$

where X = Value of σ_{11} at the longitudinal tensile or compressive failure

Y = Value of σ_{22} at the transverse tensile or compressive failure

S = Value of σ_{12} at the longitudinal shear failure

Tsai-Wu

$$F_1\sigma_{11} + F_2\sigma_{22} + F_{11}\sigma_{11}^2 + F_{22}\sigma_{22}^2 + 2F_{12}\sigma_{11}\sigma_{22} + F_{66}\sigma_{12}^2 \geq 1 \qquad (2.31)$$

$$F_1 = \frac{1}{X_T} - \frac{1}{X_C}\ ;\ F_2 = \frac{1}{Y_T} - \frac{1}{Y_C}$$

$$F_{11} = \frac{1}{X_T X_C}\ ;\ F_{22} = \frac{1}{Y_T Y_C}\ ;\ F_{66} = \frac{1}{S^2}\ ;\ F_{12} \text{ by biaxial test.}$$

where X = Value of σ_{11} at the longitudinal tensile or compressive failure

Y = Value of σ_{22} at the transverse tensile or compressive failure

S = Value of σ_{12} at the longitudinal shear failure

Modified Tsai-Wu

Matrix failure $F_2\sigma_{22} + F_{22}\sigma_{22}^2 + F_{66}\sigma_{12}^2 \geq 1$ (2.32)

Maximum stress

The maximum stress criterion has five sub-criteria or limits corresponding to the strength of the five fundamental failure modes. If any of these limits are exceeded by the corresponding stress expressed in the principal material axes, then the material has reached failure,

Fibre tension $\sigma_{11} \geq X_T\ (\sigma_{11} > 0)$ (2.33)

Fibre compression $|\sigma_{11}| \geq X_C\ (\sigma_{11} < 0)$ (2.34)

Matrix tension $\sigma_{22} \geq Y_T\ (\sigma_{22} > 0)$ (2.35)

Matrix compression $|\sigma_{22}| \geq Y_C \ (\sigma_{22} < 0)$ (2.36)

Matrix shear $|\sigma_{12}| \geq S$ (2.37)

where X = Value of σ_{11} at the longitudinal tensile or compressive failure

Y = Value of σ_{22} at the transverse tensile or compressive failure

S = Value of σ_{12} at the longitudinal shear failure

Hashin

The Hashin criterion is used to evaluate failure in an individual composite ply; it identifies four different modes of failure for composite ply,

Fibre tension $\left(\frac{\sigma_{11}}{X_T}\right)^2 + \left(\frac{\sigma_{12}}{S}\right)^2 \geq 1 \ (\sigma_{11} > 0)$ (2.38)

Fibre compression $|\sigma_{11}| \geq X_C \ (\sigma_{11} < 0)$ (2.39)

Matrix tension $\left(\frac{\sigma_{22}}{Y_T}\right)^2 + \left(\frac{\sigma_{12}}{S}\right)^2 \geq 1 \ (\sigma_{22} > 0)$ (2.40)

Matrix compression $\left(\frac{\sigma_{22}}{2S_T}\right)^2 + \left[\left(\frac{Y_C}{2S_T}\right)^2 - 1\right]\frac{\sigma_{22}}{Y_C} + \left(\frac{\sigma_{12}}{S}\right)^2 \geq 1$ (2.41)

$(\sigma_{11} > 0)$

where X = Value of σ_{11} at the longitudinal tensile or compressive failure

Y = Value of σ_{22} at the transverse tensile or compressive failure

S = Value of σ_{12} at the longitudinal shear failure

S_T = Value of σ_{23} at the transverse shear failure

Chang-Chang

The Chang and Chang criteria is used to evaluate the failure in the matrix, fibre breakage and the fibre-matrix shearing,

Fibre breakage $$\left(\frac{\sigma_{11}}{X_T}\right)^2 + \mathrm{T} \geq 1 \ (\sigma_{11} > 0) \quad (2.42)$$

Matrix cracking $$\left(\frac{\sigma_{22}}{Y_T}\right)^2 + \mathrm{T} \geq 1 \ (\sigma_{22} > 0) \quad (2.43)$$

Matrix compression $$\left(\frac{\sigma_{22}}{2S_T}\right)^2 + \left[\left(\frac{Y_C}{2S}\right)^2 - 1\right]\frac{\sigma_{22}}{Y_C} + \mathrm{T} \geq 1 \quad (2.44)$$

$$(\sigma_{22} > 0)$$

$$\mathrm{T} = \left(\frac{\sigma_{12}}{S}\right)^2 \frac{1+\frac{3}{2}\alpha G_{12}\sigma_{12}^2}{1+\frac{3}{2}\alpha G_{12}S^2} \quad (2.45)$$

where X = Value of σ_{11} at the longitudinal tensile or compressive failure

Y = Value of σ_{22} at the transverse tensile or compressive failure

S = Value of the shear strength

S_T = Value of σ_{23} at the transverse shear failure

2.4 Basic Classical laminate theory of multilayered shells in MSC.Dytran

Since a composite laminate or lamina is made up by stacking a number of fabric plies together to achieve a specific thickness, the response of a composite laminate under loadings is different from that of an isotropic material. An effective and special means of predicting the behavior of the composite plate is adopted in MSC.Dytran. The shell structures are analyzed based on the classical lamination theory. A structure is assumed to behave like a shell when the thickness is small compared to the other two characteristic lengths [19].

The following assumptions are fundamental to lamination theory [13]:

1). The laminate consists of perfectly bonded layers (laminae).

2). Each layer is a homogenous material with known effective properties.

3). Individual layer properties can be isotropic, orthotropic, or transversely isotropic.

4). Each layer is in a state of plane stress.

5). The laminate deforms according to the following Kirchhoff assumptions for bending and stretching of thin plates i.e,

a) Normals to the midplane remain straight and normal to the deformed mid-plane after deformation.
b) Normals to the midplane do not change length.

2.5 Modeling Using MSC.Patran/Dytran.

Since technology advancement has led to the use of computer software for non-linear analysis, hence an important aspect of crashworthiness research is the demonstration and validation of analytical computational tools for accurate simulation of the airframe structural response to crash impacts [20]. Therefore, an approach used in this study was based on numerical analysis using MSC.Patran for pre-and post-processing and MSC.Dytran for solving of the numerical model.

The solver MSC.Dytran is a three dimensional analysis code used for analyzing dynamic, non-linear behavior of solid components, structures and fluids explicit solver. It uses explicit time integration and incorporates features that simulate a wide range of material and geometric non-linearity [21]. In explicit methods, if the current time step is step n, an estimate of the acceleration at the end of step n+1 will satisfy the following equation of motion:

$$Ma_n + Cv_n + Kd_n = F_n^{ext} \quad (2.28)$$

This can be rewritten as

$$Ma_n = F_n^{ext} - F_n^{int} \quad (2.29)$$

$$a_n = M^{-1} F_n^{residual} \quad (2.30)$$

where

F_n^{ext} = vector of externally applied loads (2.31)

F_n^{int} = vector of internal loads (e.g. forces generated by the elements and hourglass forces) (2.32)

$$F_n^{int} = Cv_n + Kd_n \quad (2.33)$$

M = mass matrix (2.34)

The acceleration can be found by inverting the mass matrix and multiplying it by the residual load factor. If *M* is diagonal, its inversion is trivial, and the matrix equation is the set of independent equations for each degree of freedom as follows:

$$a_{ni} = F_{ni}^{residual}/M_i \tag{2.35}$$

The central difference scheme is used to advance in time:

$$v_{n+1/2} = v_{n-1/2} + a_n(\Delta t_{n+1/2} + \Delta t_{n-1/2}) / 2 \tag{2.36}$$

$$d_{n+1/2} = d_n + v_{n+1/2}\Delta t_{n+1/2} \tag{2.37}$$

This assumes that the acceleration is constant over the time step. In explicit methods, the loop is carried out for each time step as shown in the diagram in Figure 2.14.

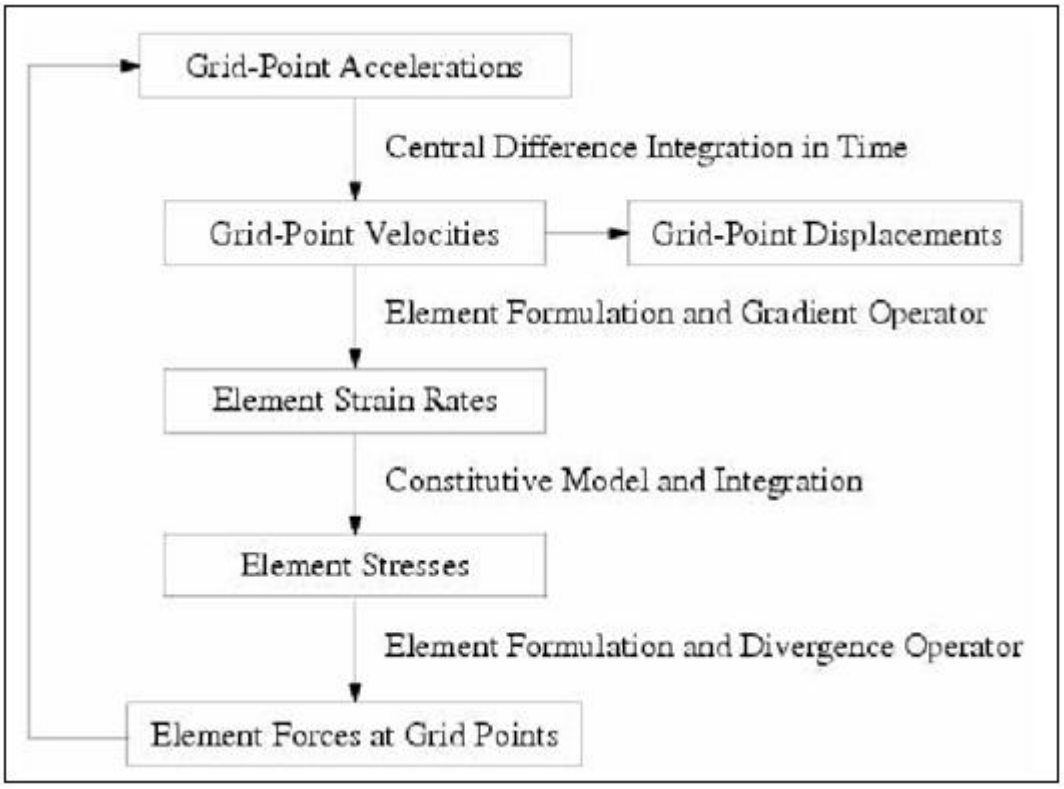

Figure 2.14 Time step loop of the explicit method. [21]

The explicit codes can remain stable by sub-dividing the shortest natural period in the mesh by the time step. This means that the time step must be less than the time taken for a stress wave to cross the smallest element in the mesh.

It is fact that, during aircraft emergency crash landings, the bottom fuselage undergoes large deformations and high degree of non-linearity. Therefore, the MSC.Dytran code with an explicit solver method was an appropriate tool for crash analysis.

2.6 Theory of contact

The aircraft impact crash analysis involves two bodies touching each other at one or more points. Therefore, the stress histories in the contact area can be predicted by accounting for the local deformations in the contact region. To predict the contact force history and the overall deformation of the impacted body, a detailed model of the contact region is not necessary. A simple relationship between the contact force and the indentation, called contact law, has been used by Timoshenko to study the impact of a beam by a steel sphere. This approach has been used extensively since then and is commonly used for the impact of composite materials and is therefore considered in this study [22].

Since MSC.Dytran uses a finite element method in solving the problems of the body under analysis, it basically contains two solvers, Lagrangian and Eulerian. In the Langrangian solver, the grid points are fixed to locations on the body under analysis. Elements of the material are created by connecting the grid points together and the collection of elements produce a mesh. Therefore, as the body deforms, the grid points move in space and the elements distort. The Lagrangian solver is therefore calculating the motion of elements of constant mass.

In the Eulerian solver, the grid points are fixed in space and the elements are simply partitions of the space defined by connected grid points. The Eulerian mesh is then a fixed frame of reference. The material of the body under analysis moves through the Eulerian mesh and the mass, momentum, and energy of material is transported between elements.

It is clear that in both solvers, the grid points form the fundamental definition of the geometry of the model to be analyzed. Furthermore, MSC.Dytran uses different types of Lagrangian elements: solid elements (CHEXA, CPENTA, and CTETRA), shell elements (CQUAD4 or CTRIA3), membrane elements (CTRIA3) beam elements (CBAR, CROD and CBEAM) and spring elements (CSPR, CVISC, CELAS and CDAMP). Most of the elements have large strain deformation and can be used to model non-linear effects.

2.7 Validation of Computational Tools

There are many different commercially available software packages that are being used in computer aided engineering techniques of predicting structural behavior under various loadings. Therefore, it is of great importance to verify the capabilities of the tool for specific application, more especially its performance accuracy in dynamic analysis. A few years back most of the tools were inadequate, since they were developed for metal structures and failed to predict the response of composite structures [23]. In order to validate a tool, experimental and numerical works are compared. This means that a model is tested and outcome is captured. After performing the experimental work, numerical simulations of the same model are performed and the results of the two investigations are compared. In most cases it was found out that in modern non-linear solvers, the finite element simulations closely correlate with the overall response of the experimental results and differences are within reasonable range [20], [24], [25], [23], [26], [27], [28], and [29]. The graphs in Figure 2.15 show some of the predicted and experimental acceleration

responses for locations on the upper and lower fuselage sidewalls obtained after performing a vertical drop test of a Boeing 737 fuselage section conducted in November 2000 at the FAA Technical Center in Atlanta [2]. A good correlation of acceptable range can be seen between the MSC.Dytran numerical and experimental plots.

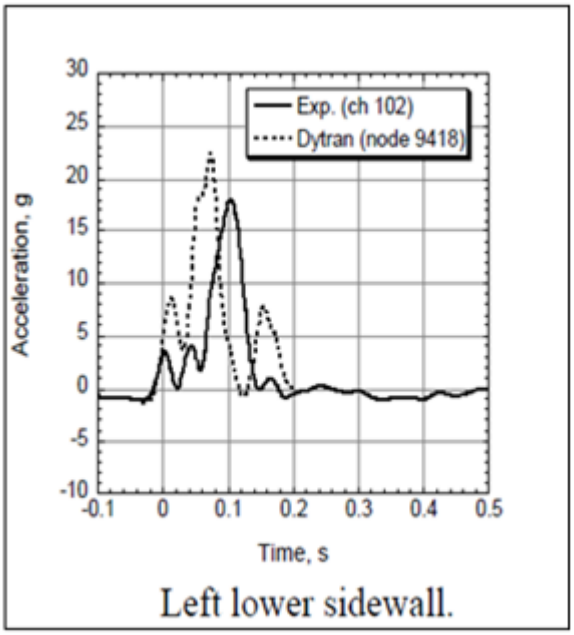

Figure 2.15 Graphs of numerical and experimental plots of the left lower sidewall acceleration responses of a vertical drop test of B737 fuselage section. [2]

Figures 2.16 and 2.17 show that the numerical model deformation executed in MSC.Dytran closely matches the experiments up to reasonable crash simulation time. The predicted damage, deformation and failure of the components of the aircraft affected by the crash impact can be identified from the output results of the finite element code being used [3].

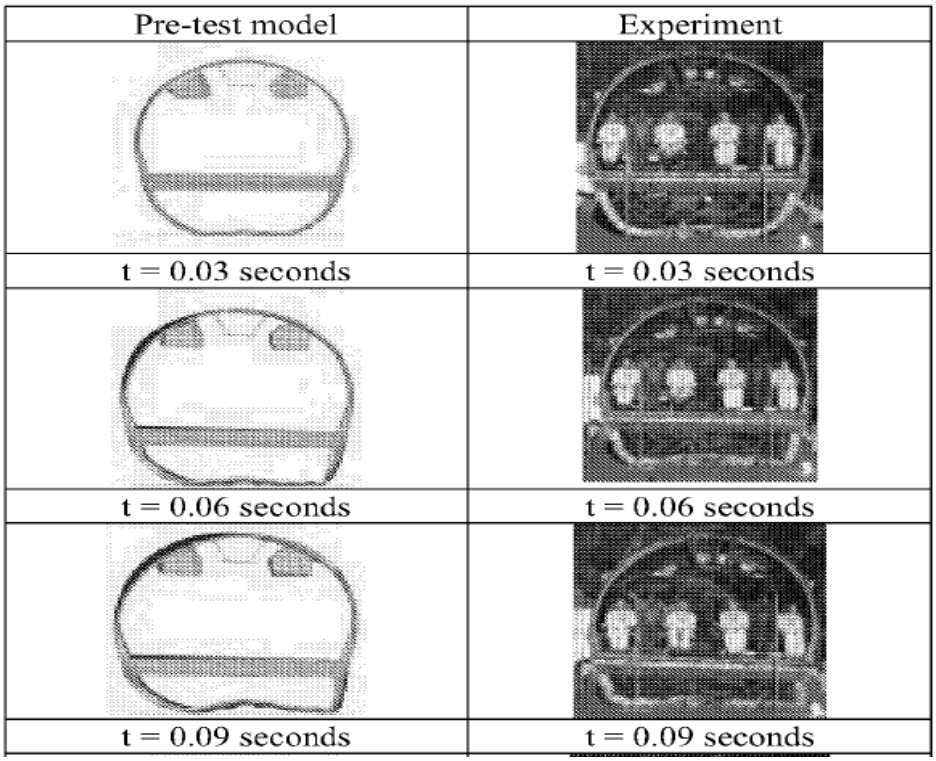

Figure 2.16 Comparison of predicted deformation of MSC.Dytran with experiments from a high speed camera. [3]

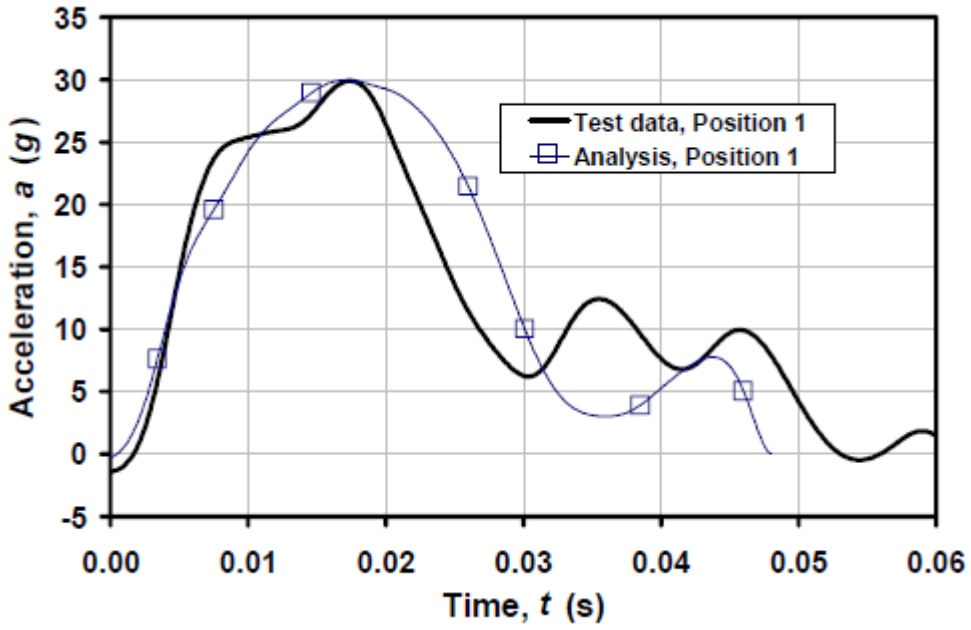

Figure 2.17 Experimental and Dytran analysis comparison of fuselage drop test. [30]

CHAPTER 3

RESEARCH METHODOLOGY

3.1 Failure criteria associated with a lamina

Failure criteria comprise an important piece of information when examining the strength of the materials to be considered for structural application. This works for both isotropic materials and orthotropic materials. But in this study more focus is on failure or strength of a lamina which is predicted by the application failure criteria. Once an appropriate failure criterion is identified, it is possible to closely predict a point in time related to material fracture or failure to carry a specific load. In most instances failure theories are very important when dealing with composite materials. They provide a reliable means of identifying weak and strong directions of the lamina and also allow the designer to set proper margins of safety.

3.1.1 Fibre-composite material with failure criteria in MSC.Dytran.

The MSC.Dytran user guide manual shows that this tool is capable of predicting the failure of a fibre composite material and is discussed in this section. The orthotropic material model is used in shell elements to build a multi-layered composite element. The material describes the elastic behavior of brittle material with failure based on the interactive stress criteria of failure per mode.

For the prediction of failure, MSC.Dytran software has a variety of models available. The first class of models contains the interactive models that predict the onset of failure, but not the failure mode. This class contains the Tsai-Hill, and Tsai-Wu failure theories. The second class not only predicts the onset of failure, but provides the fibre compression (fibre buckling), matrix-tension (matrix cracking), matrix

compression, or in-plane shear failure. Theories that fall in the latter class are the Chang-Chang, Maximum stress, Modified Tsai-Wu and Hashin failure theory.

When the failure criterion is satisfied, the next stage is to define how the remaining failure modes are affected by the failed mode. A standard model is available, which is an average of the various theories provided in the literature. However, the property degradation rules are not fixed and can be easily redefined by the user. These rules describe how the stress and strain increments are related in various directions after failure in a particular failure mode has occurred.

3.1.2 Evaluation of fibre-composite material with failure criteria in MSC.Dytran.

After a review of the theories discussed in the previous section, it was noted that the software failed to predict failure when certain failure criteria were assigned. Therefore, in this section, it was necessary to conduct an investigation on the actual capabilities of the tool on each of the failure models. The main objective is to investigate failure criteria of fibrous composite materials in the MSC.Dytran code.

Problem description

A composite halved strip is clamped at its left edge and the portions of the right edge are subjected to different impulsive initial velocities.

Model parameters

Length = 0.127m

Width = 0.0305m

Number of elements = 90

Number of layers = 8

Thickness of each layer = 0.229 mm and fibre orientation of 0° along the global x-axis of the strip.

Total thickness of the strip = 0.183 mm

Density	1540Kg/m^3
Tensile modulus 1-direction	118e9Pa
Tensile modulus 2-direction	8.2e9Pa
Failure stress	83.6e6Pa
Shear modulus 1, 2-directions	4.07e9Pa
Shear modulus 1, 3-directions	4.07e9Pa
Shear modulus 2, 3-directions	4.07e9Pa
Longitudinal tensile failure	2459e6Pa
Longitudinal compressive failure	1102e6Pa
Lateral tensile failure	5e8Pa
Lateral compressive failure	5e8Pa
Poisson's ratio	0.34

Table 2 Material properties the composite halved strip.

Boundary conditions

The nodes on the left edge were constrained in all six degrees of freedom but those on right hand edge were constrained in x-translation and both y and z-rotations as in Figure 3.1.

Initial velocities were distributed at different portions of the strip along the z-direction; this is done to closely represent the actual behavior of the full length strip under impulsive loading and have a smooth transition to the half of the strip.

- -132m/s applied at the free end on the following nodes (Node 29:31 60:62 91:93 122:124) Figure 3.1.

- -116m/s applied towards the free end on the following nodes (Node 28:121:31) on Figure 3.2.
- -100m/s applied towards the free end on the following nodes (Node 25:27 56:58 87:89 118:120) on Figure 3.3.

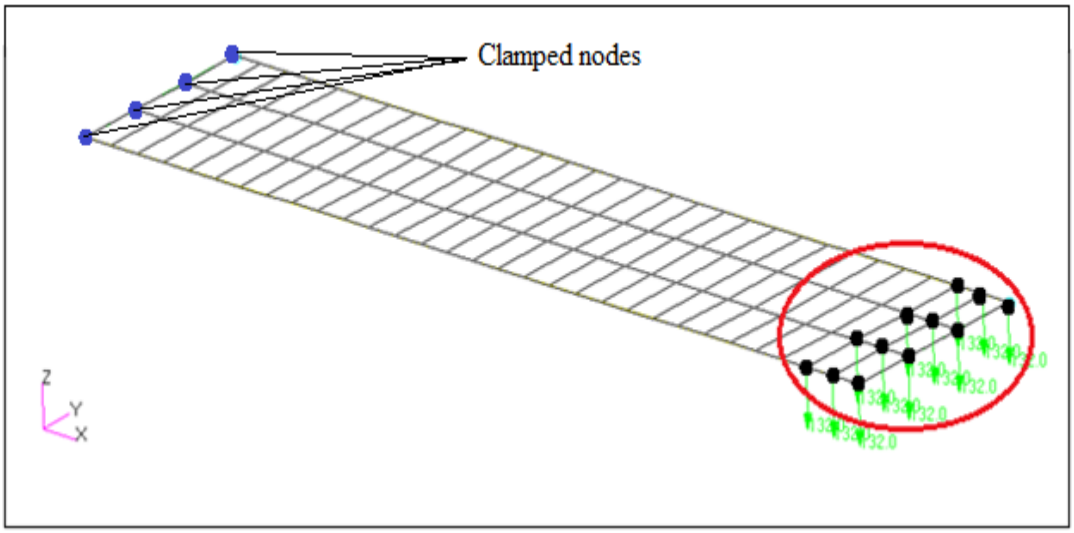

Figure 3.1 Nodes with initial velocity of -132m/s along z-axis.

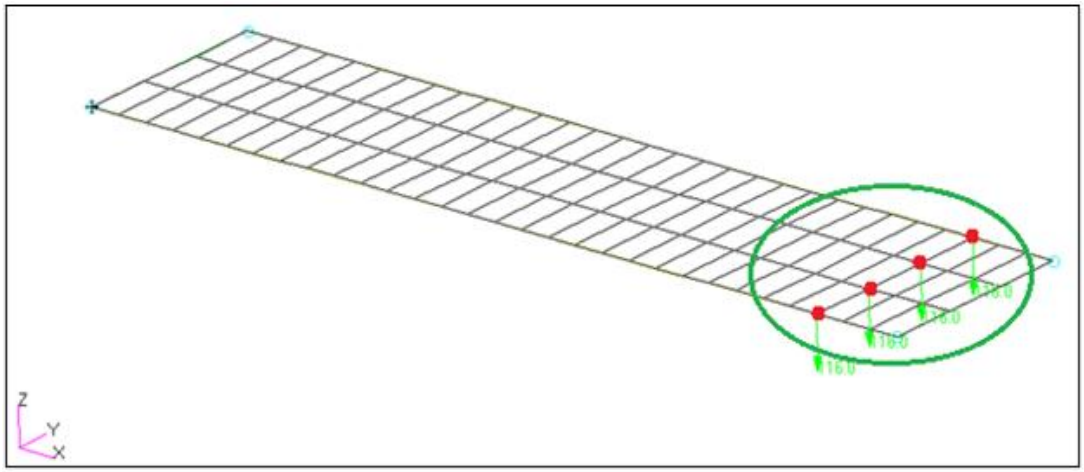

Figure 3.2 Nodes with initial velocity of -116m/s along z-axis.

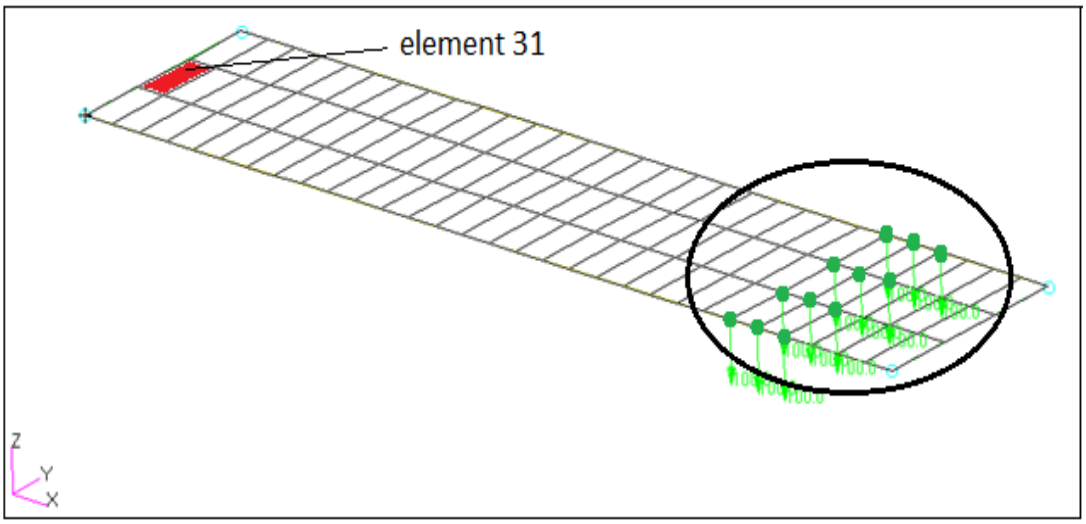

Figure 3.3 Nodes with initial velocity of -100m/s along z-axis.

The following entries are used to control the dynamic behavior of the half strip;

Time-Step control:

- End Step=10000
- End Time=0.001
- Time Step Size at Start=1e-7

Output request:

File type: Time History

Results Type:

Grid point output for z-displacement of node 31.

Output stresses on element 31.

Failure flags of element 31.

3.1.3 Modeling approach of the composite strip

The analysis is initially run without any failure criteria in order to ensure that the stresses in the strip can reach the allowable values especially at the clamped edge. The failure criteria are later introduced for the same model but the analysis is run separately for each failure criteria. This is done in order to precisely study the effect of each failure criteria and the composite lamina failure in MSC.Dyrtan code. Therefore, the major emphasis is based on the six failure criteria that are considered in the user manual of MSC.Dytran software.

List of failure criteria considered in MSC.Dytran code:

- Tsai-Hill
- Tsai-Wu
- Modified Tsai-Wu
- Maximum stress
- Hashin
- Chang-Chang

3.1.4 Results review of stress-time and failure flag-time graphs with different failure criteria.

No failure criteria defined

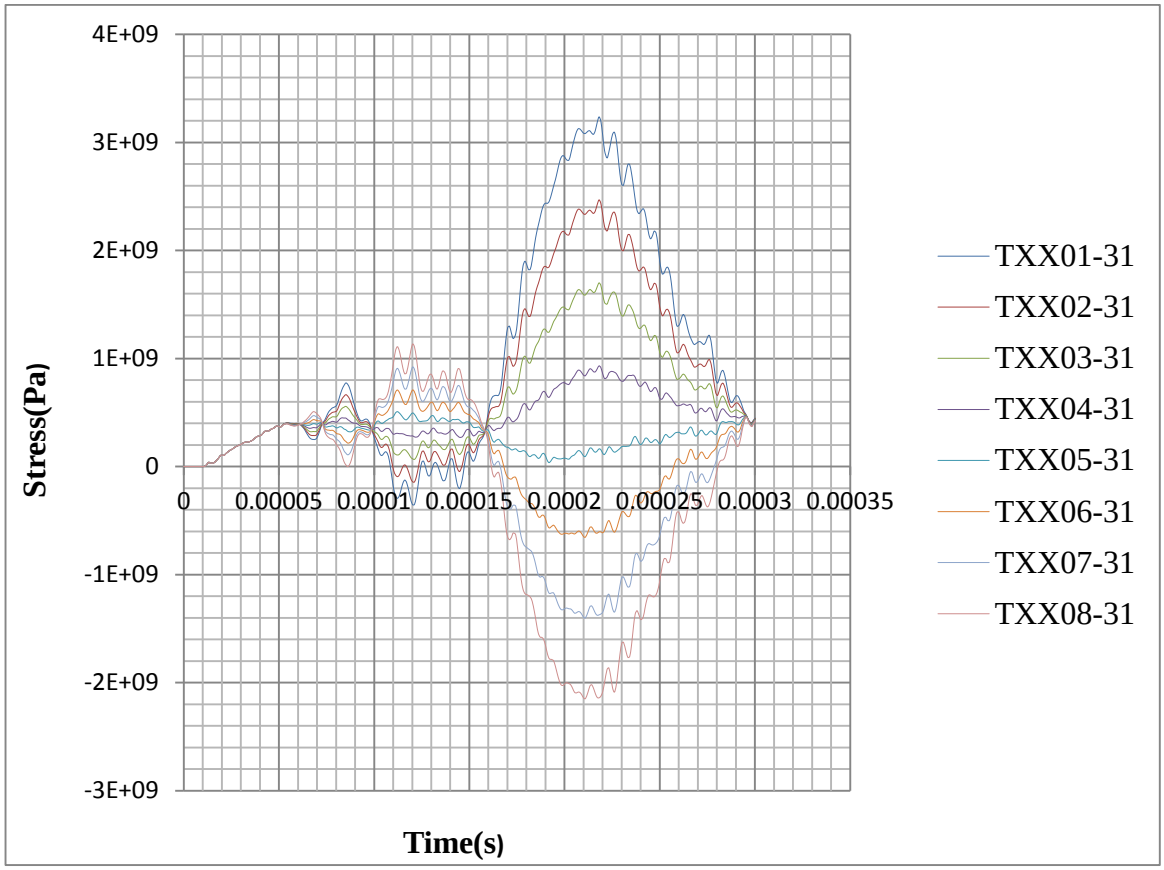

Figure 3.4 Stress vs. time plots with no failure criteria defined.

The first analysis was run without defining any failure criteria and the results of the stress response against time are displayed graphically in Figure 3.4. It is seen that the peak stresses in the outer layers exceeded the allowable longitudinal stresses in both tension and compression. This shows that the analysis approach is appropriate for obtaining stresses in the direction along the fibres of the plies at different failure times. If failure occurs, the bottom layer will first fail in compression since it reaches the maximum longitudinal allowable compressive stress. But, on the other hand, the top layer will also first fail in tension because it reaches the allowable longitudinal tensile stress before other layers. This is clearly indicated by the symmetric response

of the layers and since the longitudinal tensile stress is a much higher value compared to the longitudinal compressive stress. Therefore, the compressive mode will probably initiate fracture.

Tsai-Hill Criteria

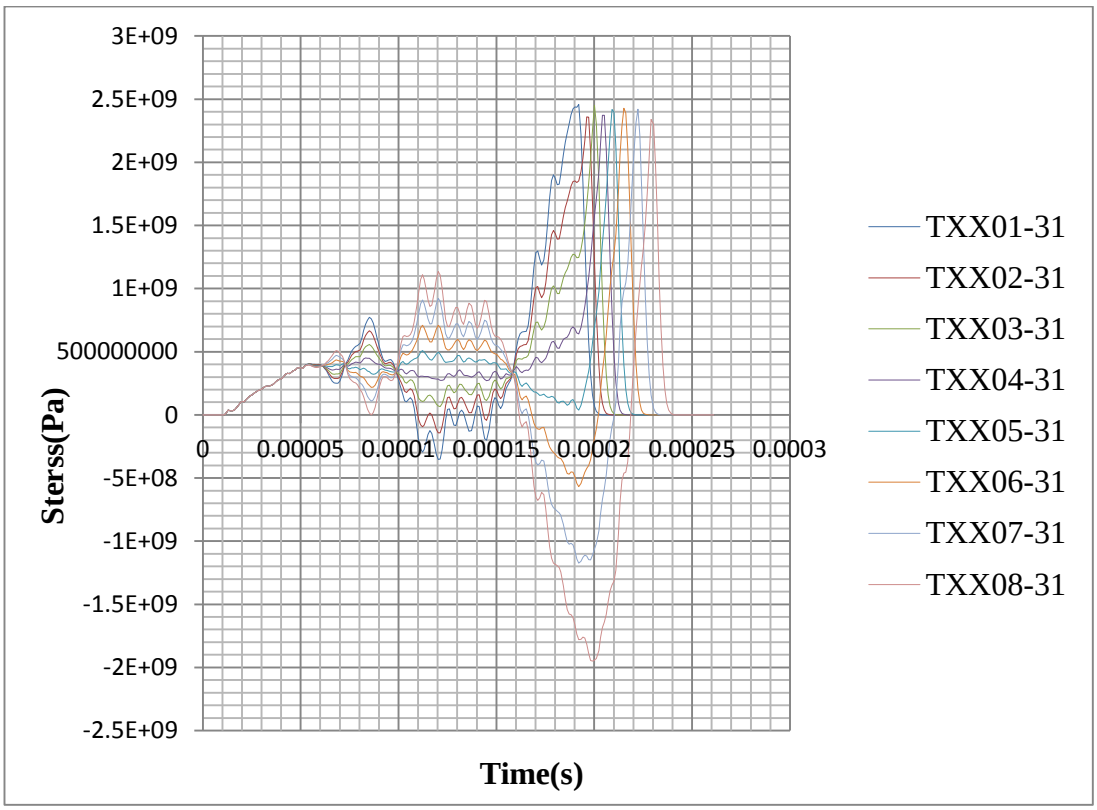

Figure 3.5 Stress vs. time plots of the Tsai-Hill criteria.

The Tsai-Hill failure criteria was defined for the prediction of failure and the results in Figure 3.5 show that layers failed progressively from the top layer through to the bottom layer of the lamina. It is also seen from the graphs that all the layers failed in the tensile mode reaching an allowable value of 2459 MPa, but the respective allowable compressive strengths were also exceeded even though no failure was predicted in this failure mode. Therefore, this implies that a Tsai-Hill failure criterion in not appropriate for predicting failure of the lamina in compression mode but it is effective in capturing the tensile failure of fibres.

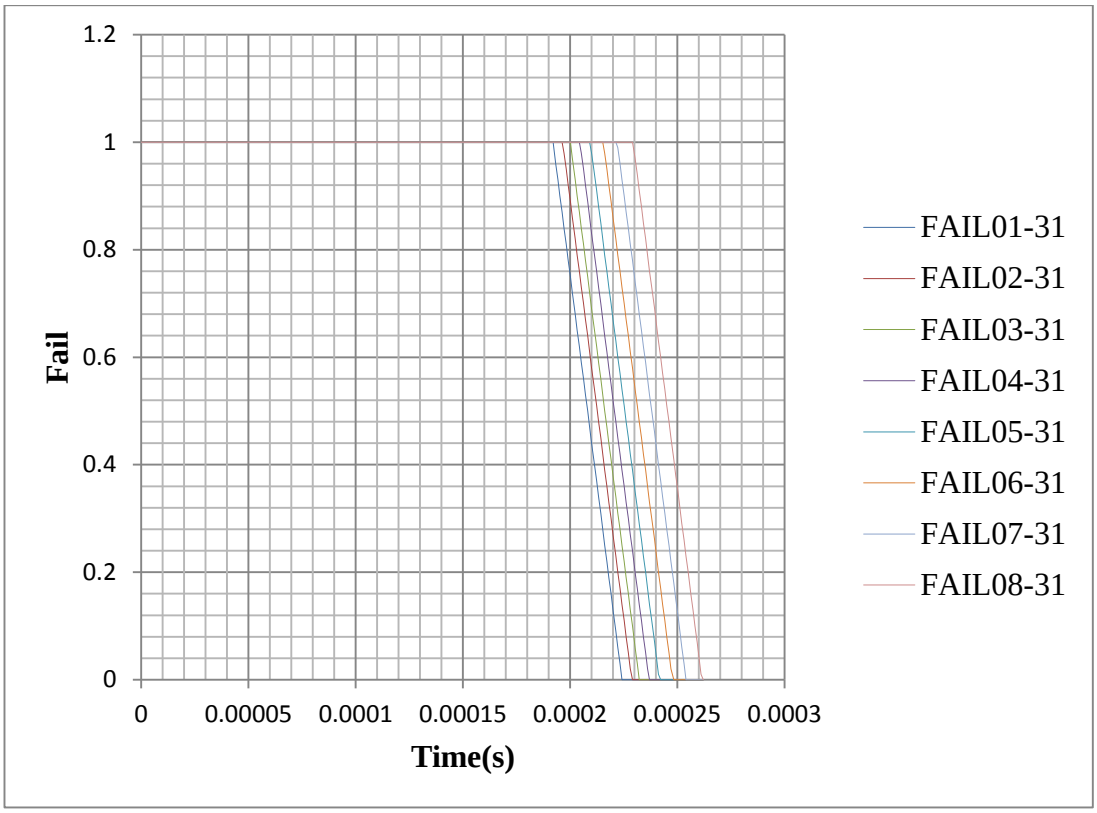

Figure 3.6 Failure flags vs. time plots of the Tsai-Hill criteria.

The ply failure flag in MSC.Dytran denotes a value between zero and one indicating failures or no failure respectively. In other words, the ply is considered to have failed when its failure flag value is equal to zero and if the value is one, it implies that no failure is predicted. Figure 3.6 shows failure flag values of the composite lamina when the Tsai-Hill criterion is defined to predict failure. It can be seen from the graphs that the plies fail progressively in tension and this response reflects the same behavior as in Figure 3.5. The failure sequence begins with layer one from the top through to eighth layer at the bottom of the lamina.

Tsai-Wu Criteria

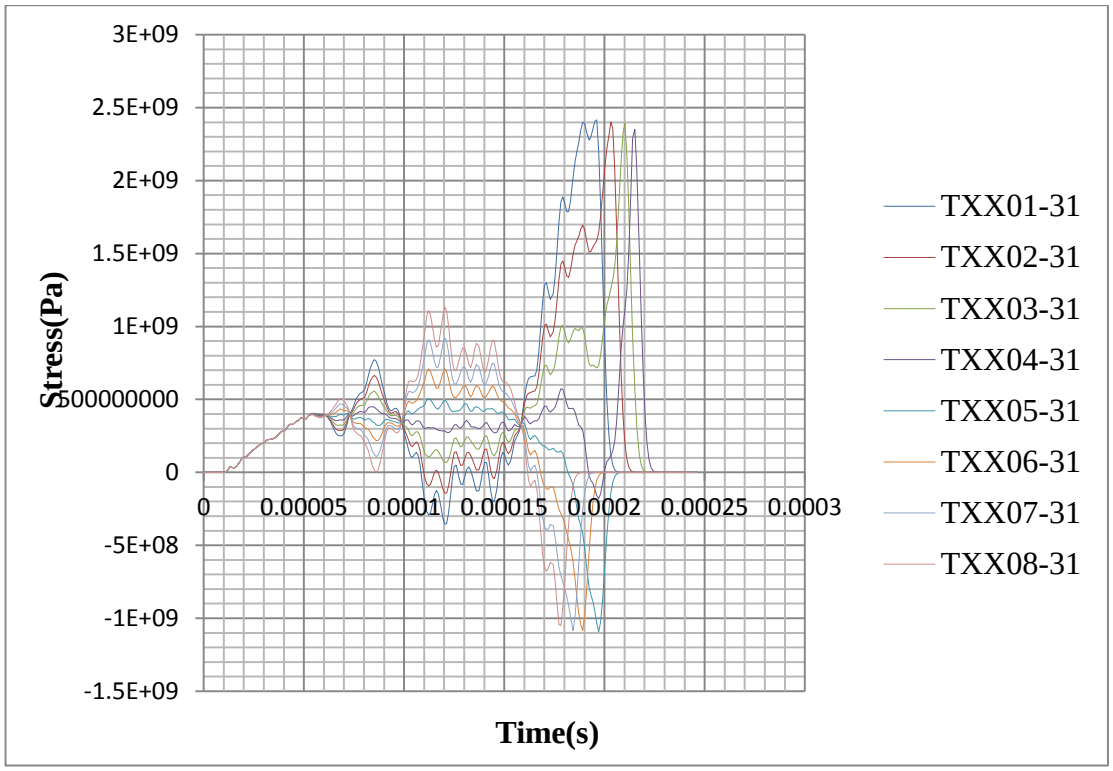

Figure 3.7 Stress vs. time plots of the Tsai-Wu criteria.

The Tsai-Wu failure criterion was defined to predict failure of the lamina and it is clearly seen in Figure 3.7 that the layers failed progressively in both the tensile and compressive modes. The respective strengths of 2459 MPa in tension, 1102 MPa in compression were reached, the Tsai-Wu criteria was satisfied. Therefore, fracture occurred and the next stage was for the stresses to relax down to zero once failure has occurred. The top four layers of the lamina show progressive tensile failure from layer one (TXX-01) through to layer four (TXX-04) but on the other hand, progressive compressive failure is also captured in the bottom four layers from layer eight (TXX-08) through to layer five (TXX-05). This shows that the Tsai-Wu failure criterion is capable of predicting failure of the composite lamina in both tensile and compressive mode in the direction of the fibres.

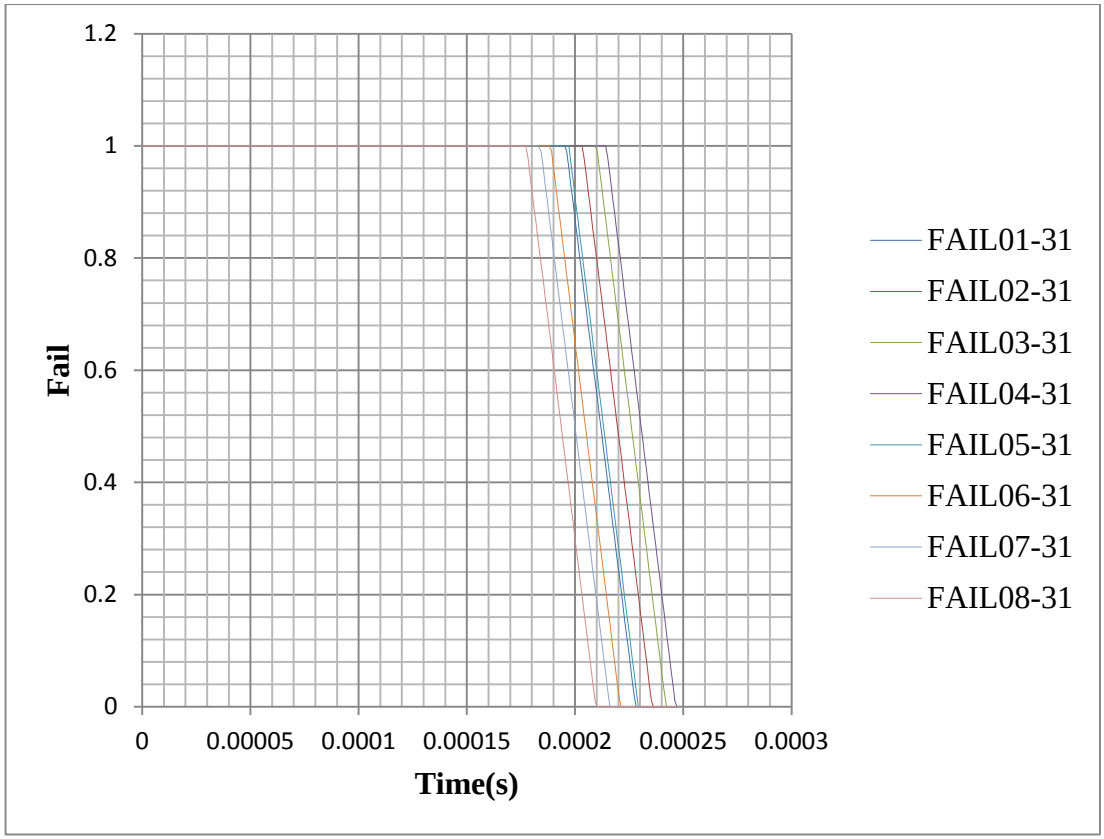

Figure 3.8 Failure flags vs. time plots of the Tsai-Wu criteria.

Figure 3.8 above shows failure flag values of the composite lamina when the Tsai-Wu criterion is defined to predict failure. The failure sequence in compressive mode begins with layer eight from the bottom through to layer five towards the middle of the lamina but the sequence in tensile mode begins with layer one through to layer four which is also towards the middle of the lamina. It can be seen from the graphs that the plies first fail progressively in compression and later in tension which agrees with the response seen in Figure 3.7 for the same failure criteria.

Modified Tsai-Wu Criteria

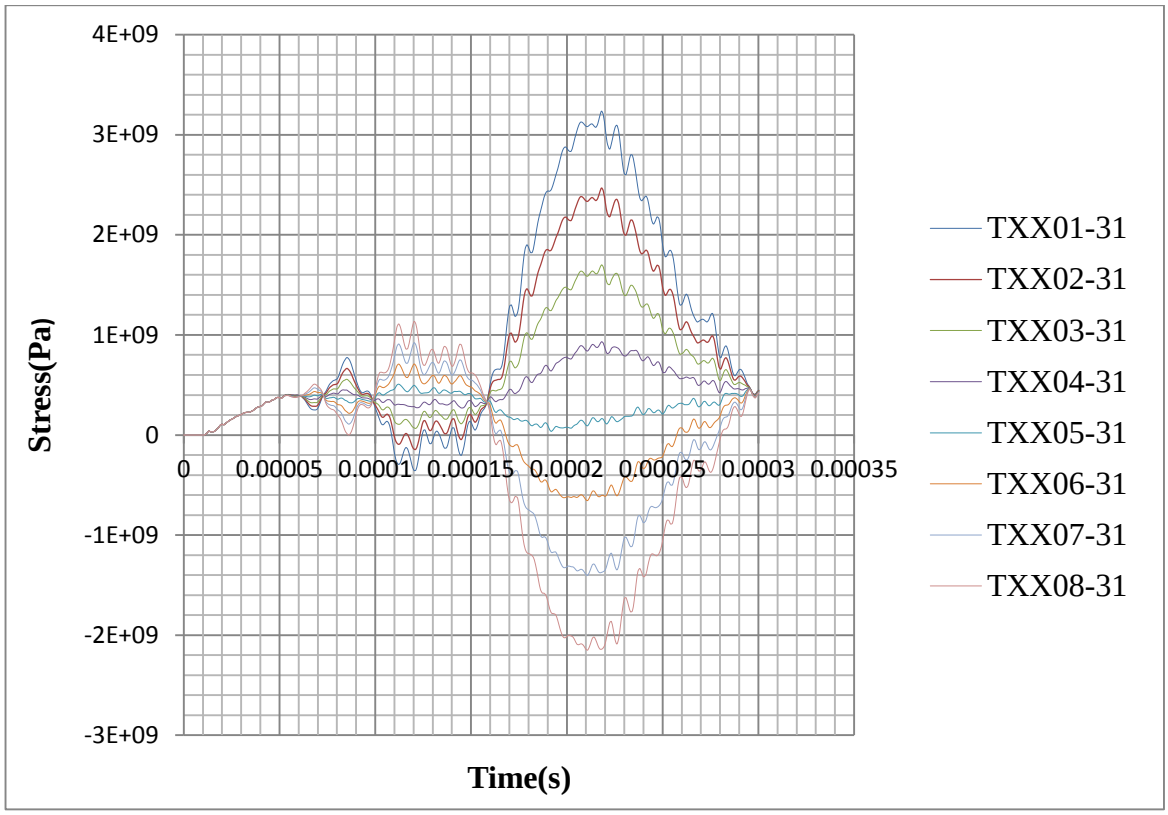

Figure 3.9 Stress vs. time plots of the Modified Tsai-Wu criteria.

The modified Tsai-Wu criterion was defined and the results of the stress response against time are shown in Figure 3.9. It is seen on the graph that the peak stresses in the lamina exceeded the allowable values of 2459 MPa, 1102 MPa in both tension and compression respectively. This shows that the Modified Tsai-Wu criterion is not capable of predicting progressive failure of the composite lamina in both tension and compressive modes along the direction of the fibres of the plies at different failure times.

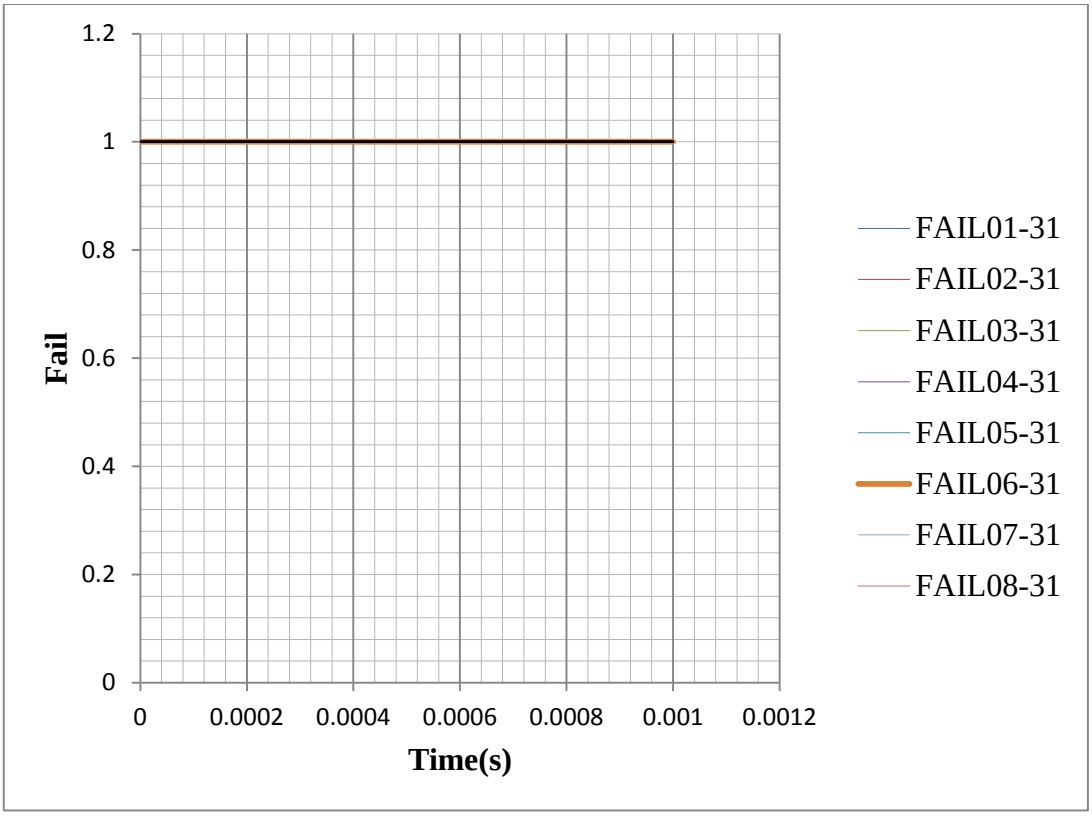

Figure 3.10 Failure flags of the Modified Tsai-Wu criteria.

The Modified Tsai-Wu criterion was defined to predict failure and the results of the failure flag against time plots are shown in Figure 3.10. It is seen from the graph that the Modified Tsai-Wu is not capable of predicting progressive failure of the composite lamina in both tension and compressive modes in the longitudinal directions of the fibres at different failure times. This correlates with the previous behavior discussed earlier from the stress-time graph in Figure 3.9 with the same criteria was assigned to predict failure.

Maximum Stress Criteria

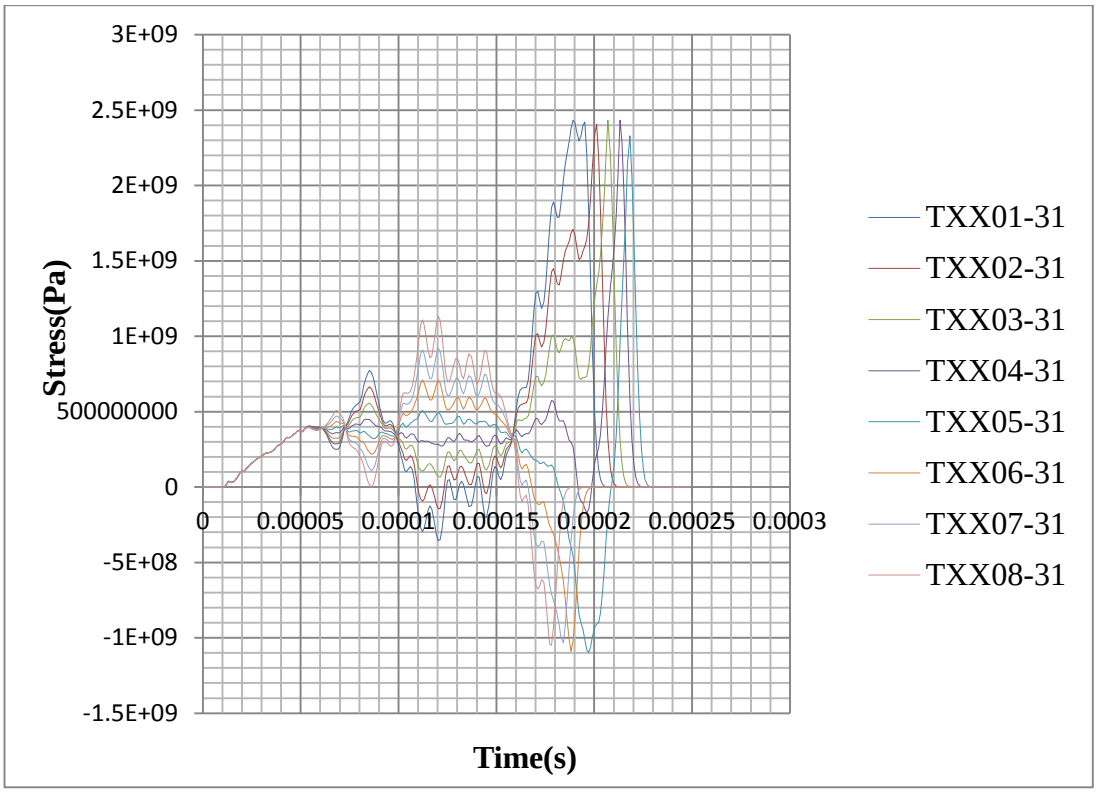

Figure 3.11 Stress vs. time plots of the Maximum stress criteria.

The Maximum Stress failure criterion was defined to predict failure of the lamina and the results in Figure 3.11 clearly show that the lamina failed progressively in both the tensile and compressive modes. The respective strengths of 2459 MPa in tension, 1102 MPa in compression were reached. The Maximum Stress criterion was satisfied. Therefore, fracture occurred and the next stage was for the stresses to relax down to zero. The top four layers of the lamina show progressive tensile failure from layer one (TXX-01) through to layer four (TXX-04). But on the other hand, progressive compressive failure was captured in the bottom four layers from layer eight (TXX-08) through to layer five (TXX-05). But the fifth layer of the lamina shows an outstanding response by reaching the allowable compressive stress. It continued holding up until it reached the allowable tensile stress, therefore failing due to tensile mode. This shows that the Maximum Stress failure criterion is not

capable of a predicting failure of the layers in both tensile and compressive mode in the direction of the fibres.

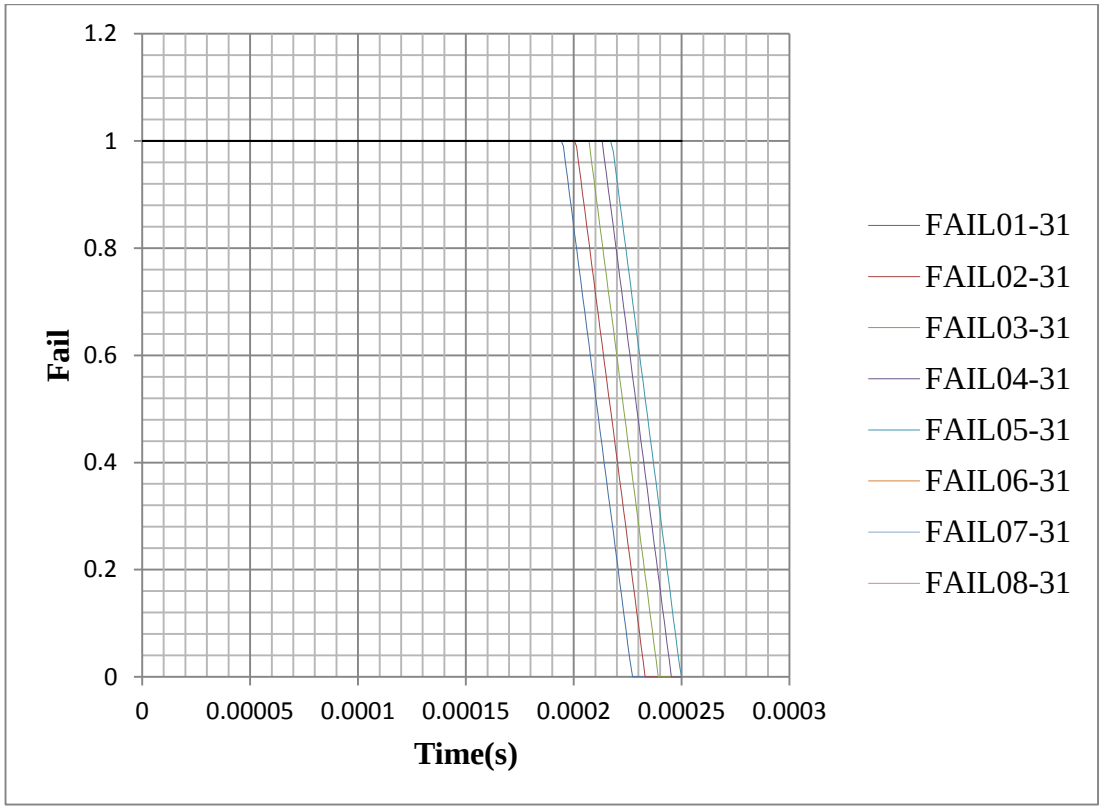

Figure 3.12 Failure flags vs. time of the Maximum stress criteria.

Figure 3.12 is a graph showing the result of failure flag against time with the Maximum stress criterion selected to predict failure of the composite lamina. It is seen from the graph that the lamina failed progressively from layer one through to layer five which shows a correlation with the result displayed in Figure 3.11 of the stress-time plots. Based on the results from Figure 3.11, the graph only shows the failure effect of tensile mode in the longitudinal direction of fibres, it is seen that the failure effect of the compressive mode is not captured but it is displayed in Figure 3.11 of the stress-time graph.

Hashin Criteria

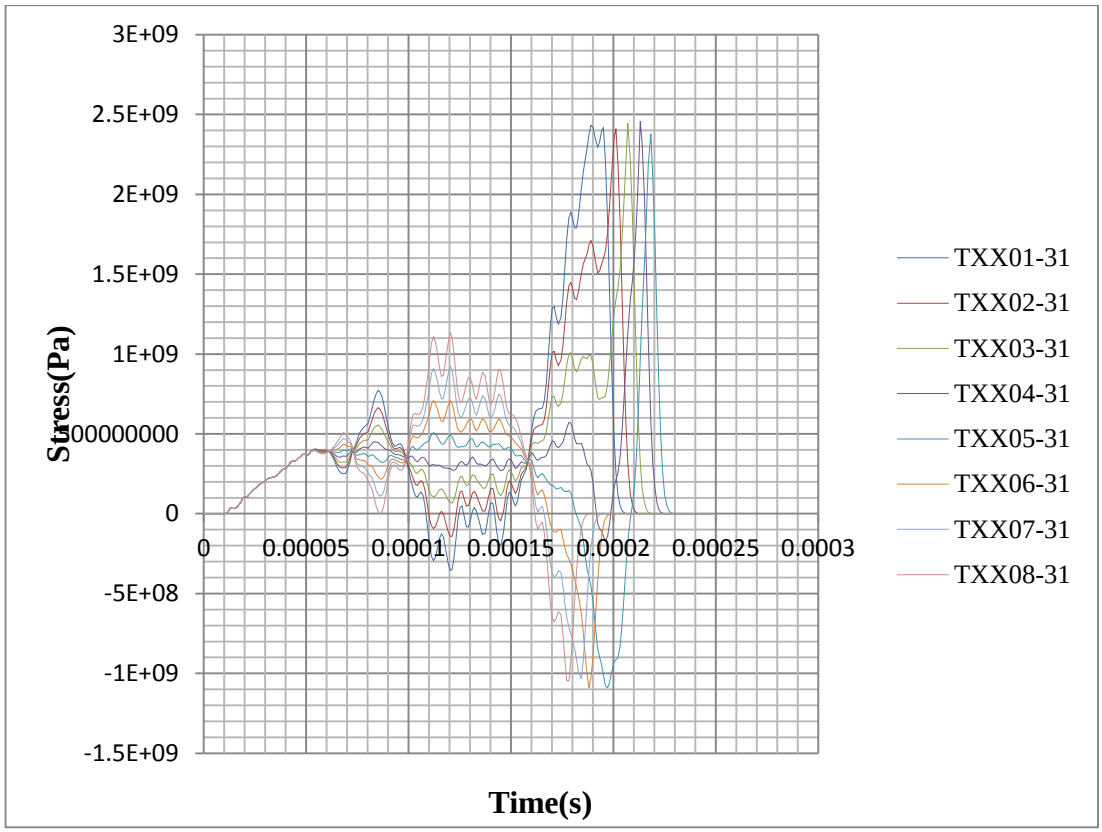

Figure 3.13 Stress vs. time plots of the Hashin criteria.

The Hashin failure criterion was defined to predict failure of the lamina and the results in Figure 3.13 clearly show that the lamina failed progressively in both the tensile and compressive modes. The respective strengths of 2459 MPa in tension, 1102 MPa in compression were reached. The Hashin criterion was satisfied, therefore fracture occurred and the next stage was for the stresses to relax down to zero once failure has occurred. The top four layers of the lamina show progressive tensile failure from layer one (TXX-01) through to layer four (TXX-04). But on the other hand, the progressive compressive failure is also captured in the bottom four layers from layer eight (TXX-08) through to layer five (TXX-05). But the fifth layer of the lamina shows an outstanding response by reaching the allowable compressive stress and continued holding up until the allowable tensile stress, therefore failing due to tensile mode. This shows that the Hashin failure criterion is partially capable

of predicting failure of the composite lamina in both tensile and compressive mode in the direction of the fibres. But the response of the fifth layer of the lamina is not clear.

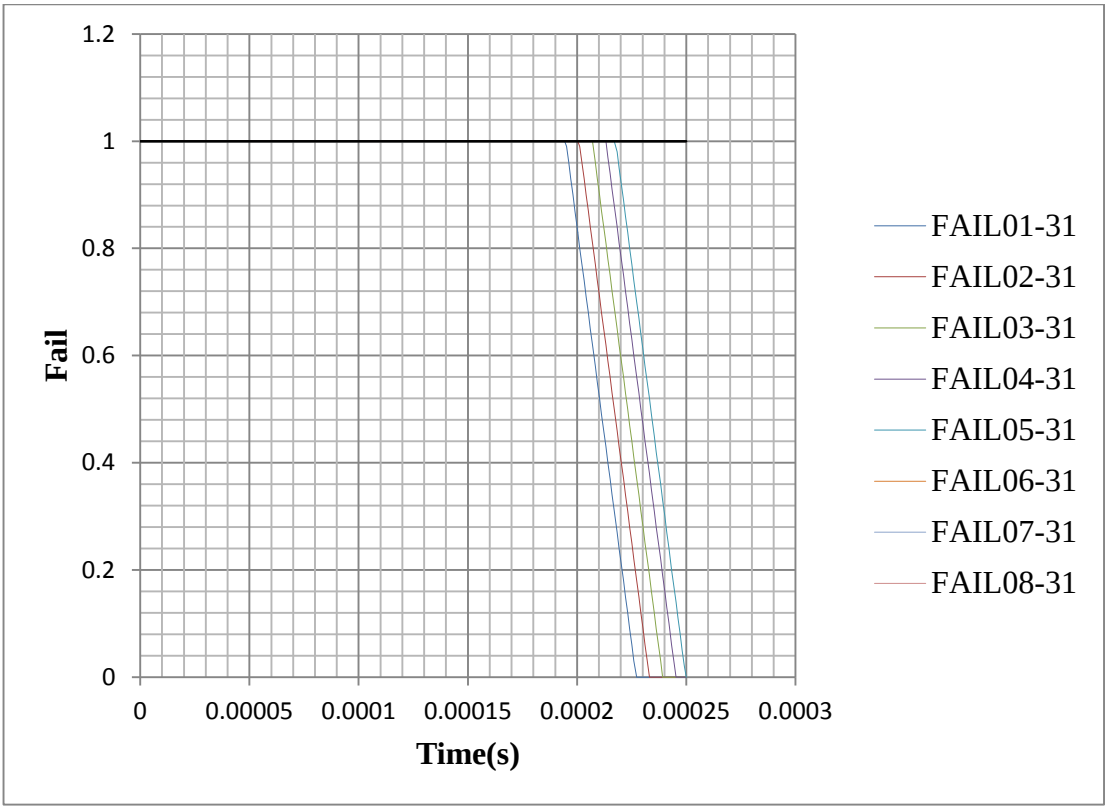

Figure 3.14 Failure flags vs. time of the Hashin criteria.

Figure 3.14 is a graph showing the result of failure flag against time with the Hashin criterion selected to predict failure of the composite lamina. It is seen from the graph that the lamina failed progressively from layer one through to layer five which shows a correlation with the result displayed in Figure 3.13 of the stress-time plots. Based on the results in Figure 3.14, the graph only shows the failure effect of tensile mode in the longitudinal direction of fibres, it is also seen that the failure effect of the compressive mode was not captured but it is displayed in Figure 3.13 of the stress-time graph. This result is almost the same as those of obtained from the failure flag against time where the Maximum stress was defined to predict failure of the lamina.

Chang-Chang Criteria

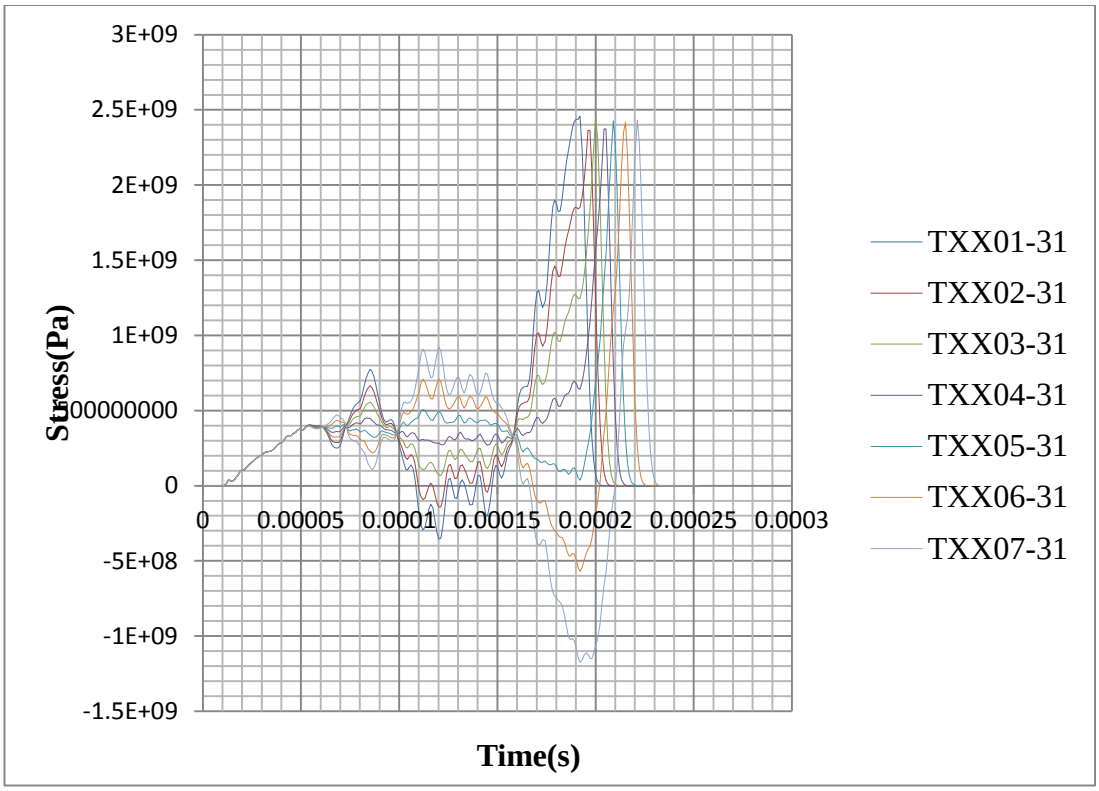

Figure 3.15 Stress vs. time plots of the Chang-Chang criteria.

The Chang-Chang failure criterion was defined to predict failure of the lamina and from the results in Figure 3.15 it is clearly shown that the lamina failed progressively in the tensile modes. The respective strengths of 2459 MPa in tension, 1102 MPa in compression were reached. The Chang-Chang criterion was satisfied. Therefore, fracture occurred and the next stage was for the stresses to relax down to zero due to tensile failure. The layers of the lamina show progressive tensile failure from layer one (TXX-01) through to layer eight (TXX-08). This shows that the Chang-Chang failure criterion is capable of predicting failure of the composite lamina for the tensile mode along the fibre direction, but it is not suitable for predicting failure in the compressive mode.

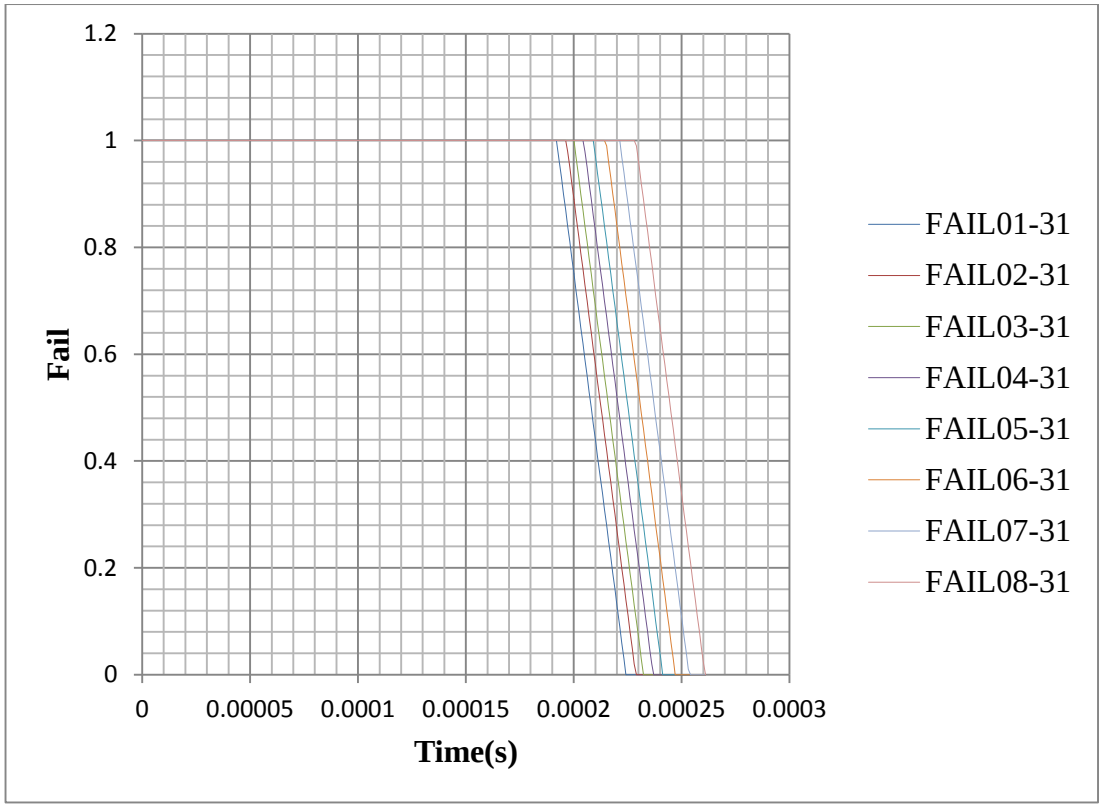

Figure 3.16 Failure flags vs. time plots of the Chang-Chang criteria.

The results of the Chang-Chang criteria selected to predict failure were discussed earlier on in Figure 3.15. This showed the stresses against respective failure times. Therefore, further examination was done by plotting the failure flag against time as shown in Figure 3.16 above. Hence, it can be seen from the graphs that the plies fail progressively in tension mode from layer one through to layer eight. This failure sequence strongly agrees to that in Figure 3.15, this happens when the same criterion is defined to predict failure of the lamina plies.

3.1.5 Results review of displacement-time graphs with different criteria.

In this section the vertical displacement versus time histories of node 31 under initial velocity excitation were investigated. This was done with different failure criteria defined for the composite strip response.

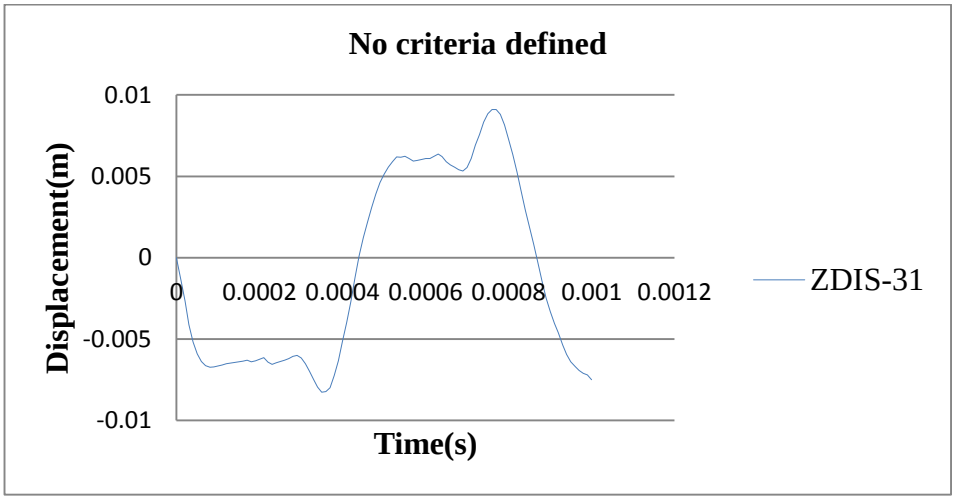

Figure 3.17 Displacement vs. time plots of node 31 with no failure criteria defined.

The graph in Figure 3.17 displays the displacement of node 31 with no criteria defined and the plots in Figure 3.18 show the results with different criteria. The displacement of node 31 was similar at the beginning of the plots up to a time value closer to t=0.4 milliseconds for all the graphs. But the graphs show slightly different response just after t=0.4 milliseconds. None of the graphs return to the zero. Since the composite lamina fractures at about t=0.2 milliseconds, its behavior was the same just before failure occurred and this was predicted between t=0.2 milliseconds and t=0.4 milliseconds. This response perfectly relates the failure times seen in stress-time and fail-time graphs discussed in the previous section. Furthermore, the response from the plot with no criteria and the graph with Modified Tsai-Wu defined also relates to that of the same failure conditions defined earlier in this study.

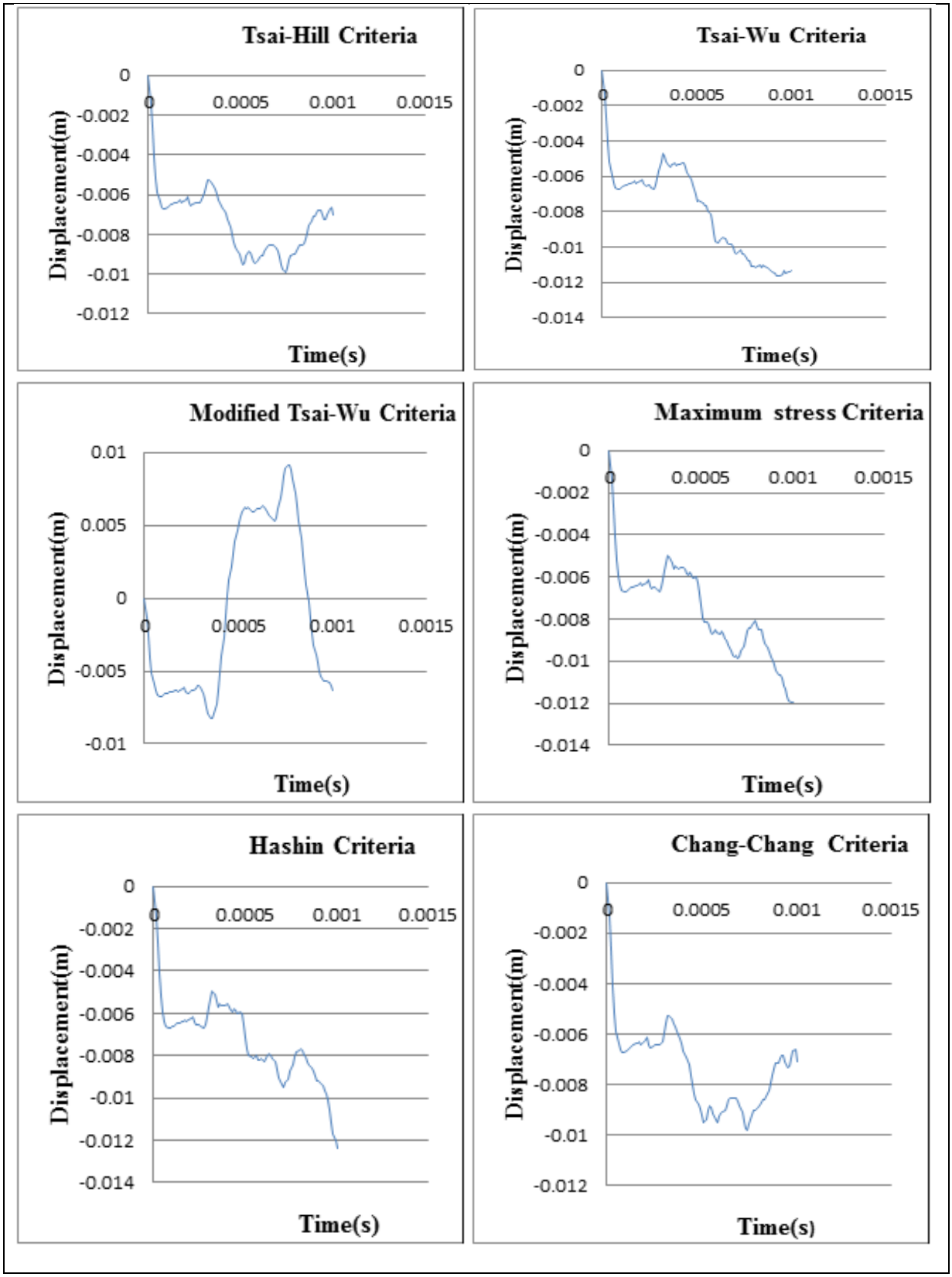

Figure 3.18 Displacement vs. time plots of node 31 with failure criteria defined.

3.1.6 Progressive ply failure in MSC.Dytran

It is essential to have a thorough understanding of a laminate behavior under various loading conditions in MSC.Dytran. This is due to the fact that most common FE codes use linear finite element solution and is focused on failure calculations derived from a theory based on the first ply failure analysis. But the actual truth is a composite laminate can continue to withstand significant loadings even though the first ply has failed long time in the composite. This is due to the nature of the laminate layup. The remaining layers of the laminate continue holding until each one of them has failed. The laminate completely fails after the final layer has failed. This type of composite laminate failure of first ply failure through to the final ply is termed progressive ply failure.

Therefore, a Tsai-Wu failure criterion was defined to control failure of the impulsively loaded composite strip defined earlier. At t=0.256 milliseconds, it is seen that the elements on the clamped end were still present in the analysis. In MSC.Dytran, when an element has failed in the model, it is eliminated from the analysis. On the other hand, the ply failure index denotes a value between zero (fail) and one (not fail) [31]. Therefore, some of the plies in the laminate failed while others continued carrying load and there was no element failure as shown in Figure 3.19 but a value of zero indicating failure is denoted at the clamped end.

In addition, at t=0.272 milliseconds in Figure 3.20, the composite strip was already separated from the clamped end between t=0.256 milliseconds and t=0.272seconds, and this shows that the elements at the clamped edge are eliminated from the analysis at that time; this also indicates that the laminate element has completely failed. The failure flags versus time graph of the composite are shown in Figure 3.21, the ply failure sequence starts from the first through to the eighth ply which is the only layer finally carrying the load. But eventually the eighth ply fails just after

t=0.261 milliseconds and this indicates complete failure of the laminate. It is evident that MSC.Dytran uses progressive ply failure for composite laminate under significant loading conditions.

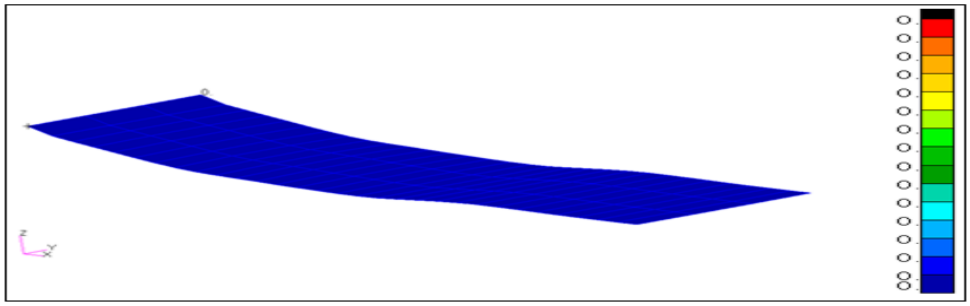

Figure 3.19 No failure at t=0.256 milliseconds with Tsai-Wu failure criteria.

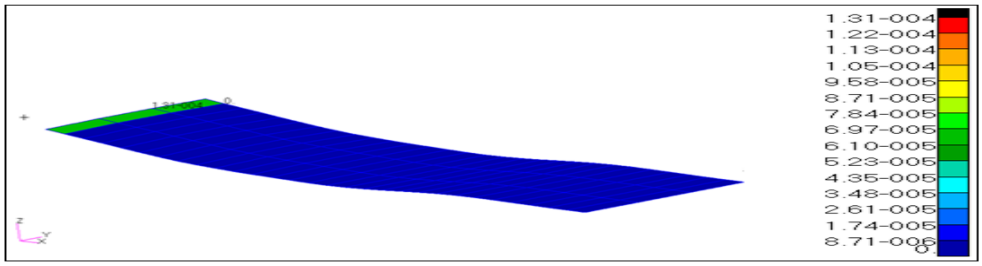

Figure 3.20 Failure at t=0.272 milliseconds with Tsai-Wu failure criteria.

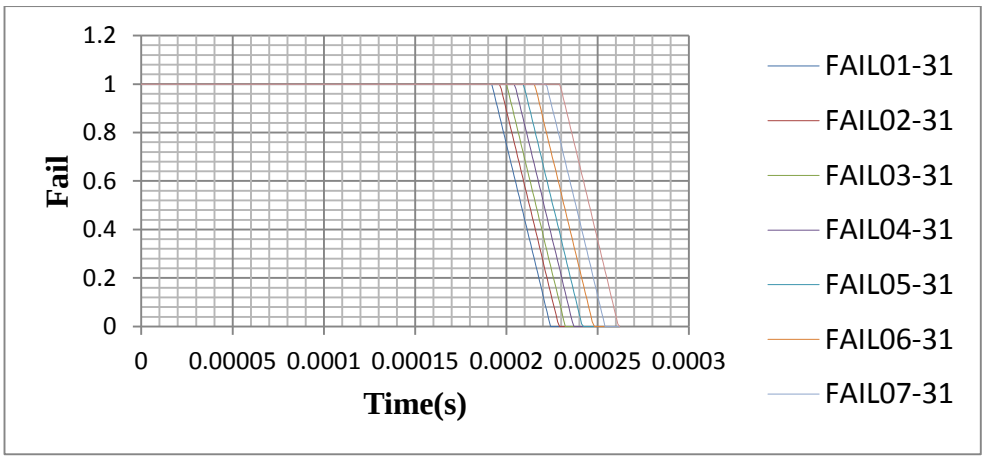

Figure 3.21 Failure flag plot up to t=0.261 milliseconds with Tsai-Wu failure criteria.

3.2 Evaluation of the fuselage sandwich core

3.2.1 Modeling the sandwich core

The fuselage sandwich core comprises of a foam material sandwiched in the fabric layers. Therefore, a similar approach used by Karen E. Fasanella et al of representing the Rohacell foam with DYMAT24 material model was adopted in this study [32]. It was necessary to evaluate the failure behavior of this elastoplastic, non-linear, plastic material with isotropic hardening and a piece-wise linear stress-strain curve. This material model can be used with solids, shells and Hughes-Liu beam elements [21]. The properties used for the Rohacell foam material are listed in Table 3 below and material properties for the composite layers are similar to those in Table 2.

Material	**Formulation**	**ρ**(Kg/m^3)	**E**(MPa)	**Poisson's ratio**	**Yield stress**(MPa)	**Plastic strain at failure**(m/m)
Rohacell foam	DYMAT 24	44.89	13.79	0,3	0.62	0,02

Table 3 Rohacell foam material properties. [32]

A similar modeling approach used in the previous section was followed to predict the failure flags of the sandwich core. But in this instance a Rohacell foam material model was placed between two carbon fibres to form a single strip as shown in Figure 3.22.

Figure 3.22 Sandwich core of Rohacell foam and two plies of carbon fibre.

3.2.2 Failure flags of the sandwich core before and after failure prediction

The response of each layer was evaluated after several time steps. Figure 3.23 shows the failure flag results of layer 1(carbon fibre) before and after failure prediction. It is seen that at t=1.153 milliseconds, the layer was still integrated, but at t=1.154 milliseconds, element 31 is missing which implies that failure has occurred.

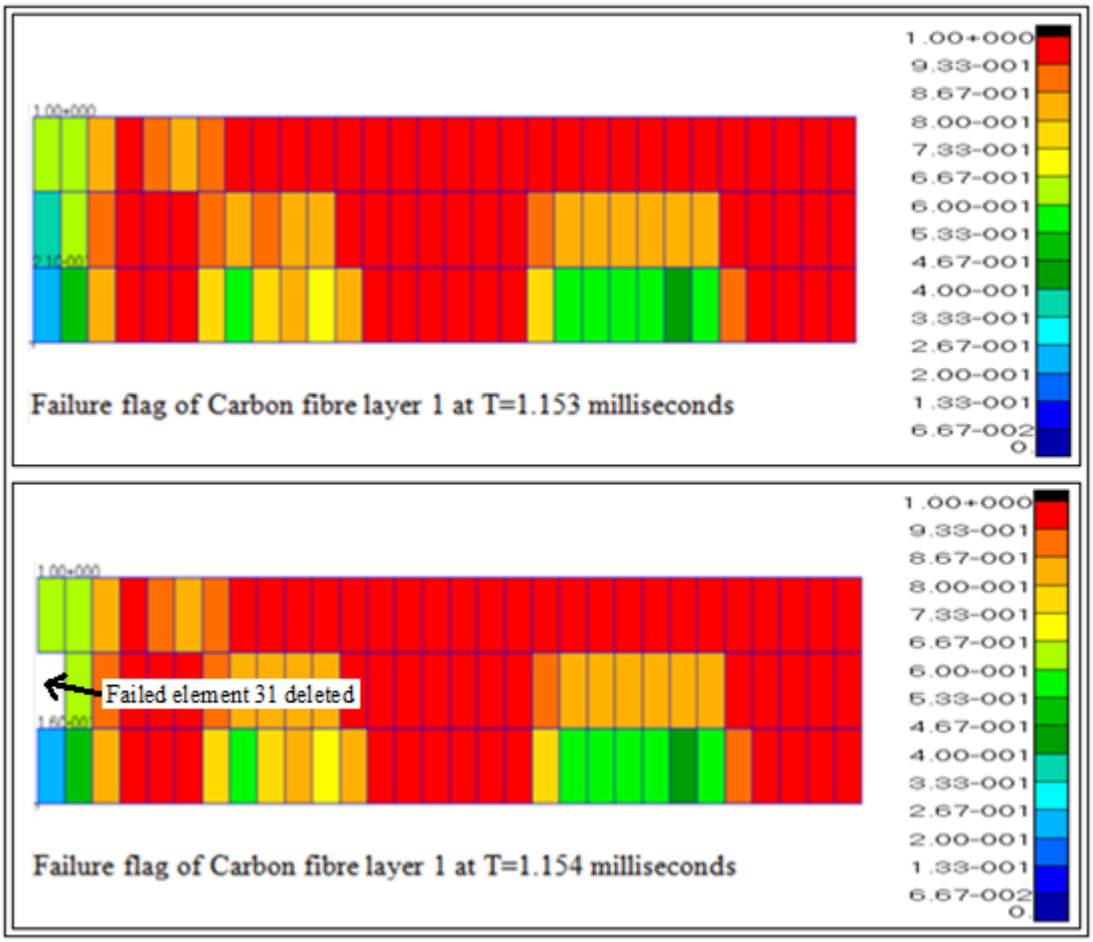

Figure 3.23 Failure flag plots of layer 1 defined with carbon fibre properties.

Figure 3.24 displays the failure flag results for the foam core. It is illustrated that at t=1.153 milliseconds, the elements were still active in the analysis. But later at t=1.154 milliseconds element 31 was eliminated from the analysis. The failure flag plots of layer 3(carbon fibre) are displayed in Figure 3.25 and the results showed similar response to other layers.

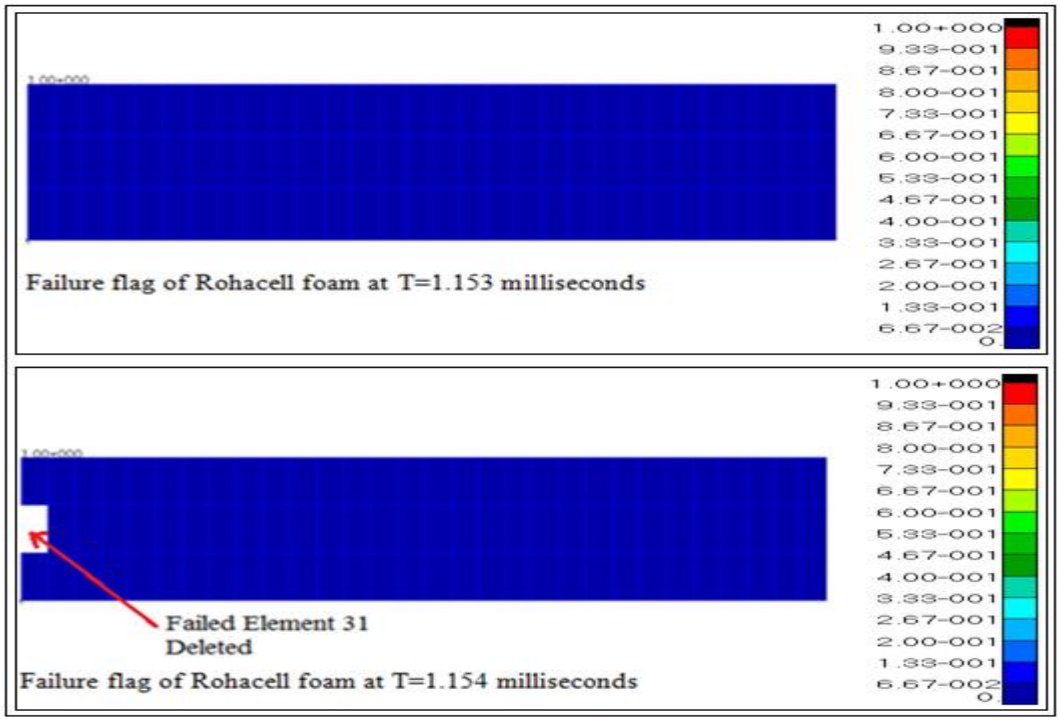

Figure 3.24 Failure flag plot of layer 2 defined with Rohacell foam core properties.

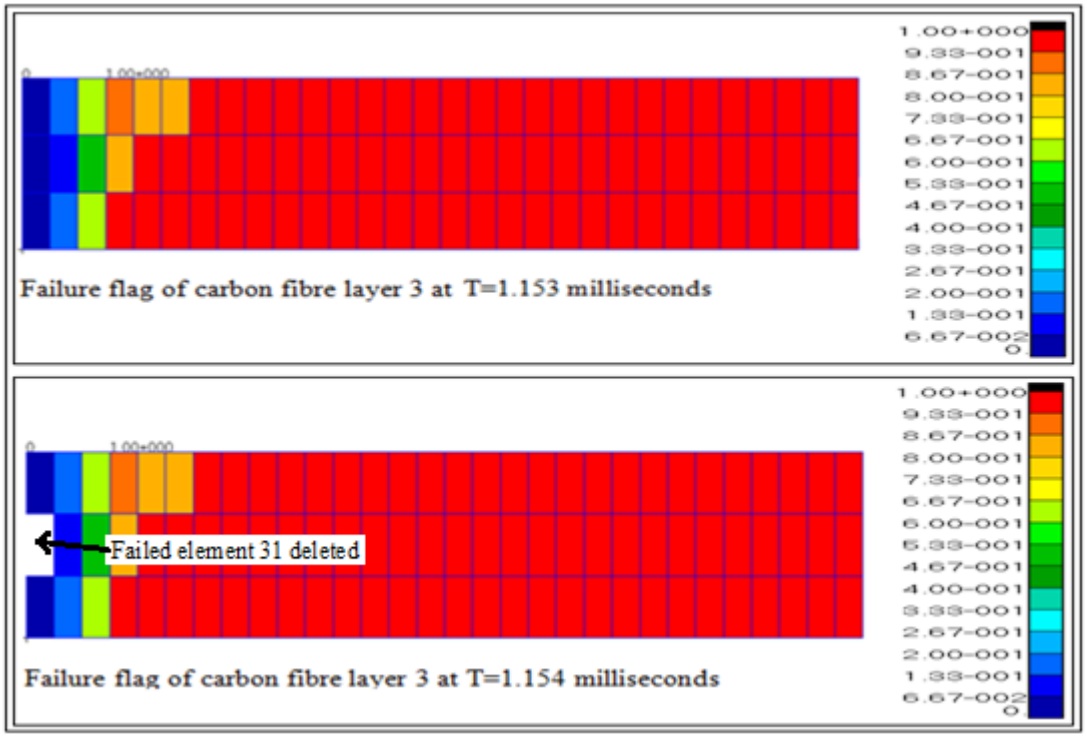

Figure 3.25 Failure flag plot of layer 3 defined with carbon fibre properties.

3.2.3 Failure flag plots of the sandwich core materials

The results of the failure flags were obtained after the Tsai-Wu failure criteria was defined to control the failure response of the carbon fibre layers and the Rohacell foam failure behavior was controlled by the maximum plastic strain. The failure flag plots of carbon fibre layers drop down to a value of zero once the maximum allowable stress was reached. This response is seen in Figures 3.26 and 3.28 of the carbon fibre failure flags against time. But the failure flag for the foam in Figure 3.27 does not drop down to zero since it was defined by a DYMAT24 model.

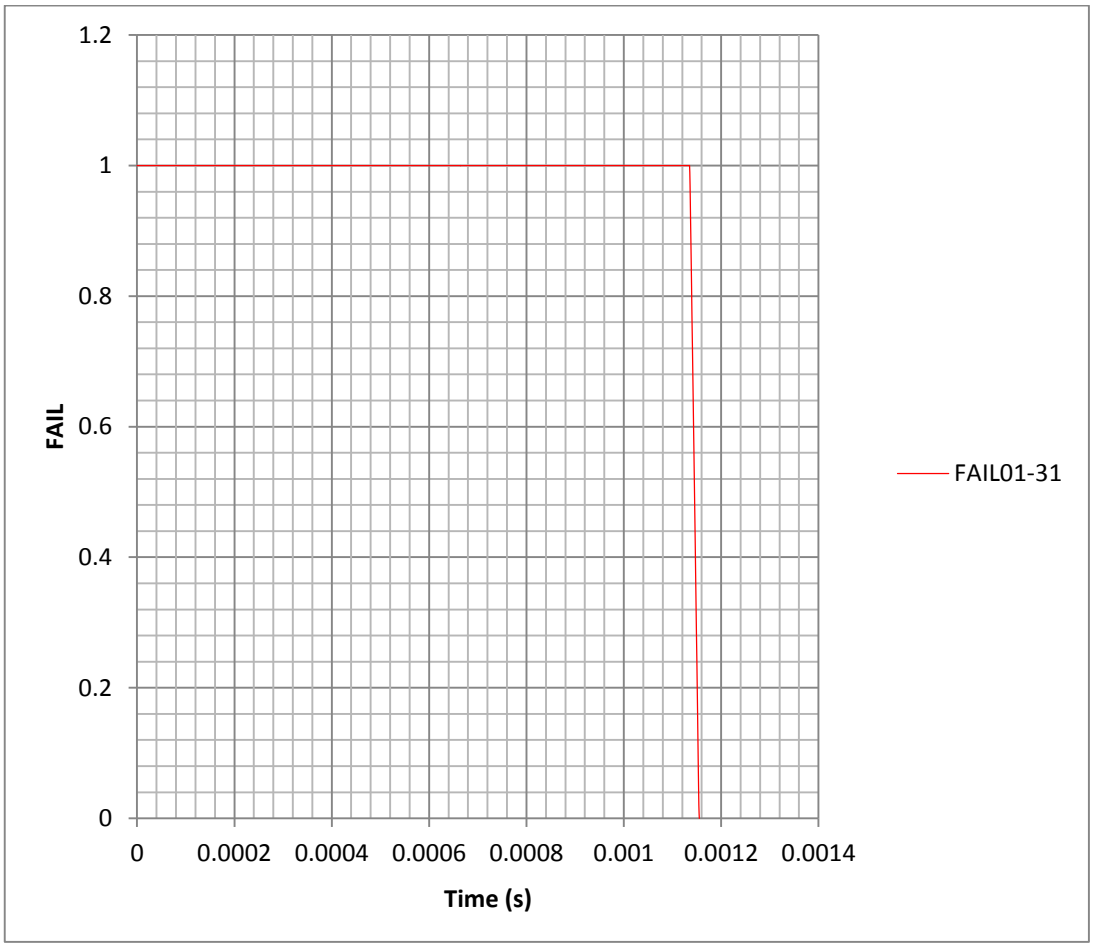

Figure 3.26 Carbon fibre failure flag of element 31 layer 1.

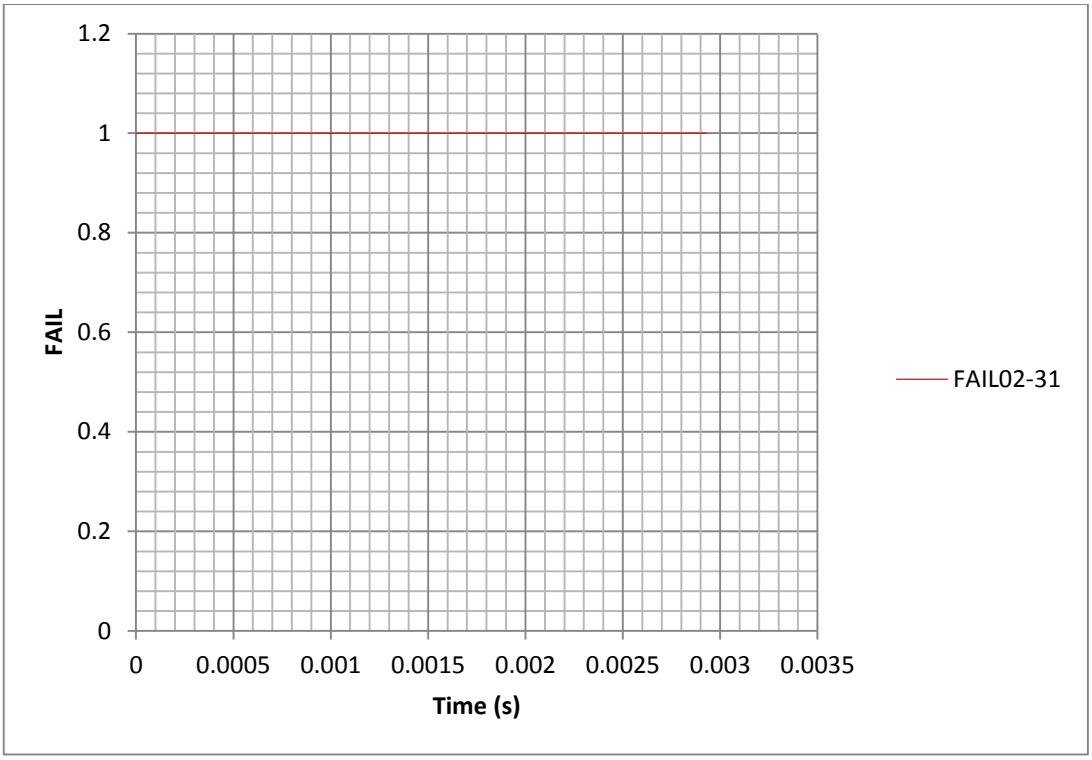

Figure 3.27 Rohacell foam failure flag not dropped down to zero after failure of element 31 of layer 2.

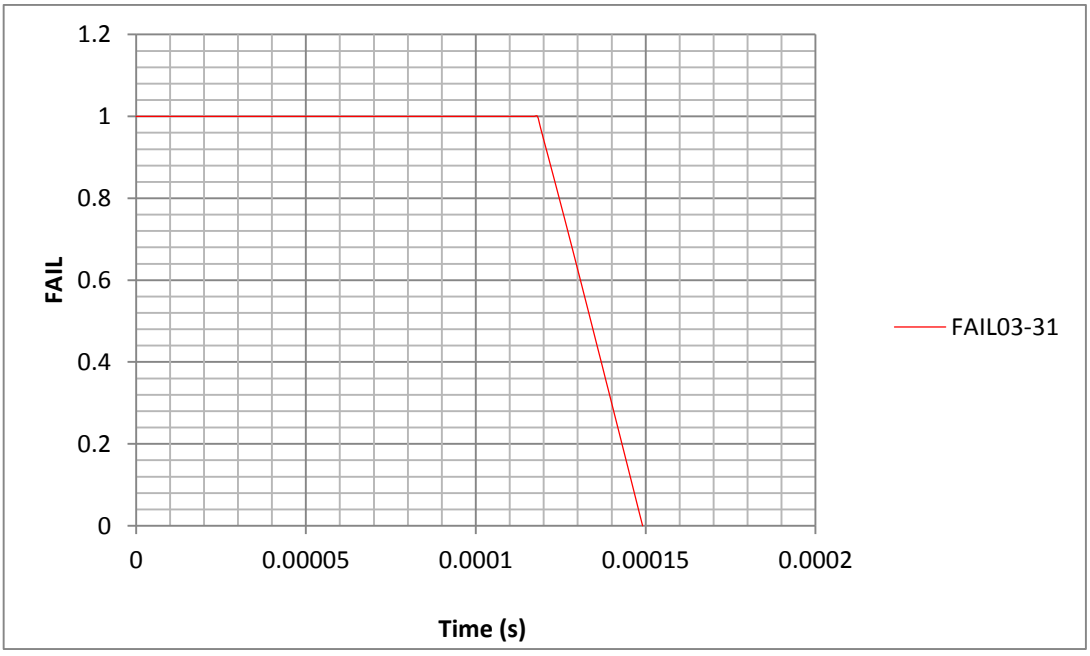

Figure 3.28 Carbon fibre failure flag of element 31 of layer 3.

3.3 Evaluation of failure criteria associated with beams with MSC.Dytran

As stated earlier, the stiffeners, engine frame tubes, stabilizers and the wings were represented by 1-D elements. Therefore, it was necessary to study the failure behavior of 1-D elements under extreme loading conditions. A cantilevered beam with a concentrated mass at its free end is displayed in Figure 3.29. A clamped node was constrained in all six degrees of freedom such that the beam can deflected downwards. A downward initial velocity of 10m/s was applied on three adjacent nodes towards the free end. The node with a concentrated mass is also constrained to move vertically downwards without any sideways displacement to enforce high stresses in the beam at the clamped location.

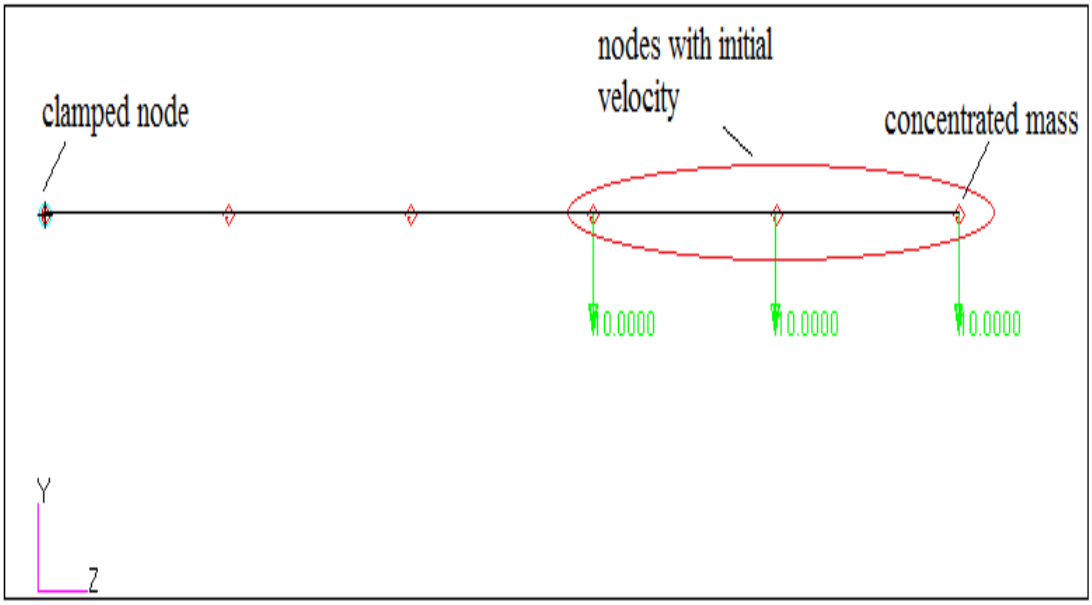

Figure 3.29 Clamped nodes, nodes with initial velocity and concentrated mass.

The failure flag plot in Figure 3.30 indicates that at t=1.762 milliseconds the clamped element reached its allowable stress. But later the clamped element is completely removed from the analysis at t=181.9 milliseconds since it has failed.

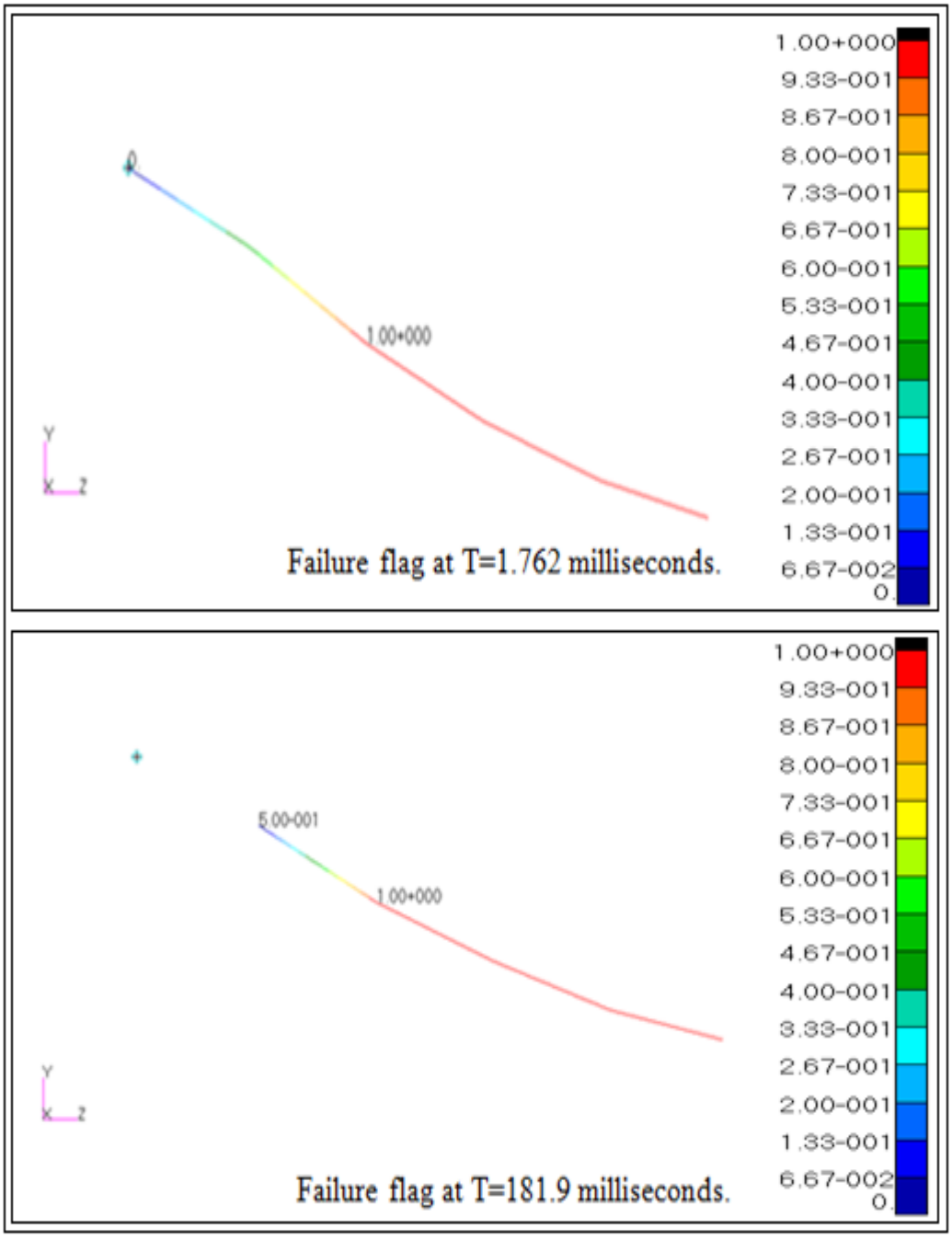

Figure 3.30 Beam failure flag at t=1.7362 milliseconds and t=181.9 milliseconds.

The stress-time and failure flag-time of the beam are displayed in Figures 3.31. It can be seen that both the plots of the stresses and failure flags drop down to zero when the allowable stress is reached. In addition, both graphs drop down to zero between t=0.1 milliseconds and t=0.12 milliseconds.

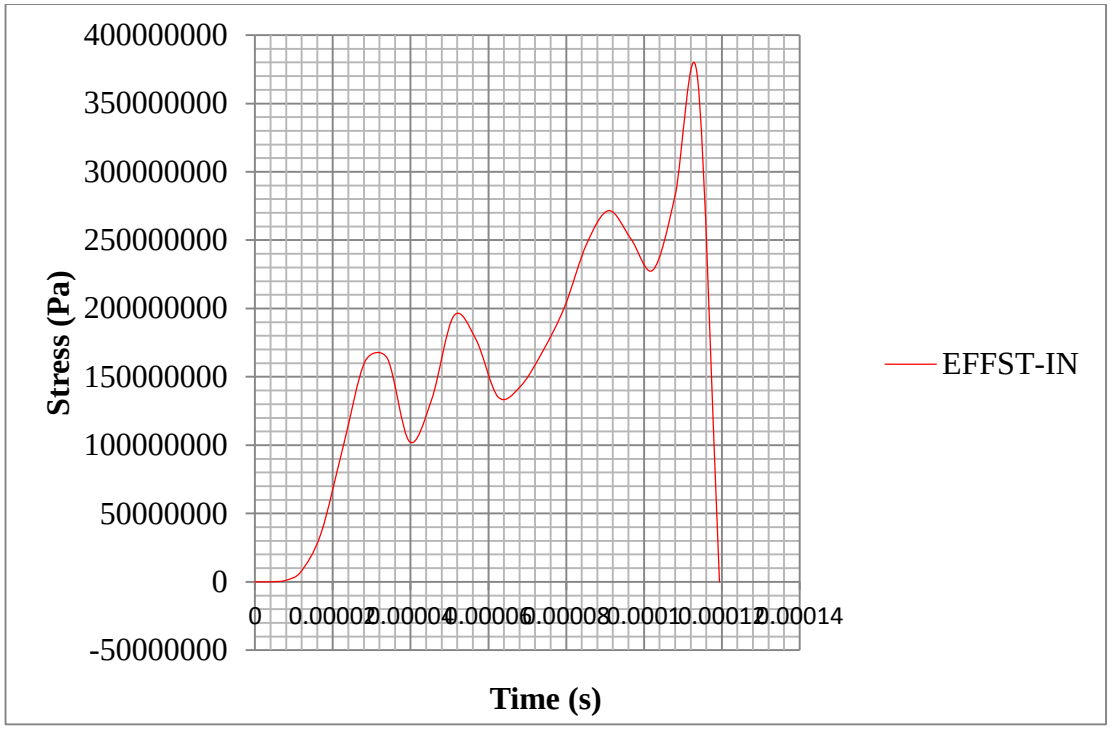

Figure 3.31 Beam stresses vs. time graph.

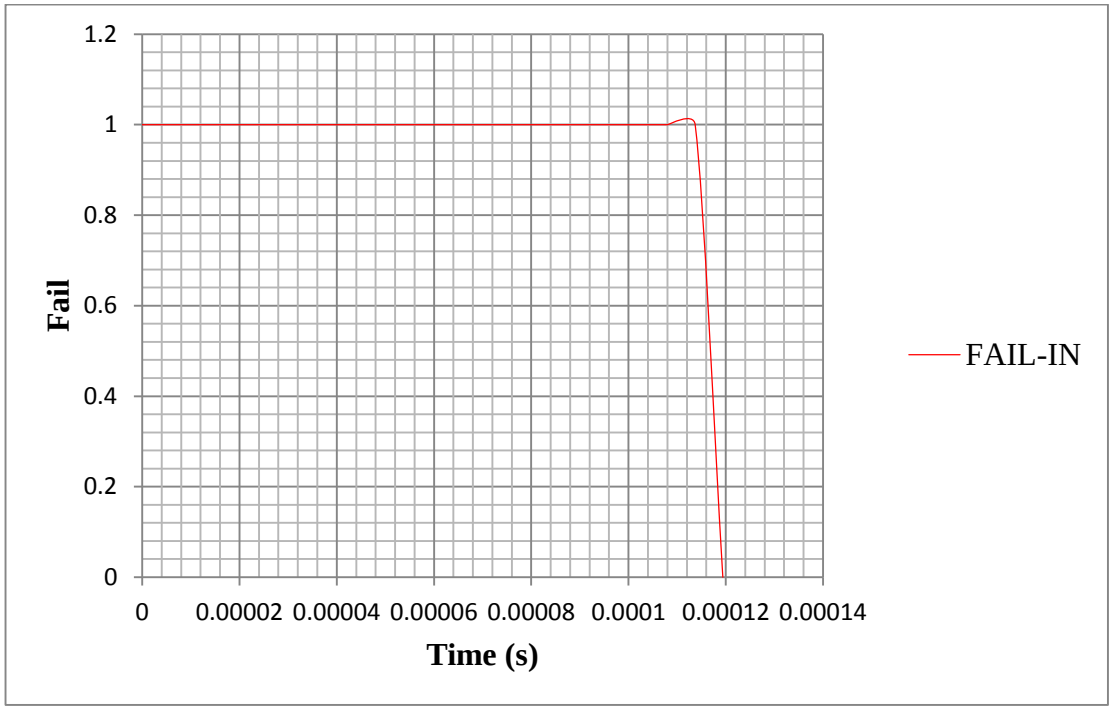

Figure 3.32 Beam failure flags vs. time graph.

3.4 Progressive crushing of a composite square tube

3.4.1 Modeling methodology of the composite square tube

In order to further illustrate the techniques and methodologies related to composite modeling, the next approach was focused on demonstrating the response of composite structures under high dynamic impact loads. The numerical simulations of similar studies of composite tubes under axial crushing possessed stable crushing process with brittle fracturing, good correlation with experiments was obtained. This provides confidence in the future use of non-linear dynamic finite codes for the design of composite structures subjected to crash loading, particularly in the automotive and aircraft industries [33], [34]. Therefore, a composite square tube, a moving rigid surface and a planar rigid wall were modeled using MSC.Patran/Dytran. The analysis model is shown in Figure 3.33; a composite tube was placed upright between the planar rigid wall and the moving rigid surface. The planar rigid wall prevents the tube from moving downwards. The rigid moving surface is impacted on the tube such that the effect of a dynamic crash load applied on composite structures can be created.

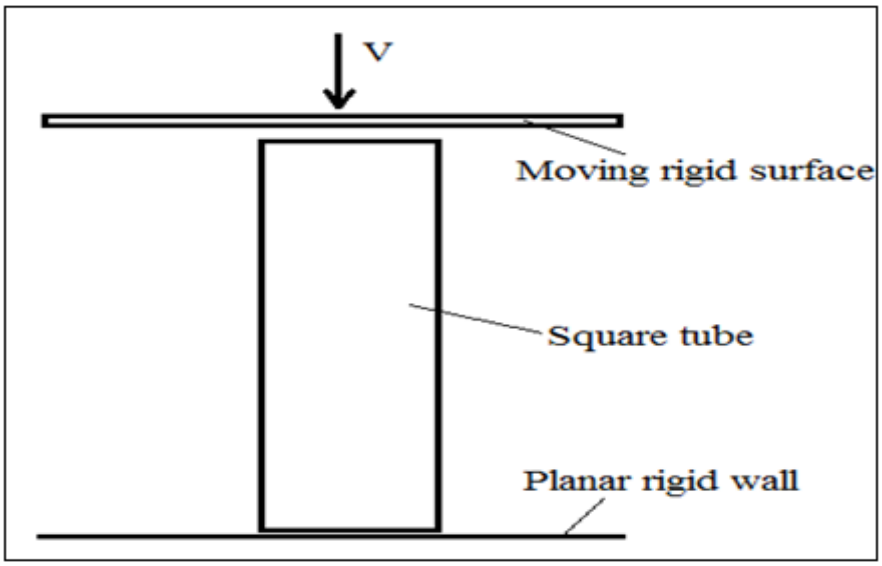

Figure 3.33 Set-up model for the composite tube crush analysis.

The composite tube geometry dimensions used in this study were obtained from the investigation done by Don H. Pham in a finite element study of a composite tube under impact load [35]. In that study, all the translational and rotational degrees of freedom at the bottom edge of the tube were constrained. This was to prevent the tube from moving along with the rigid surface. But the continuously loading of the tube causes failure at the constrained end and the remainder of the tube moves freely along with the moving rigid surface. Therefore, the progressive crushing behavior is not properly demonstrated.

Therefore, in this investigation the undesired dynamic response is prevented by constraining two horizontal translations at the bottom end of the tube. In addition, introducing the planar rigid wall at the constrained end allows for the expected crush behavior of the tube by preventing it from moving together with the impacting rigid surface.

3.4.2 Finite element model of the composite square tube

A moving rigid surface and a composite square tube are modeled using (6×6) 36 and 2656 CQUAD elements respectively. A uniform mesh with coarse elements of 25.4mm square is used throughout the rigid plate model and a fine uniform mesh of (3.048 mm×3.175 mm) is used on the tube model. In addition, a tube was modeled by using a multi-layered shell which uses one integration point per layer. This means seven integration points are used for each element of the tube since there are seven layers per tube element. The CQUAD elements use the highly efficient Belytschko-Tsay shell formulation [21]. A meshed rigid surface and composite tube are shown in Figure 3.34, but a rigid planar wall is invisible in MSC.Patran. A rigid surface defines a moving rigid plane of finite size and a master-slave contact while a planar rigid wall resembles a rigid plane of infinite size that cannot be penetrated by the grid points and the plane is fixed in space.

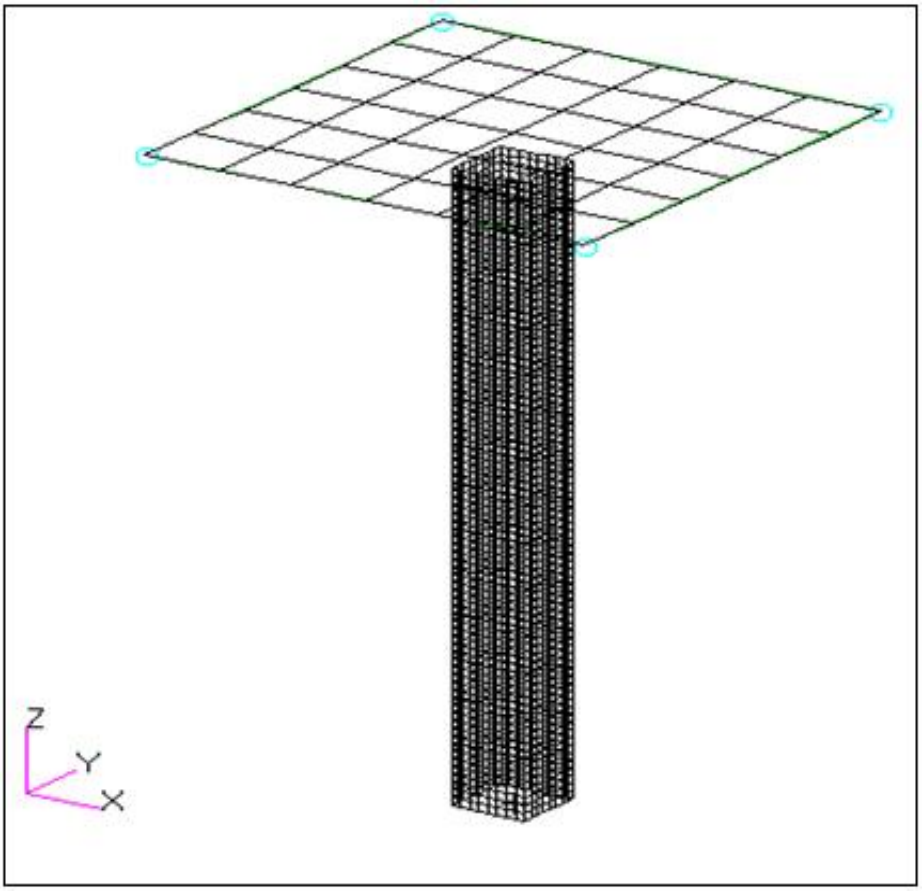

Figure 3.34 Meshed models of the moving rigid surface and the square tube.

3.4.3 Material properties for the composite square tube model

The glass fibre reinforced plastic tube was defined by using the MAT8 composite material, which is an orthotropic material for shell elements. The stacking sequences of seven plies per element were arranged in the order of [0°/45°/90°/-45°/90°/45°/0°] and material orientation was defined using the PCOMP data entry. The PCOMP entry defines the properties of a multi-ply laminate composite material. The MAT8 composite material was associated with the PCOMP data entry for assigning the orthotropic properties. The material properties of the composite laminate are shown in Table 4.

The moving rigid surface was defined using the MATRIG material entry, which defines the properties of a rigid body that cannot be deformed and therefore, it does not allow the slave grid points to pass through.

Properties	**Values**
Longitudinal Modulus (E_1)	20.7 GPa
Transverse Modulus (E_2)	20.7 GPa
Poisson's ratio	0.12
Longitudinal Shear Modulus (G_{12})	3.72 GPa
Transverse Shear Modulus (G_{13})	3.72 GPa
Density	1934kg/m^3
Cured ply thickness	0.2286 mm
Longitudinal Compressive Strength	258.56 MPa
Longitudinal Tensile Strength	258.56 MPa

Table 4 Material properties of the tube wall laminate ply. [35]

3.4.4 Boundary conditions for the composite tube crushing

In order for the rigid moving surface to impact the composite tube, all the nodes belonging to the moving surface were initiated with a velocity of 25.4 m/s. This was done in the direction towards the tube. In addition, the moving rigid surface was assigned a mass of 22.7 kg. Since the moving surface had to impact, in order to crush the tube, a contact mechanism was defined between the interacting bodies of the model. Therefore, a master-slave contact was defined between the tube and moving rigid surface. On the other hand, the grid points of the composite tube cannot penetrate the rigid planar wall. Since the composite tube is likely to fold into itself under the impact loading of the moving plate, a self-contact method was defined to the composite tube.

3.4.5 Results review of the composite tube crushing

The results plots displaying the crushing sequence of composite tube were created using the MSC.Patran and are divided into two groups. The first group shows the stress plots of the composite tube without any failure criterion defined in the analysis. This was done to first verify that the stresses in the composite tube can reach or exceed the failure stress of the material before any failure theory can be introduced. This assures that the composite tube will fail once the failure criterion is defined for the model. Figure 3.35 shows the response of the composite tube at different times with no failure criterion assigned to the model and the allowable stress value was exceeded.

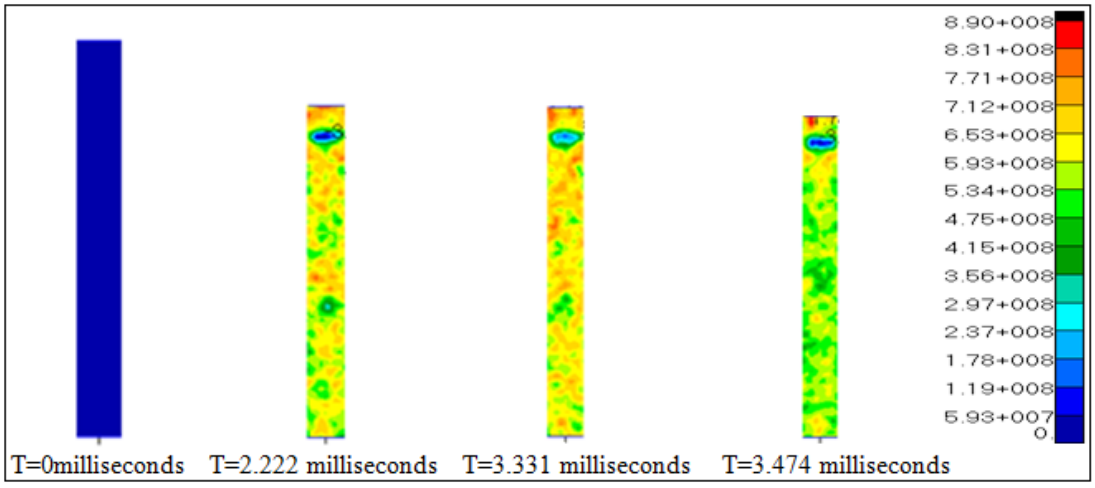

Figure 3.35 Composite tube plots with no failure criteria defined.

The second group comprises of the results obtained from a simulation in which the Tsai-Wu criteria was defined to control the failure response of the composite tube. Figure 3.36 displays the composite tube crushing sequence when the Tsai-Wu failure theory is defined to control the failure process. Since in MSC.Patran/Dytran the failed elements are excluded from the analysis, the height of the tube was reduced at the t=3.934 milliseconds.

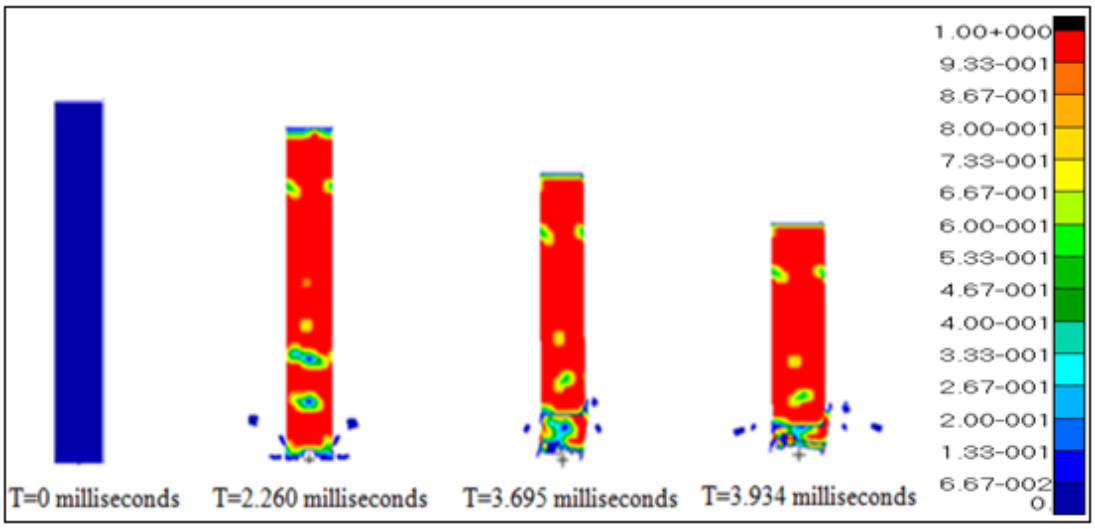

Figure 3.36 Composite tube plots with Tsai-Wu failure criteria defined.

3.5 Crash modeling approach of the Ravin 500 light composite aircraft.

3.5.1 Description of the FEM model of the aircraft

The geometrical model of the Ravin 500 low-wing aircraft was developed from a computer aided drawing tool. The model includes the fuselage section, fire-wall, bulkheads and floor structure. But the information related to the detailed geometry of the wing, horizontal and vertical stabilizers structures was not available; therefore, several assumptions were made to closely represent the weight effects of the missing components and were kept as simple as possible to provide reasonable model for crash analysis. Nevertheless, apart from the lack of wing structural data, the wing structure of this type of aircraft does not make any significant contribution in terms of energy absorption during crash but instead the wing spar crossing affects the passenger cabin, therefore, being hazardous to the occupants [23], [3]. For this reason it makes it easy to represent the wing by means of 1-D beam elements but the center of mass of the wing must be obtained in order to correctly locate or represent its weight by the concentrated load effect. The center of gravity of the wings, engine, vertical and horizontal stabilizers were estimated after measuring the size of each part. But the rigid attachment of the wings, horizontal and vertical stabilizers to the fuselage was achieved by means of RBE2 (Rigid Body Elements) entry. In MSC.Dytran, the degrees of freedom attached to the RBE2 move by the same amount throughout the analysis. Furthermore, the components that have very small or contribute no effect on the structural response during the crash event were also ignored, for example: the windows have very small value of the stiffness as compared to the glass fibre epoxy composite which is the primary structural material of the aircraft. The available geometry model was saved in the International Graphics Exchange System (IGES) and later imported into the pre-processing software package, MSC.Patran [36].

The surfaces, curves and solid components of the aircraft were defined to enable meshing of the structure. The meshing was performed to generate the finite element model of the airframe by both manual and automatic approach. Figure 3.37 shows a

meshed half model of the aircraft with main components labeled and the layup nominal schedule for the fuselage skin is displayed in Table 5.

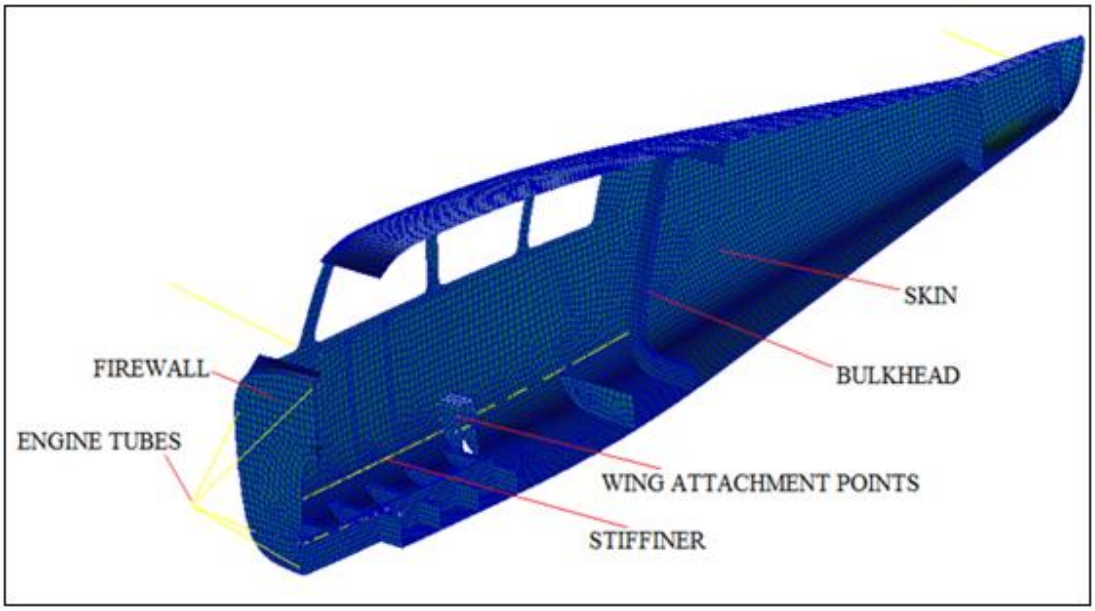

Figure 3.37 Half model of the Ravin 500 light composite aircraft.

Skin layup	Fibre orientations	Ply thickness
1xEthelyne double biaxial	0°/90°	0.14 mm
1xEthelyne double biaxial	+-45°	0.14 mm
1xEthelyne double biaxial	0°/90°	0.14 mm
1xEthelyne double biaxial	+-45°	0.14 mm
Airex foam core 80kg/m^3		10 mm
1xEthelyne double biaxial	+-45°	0.14 mm
1xEthelyne double biaxial	0°/90°	0.14 mm
1xEthelyne double biaxial	+-45°	0.14 mm
1xEthelyne double biaxial	0°/90°	0.14 mm

Table 5 Nominal layup schedule for the aircraft fuselage skin.

Figure 3.38 shows the main components of the aircraft floor structure. The floor structure was integrated into the aircraft fuselage by an equivalence technique that connects coexisting nodes at a point to a single node. Figure 3.39 displays connected portions of both the floor structure and the fuselage section. The corresponding nominal layup schedule for internal frame and the bulkheads is displayed in Table 6.

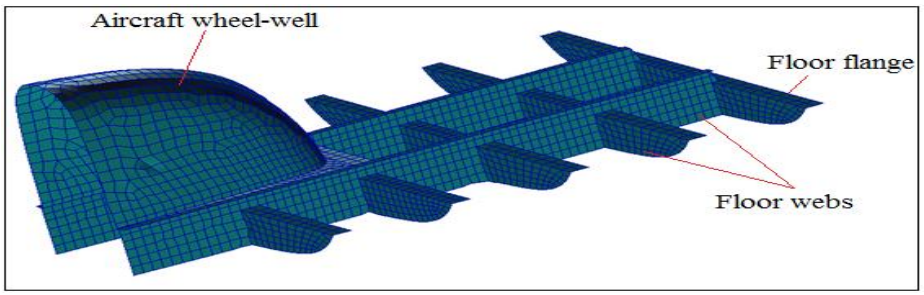

Figure 3.38 Components of the Ravin floor structure.

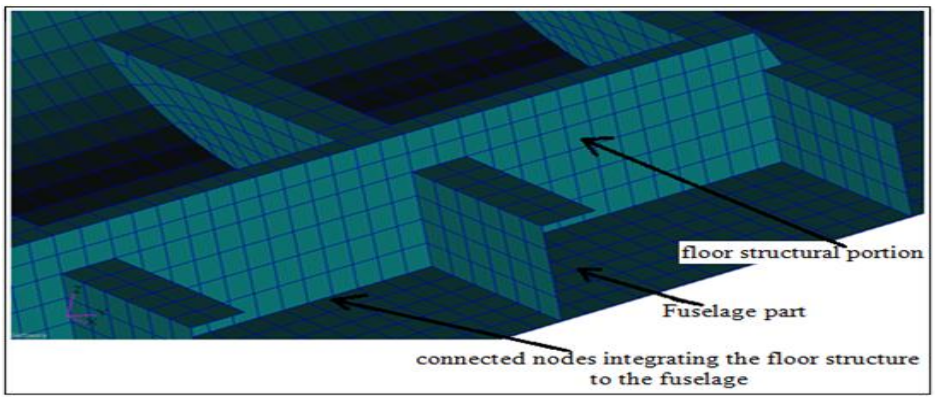

Figure 3.39 Connected portions of both the floor structure and the fuselage section.

Layups for the Internals	Fibre orientations	Ply thickness
2xEthylene double biaxial	+-45°	0.28 mm
Airex foam core 80kg/m³		5 mm
2xEthylene double biaxial	+-45°	0.28 mm

Table 6 Nominal layup schedule for the aircraft internal structure.

3.5.2 Material properties for the aircraft crash model

The fuselage skin and internals equivalent material models displayed in Table 7 and Table 8 respectively were prepared from the typical fibre reinforced plastic properties for glass for glass fibre laminates. In addition, the foam core in Table 9 and steel beam properties in Table 10 were also based standard values. The soil properties used in the model were obtained from the work done by Edwin L. Fasanella et al [37].

Property	**Value**
E1	15.3GPa
E2	15.3GPa
G12=G13	6.20GPa
G23	3.13GPa
Poisson's ratio	0.31
Density	1984kg/m^3
Longitudinal Tensile Failure	277MPa
Longitudinal Compressive Failure	162MPa
Failure Stress	86MPa
Lateral Tensile Failure	277MPa
Lateral Compressive Failure	162MPa

Table 7 Equivalent material properties for fuselage facings (orthotropic).

Property	**Value**
E1	9.81GPa
E2	9.81GPa
G12=G13	9.1GPa
G23	3.13GPa
Poisson's ratio	0.57
Density	1984kg/m^3
Longitudinal Tensile Failure	95MPa
Longitudinal Compressive Failure	95MPa
Failure Stress	155MPa
Lateral Tensile Failure	95MPa
Lateral Compressive Failure	95MPa

Table 8 Equivalent material properties for internal facings (orthotropic).

Property	Value
Elastic Modulus	66MPa
Modulus of Rigidity	30MPa
Poisson's ratio	0.01
Density	80kg/m^3
Yield Stress	0.95MPa
Plastic Stress at Failure	0.95MPa
Plastic Strain at Failure	0.2m/m

Table 9 Material properties for foam core (isotropic).

Property	Value
Density	7850kg/m^3
Elastic Modulus	200GPa
Poisson's ratio	0.3
Yield Stress	400MPa
Maximum Plastic Strain	0.001

Table 10 Material properties for the steel beam elements.

Property	Value
Density	2201.6kg/m^3
Elastic Modulus	4MPa
Poisson's ratio	0.3
Yield Stress	68.9KPa
Strain Hardening	800KPa

Table 11 Material properties for soil model (isotropic). [37]

3.5.3 Boundary conditions of the aircraft crash model

3.5.3.1 Concentrated masses applied to the model

As stated some of the aircraft components were to be represented by concentrated masses. Therefore, the lump masses were located at the center of gravity of the specific component provide the effect of the weight contribution to the overall structure. Table 12 shows the magnitudes of estimated masses for each wing, engine, vertical and horizontal stabilizers. The representations of respective concentrated loads are displayed in Figure 3.40 with appropriate labels.

Components	Mass (kg)
Engine	162
Wing	250
Horizontal stabilizer	33
Vertical stabilizer	42

Table 12 Components with concentrated masses.

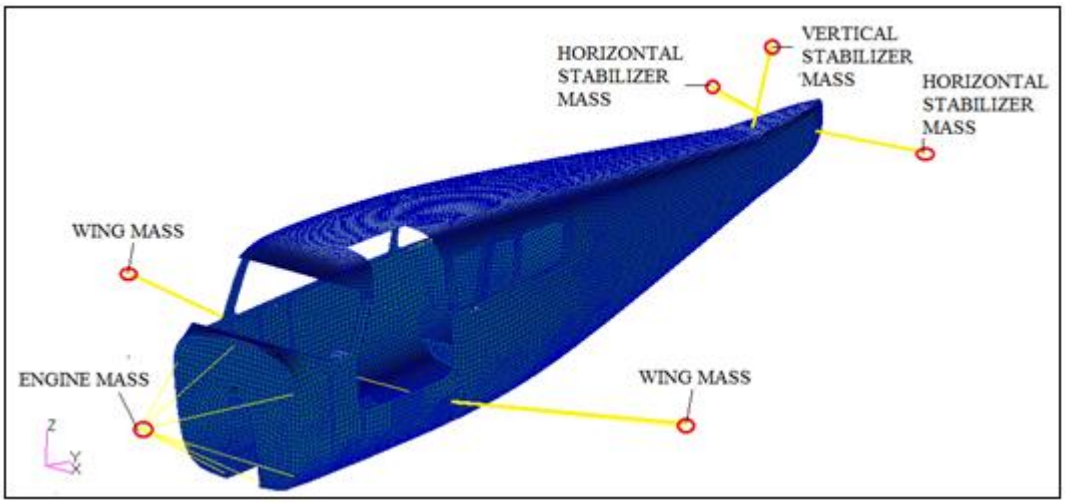

Figure 3.40 Concentrated masses representing the wings, stabilizers and engine loadings.

3.5.3.2 Contact definition in the crash model

An adaptive self-contact was defined between the shell elements of the aircraft. This contact definition prevents the aircraft shell elements from penetrating themselves. In most aircraft crash models, the aircraft surface is likely to buckle as the structure gets heavily deformed. It is important to assign this type of contact in all the shell elements of the structure since it's not easy to identify the points of contact beforehand. A master-slave contact was defined between the impacted soil and the bottom fuselage section of the aircraft structure. These contact surfaces were defined to prevent shell elements of the aircraft from penetrating the soil model during impact.

3.5.3.3 Aircraft crash parameters

Since there are no specific regulations that provide dynamic design requirements of the light composite aircraft structure, the crashworthiness analysis was conducted using closely similar parameters to the aircraft stall conditions. Various researchers have proposed different crash conditions depending on the goals of their investigations. Therefore, only four conditions of analysis are considered in this study. It is common practice to test the crashworthiness of an aircraft at various angles but maintaining the same crash velocity [38], [39], [4]. Changing the flight-path angle has more effect on the structural damage and acceleration in the forward portion of the fuselage from nose to firewall than the cabin area [39]. Therefore, the first three crash conditions were conducted at the same crash velocity and the flight path angle was changed by 5^{o} from 10^{o} to 20^{o}. But in the fourth crash scenario, the crash angle was increased to 30^{o} based on the study that was conducted by the AGATE Advanced Crashworthiness Group and they developed the impact conditions for their accident investigation purpose [40]. The crash conditions adopted in this study are listed in Table 13.

Flight path angle	Flight path velocity	Terrain
10°	22m/s	Soil
15°	22m/s	Soil
20°	22m/s	Soil
30°	22m/s	Soil

Table 13 Different aircraft crash conditions used for the crash model.

Both the initial velocity and the crash angle are referenced from the soil horizontal plane as displayed in Figure 3.41. These two parameters define the initial flight conditions of the aircraft at the beginning of the analysis and before making contact with the soil. In addition, it was also important to apply the gravitational acceleration to the masses of the model, therefore, a downward gravity acceleration of -9.81m/s^2 was applied along the global z-axis of the model.

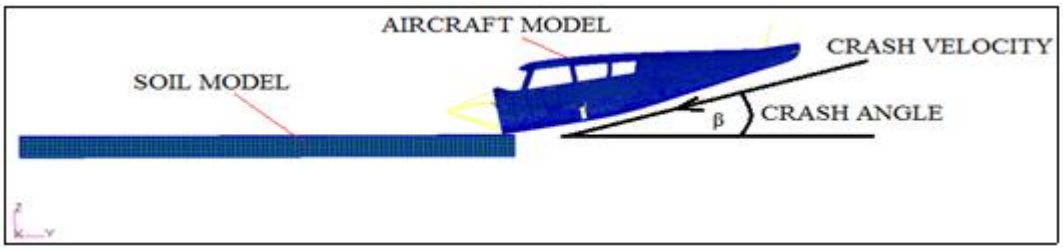

Figure 3.41 Soil model, aircraft model, crash velocity and crash angle.

CHAPTER 4

RESULTS AND DISCUSSION

4.1 Progressive ply failure effect in aircraft crash analysis

In order to illustrate the effect of various techniques and theories discussed in the previous sections, it was necessary to make a comparison of the results obtained from a large scale model. An attempt was made to investigate the progressive ply failure behavior of the aircraft fuselage plies after a series of simulations were performed. The failure index of element 37470 was checked at time step just before and after failure.

The focus was on the outer plies of the laminate facings which were expected to fail first based on progressive ply failure approach. Therefore, in Figure 4.1 it is seen that at t=55.4 milliseconds, element 37470 was still active in the analysis with both layer 1 and layer 9 integrated to the structure. This means that all the element plies were still active at this time according to the progressive ply failure based technique.

But later in next time step at t=56.4 milliseconds element 37470 has been eliminated from the analysis as seen in Figure 4.2. This indicates that all the ply stacking of the element 37470 have failed. Furthermore, this shows that the first ply failure based approach would still work reasonably well for the aircraft crash analysis since the last ply fails relatively quickly after the first ply.

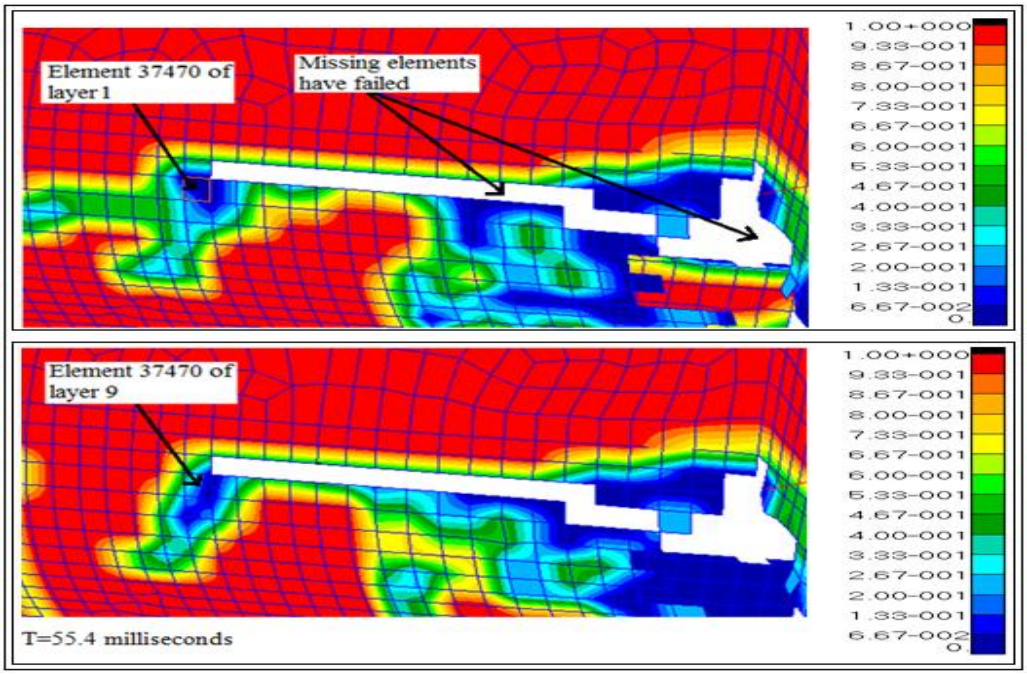

Figure 4.1 Element 37470 not failed at t=55.4 milliseconds for both layer 1 and 9 of the fuselage at 20 crash angle.

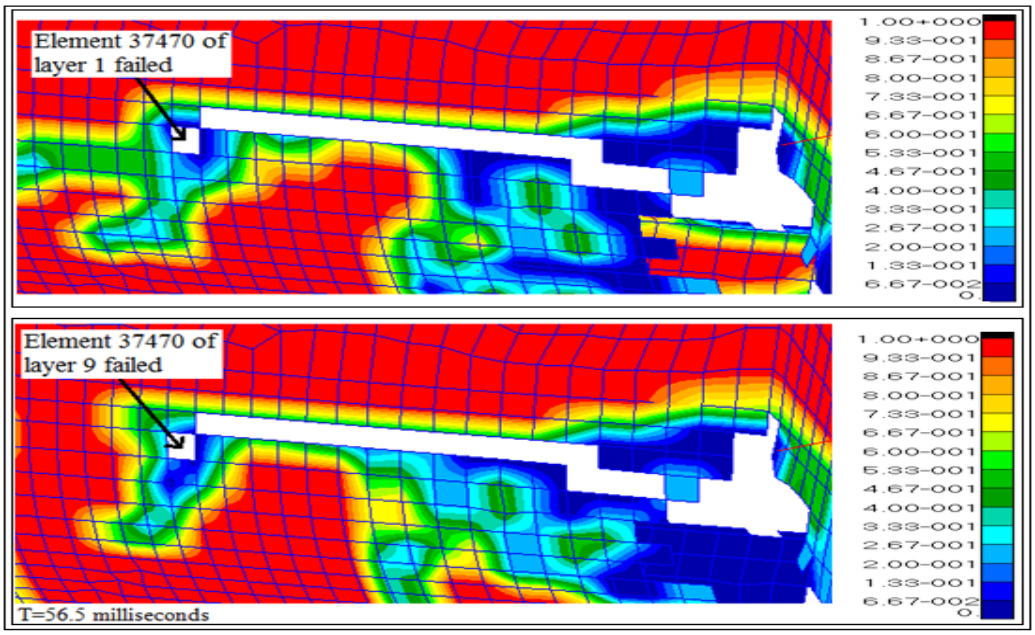

Figure 4.2 Element 37470 failed at t=56.5 milliseconds for both layer 1 and 9 of the fuselage at 20 crash angle.

4.2 Effect of varying aircraft crash angle

Comparisons of the aircraft structural damage induced by the crash events at 10°, 15°, 20° and 30° crash angles are shown in Figures 4.1, 4.2, 4.3, 4.4, 4.5 and 4.6. The crash sequences at each scenario clearly indicate that varying the crash impact angle influence the amount of structural failure. There is a small amount of damage on the aircraft at a 10° crash angle but the structure was severely damaged at a 30° crash angle. In addition, it is visible in Figures 4.4, 4.5 and 4.6 that composite structures exhibit a crushing behavior under high dynamic impact loads.

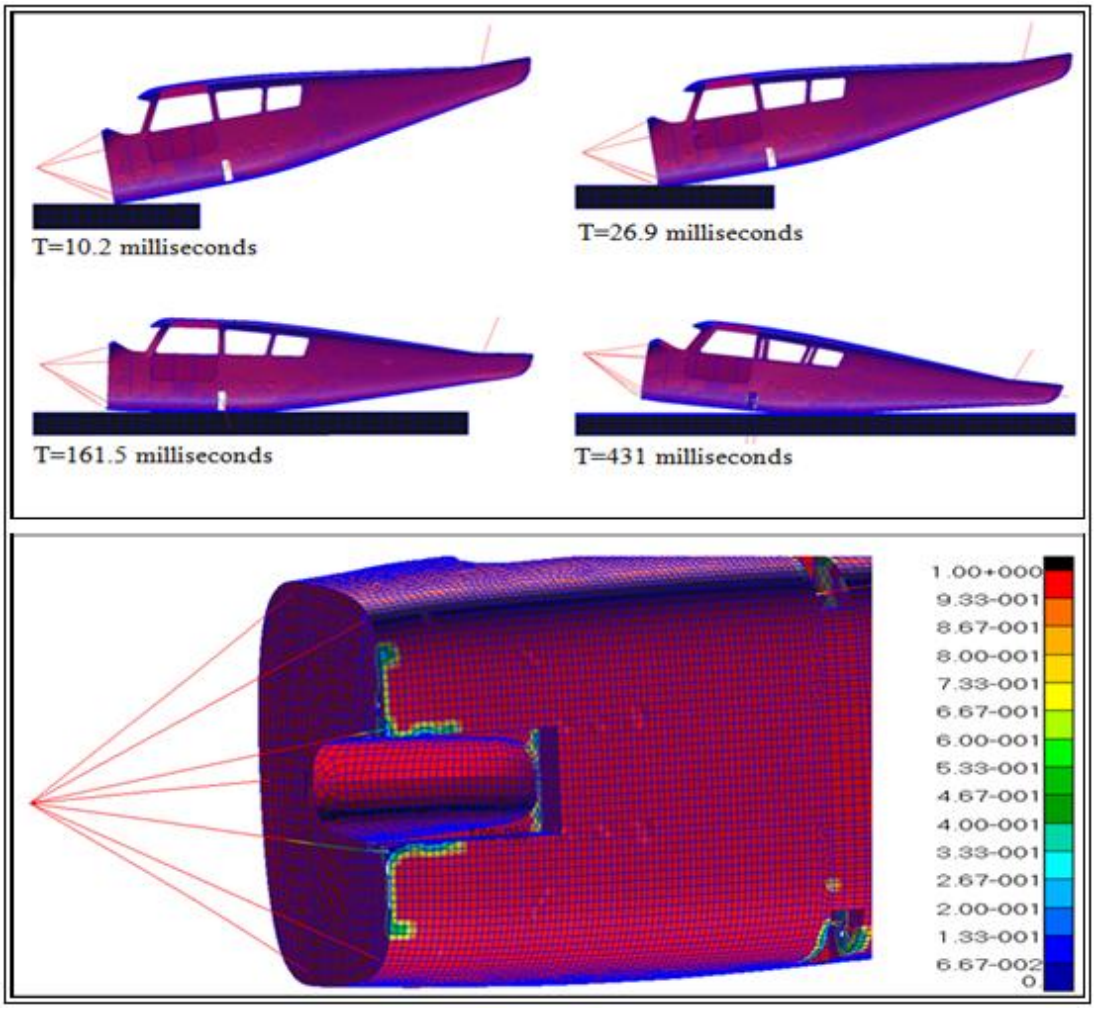

Figure 4.3 Aircraft crash sequence at 10° crash angle and a portion of a fuselage with minimum amount of damage.

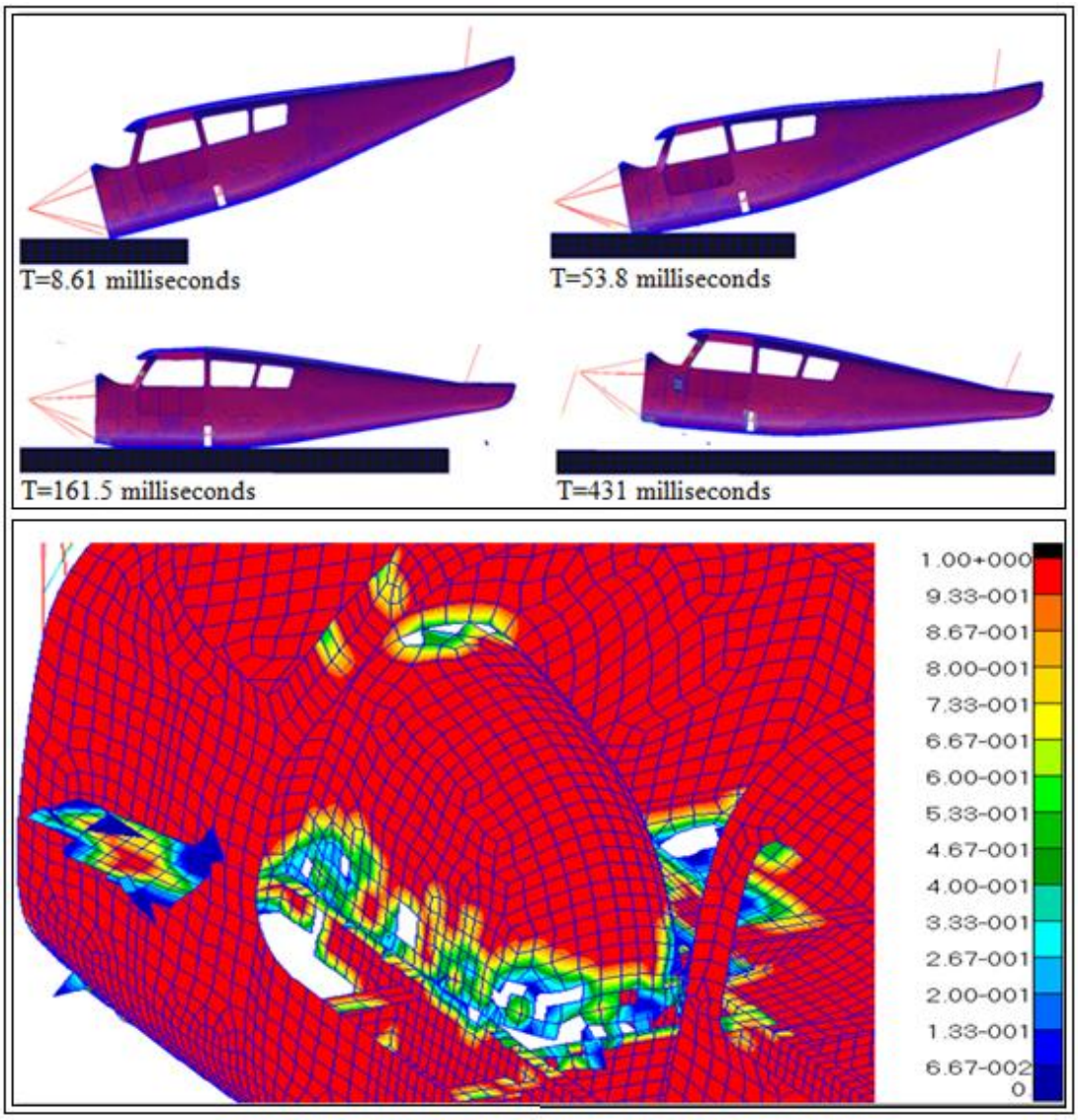

Figure 4.4 Aircraft crash sequence at 15° crash angle and failure in the wheel-well structure.

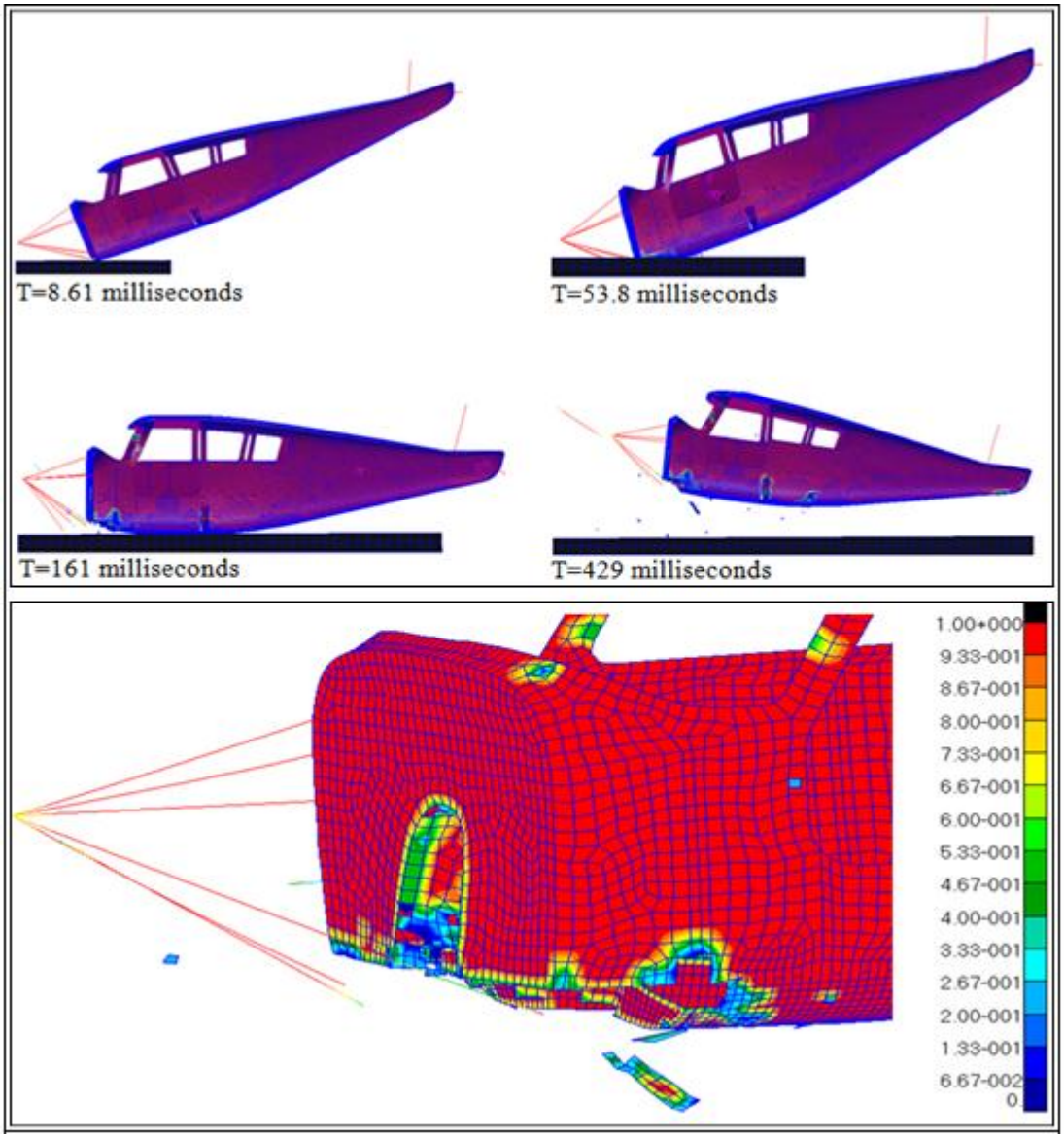

Figure 4.5 Aircraft crash sequence at a 20° crash angle and crushed forward, fuselage structure.

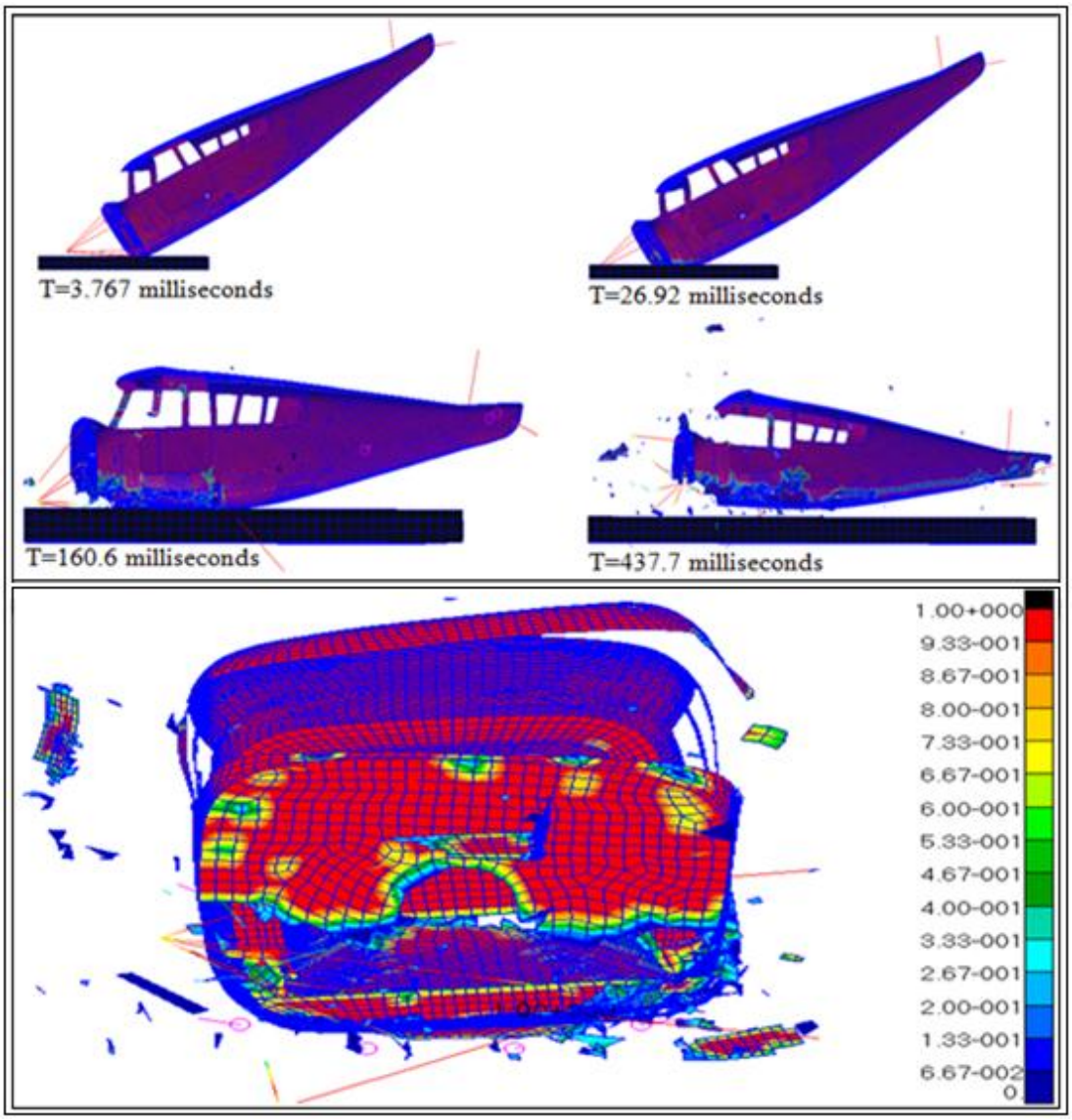

Figure 4.6 Aircraft crash sequence at a 30° crash angle and the entire fuselage heavily damaged.

CHAPTER 5

CONCLUSIONS AND RECOMMENDATIONS

The crashworthiness of a light composite aircraft onto the soil was carried out with the use of finite element non-linear analysis code MSC.Dytran. The failure criteria were investigated by conducting a basic composite plate analysis to evaluate the capabilities of the criteria in the analysis code. The Tsai-Wu failure theory was found to be capable of predicting failure of a composite laminate. Therefore, the prediction of composite aircraft structural response or failure was achieved by using the Tsai-Wu criteria. Even though simulation reduces the expenses of testing, it does not totally eliminate the testing process. The simulation results depend largely on the quality of the model and lot of assumptions are considered in areas that the software may be limited, but properly conducted experimental work minimizes the room for speculation. Therefore, it is advisable to perform experimental tests to validate the results in this type of investigation.

Based on the simulation results, a comparison of the aircraft structural damage induced by the crash scenarios at 10°, 15°, 20° and 30° angles was done to evaluate the effect of varying the crash angles. The crash sequences at each event clearly indicate that the steeper the crash angle the greater the damage on the aircraft structure. In addition, it is visible in that composite structures exhibit a crushing behavior under high dynamic impact loads.

The performed analysis have enabled for the establishment of some criteria for designing the light composite aircraft. Therefore, it is important to focus more on the following aspects in order to develop of a crashworthy light composite aircraft design;

- The forward bottom fuselage must be strengthened to withstand the high impact forces during entry into the surface.
- The subfloor structure may be fitted with some energy absorbing mechanism that can dissipate impact energy from being transferred to the occupant's locations.
- The cabin area may be installed with secondary safety features that can minimize the effect of impact to the occupants.
- The engine frame or mounting tubes may be designed to partially contact the impact surface during crash event; their failure will lead to energy absorption process at early crash stages.
- The windows and doors panels must be strong enough to sustain the loads of the roof as its structure is likely to collapse down reducing the passenger space within the aircraft.

REFERENCES

[1] Adept Airmotive, http://www.adeptairmotive.com/ (Accessed: 15 May 2011).

[2] Jackson, E.K and Fasanella, E.L, Crash Simulation of a Vertical Drop Test of a B737 Fuselage Section with Overhead Bins and Luggage, US Army Research Laboratory, NASA Langley Research Center.

[3] Fasanella, E.L and Jackson, E.K, (2002), Best Practices for Crash Modeling and Simulation, U.S Army Research Laboratory, Vehicle Technology Directorate, NASA Langley Research Center.

[4] Castle, B.C and Emilio, A, (1983), Crash Tests of Three Identical Low-Wing Single-Engine Airplanes, NASA Technical Paper 2190.

[5] Greer D.L, Breeden, J. S and Heid, T.L, (1964), Crashworthy Design Principles, Federal Aviation Agency, Washington D.C.

[6] Simula Inc, 2223 South 48th Street Tempe, Arzona, (1980), Aircraft Crash Survival Design Guide Volume III, U.S. Army Research and Technology Laboratories.

[7] Simula Inc, 2223 South 48th Street Tempe, Arzona, (1980), Aircraft Crash Survival Design Guide Volume II, U.S. Army Research and Technology Laboratories.

[8] Reed, W.H and Avery, J.P, (1966), Principles for Improving Structural Crashworthiness for STOL and CTOL Aircraft, U.S. Army Aviation Material Laboratories.

[9] Dennis F. S, Basic Principles of Crashworthiness, Colonel USA (Ret), Injury Analysis LLC, 2839 Via Conquistador, Carlsbad, CA 92009-3020 USA.

[10] Emilio, A. and Victor L. V, Light Airplane Crash Tests at Impact Velocities of 13 and 27 m/s, NASA Technical Paper 1042, Langley Research Center, Hampton, Virginia.

[11] Todd R. H, Jill M. V, Small Airplane Crashworthiness Design Guide, NASA Langley Research Center.

[12] William F. Smith, Javad Hashemi, Foundations of Materials Science and Engineering, Fourth Edition, McGraw-Hill International Edition.

[13] Herakovic, C.T (1998), Mechanics of Fibrous Materials, John Wiley and Sons Inc, New York.

[14] Jordan, K.G, (2004), Development of Prototype UCAV Airframe Components using Advanced Composite Materials, Dissertation for Degree of Master of Technology in Mechanical Engineering, Durban Institute of Technology.

[15] Reid S.R and Zhou G, Impact Behaviour of Fibre-Reinforced Composite Materials and Structures, Woodhead Publishing Limited, Cambridge England.

[16] Federico P.A., Study of Failure Criteria of Fibrous Composite Materials, George Washington University, Joint Institute for the Advancement of Flight Sciences, Langley Research Center, Hampton, Virginia.

[17] Hakan K, Rami H, (2003), Progressive Damage and Nonlinear Analysis of Pultruded Composite Structures, Department of Structural Engineering and Mechanics, School of Civil and Environmental Engineering, Georgia Institute of Technology. Composites PartB, Vol. 34, p. 235-250.

[18] Wen-Pin L and Hsuan-Teh H, Parametric Study on the Failure of Fibre-Reinforced Composite Laminates Under Biaxial Tensile Load, Department of Civil Engineering, Chinese Military Academy, Department of Civil Engineering, National Cheng Kung University.

[19] MSC.Dytran (2008) Theory Manual, MSC.Software Corporation, 2 MacArthur Place, Santa Ana, CA 92707.

[20] Edwin L. Fasanella, Karen E. Jackson, and Karen H. Lyle, Finite Element Simulation of a Full-Scale Crash Test of a Composite Helicopter, US Army Research Laboratory.

[21] MSC.Dytran User's manual Version 4.0, (1997), The MacNeal-Schwendler Corporation, Los-Angeles, California.

[23] Bossak M. and Kaczkoski, J., (2003), Global/local analysis of Composite Light Aircraft Crash Landing, Institute of Mechanics and Design, Warsaw University of Technology, Poland. Computers and Structures, Vol. 81, p. 503-514.

[22] Serge A., Impact on Composite Structures, Southern Illinois University at Carbondale, Cambridge University Press.

[24] Fasanella, E.L and Karen E. J, Water Impact Test and Simulation of a Composite Energy absorbing Fuselage Section, US Army research Laboratory.

[25] Michal, M, Jan S, The Sailplane Cockpit Structure During Emergency Landing Condition, , Brno University of Technology, Institute of Aerospace Engineering, Czech Republic, 25th International Congress of the Aeronautical Sciences.

[26] Karen, E.J and Fasanella, E.L, Impact Testing and Simulation of a Crashworthy Composite Fuselage, US Army Research Laboratory.

[27] Heimbs S, Cichosz J, Klaus M, Kilchert S, Johnson A.F, (2010), Sandwich Structures with Textile-Reinforced Composite Foldcores Under Impact Loads. Composite Structures, Vol. 92, p. 1485-1497.

[28] Hamidreza Z, Matthias K, Henrik A, (2008), An Experimental and Numerical Crashworthiness Investigation of Thermoplastic Composite Crash Boxes, Institute of Dynamics and Vibrations, Germany. Composite Structures, Vol. 85, p. 245-257.

[29] Jiang W, Yang J.L, (2009), Energy Absorption Behaviour of a Metallic Double-Sine-Wave Beam Under Axial Crushing, The Solid Mechanics Research Centre, Beijing University of Aeronautics, China. Thin-Walled Structures, Vol. 47, p. 1168-1176.

[30] Ashish, K.S, Fasanella, E.L, Chad, S., Karen, J. and Mullins, B.R, Comparison of Hard Surface and Soft Soil Impact Performance of Crashworthy Composite Fuselage Concept, Bell helicopter Textron Inc and U.S. Army Research Laboratory Vehicle Directorate.

[31] MSC.Dytran (2010) Reference Manual, MSC.Software Corporation, 2 MacArthur Place, Santa Ana, CA 92707.

[32] Karen, E.J and Fasanella, E.L, Crash Simulation of a Half-Scale Model Composite Fuselage Concept, U.S. Army Vehicle Technology Center, NASA Langely Research Center.

[33] Jiancheng, H., Xinwei, W, (2009), Numerical and Experimental Investigations on the Axial Crushing Response of Composite Tubes, College of Aerospace Engineering, Nanjing University of Aeronautics and Astronautics, People's Republic of China, Composite Structures, Vol. 91, p. 22-228.

[34] Bisagni, C., Di Pietro, G., Fraschini, L and Terletti, D, (2005), Progressive Crushing of Fibre-reinforced Composite Structural Components of a Formula One Racing Car, Italy. Composite Structures, Vol. 68, p. 491-503.

[35] Pham, D., (2002), Finite Element Study of a Composite Tube Under Impact Load, Visteon Corporation, SAE Technical papers series.

[36] MSC.Patran User's Manual, MSC.Software Corporation, 2 MacArthur Place, Santa Ana.

[37] Fasanella, E.L, Jones, Y., Knight, N.F and Kellas, S, Low Velocity Earth-Penetration Test and Analysis, US Army Research Laboratory, Vehicle Technology Directorate Hampton.

[38] Castle, B.C and Alfaro-Bou, E, (1979), Light Airplanes Crash Tests at Three Roll Angles, NASA Technical Paper 1477.

[39] Castle, B.C and Alfaro-Bou, E, (1978), Light Airplanes Crash Tests at Three Flight Path Angle, NASA Technical Paper 1210.

[40] Hooper, S.J, Design and Construction of a Crashworthy Composite Airframe, Marilyn Henderson National Institute for Aviation Research, Wichita State University.